

## Abstract

# Advances in dynamic response reconstruction using non-linear time domain system identification.

By

Charl R Cater

A thesis submitted for the degree of

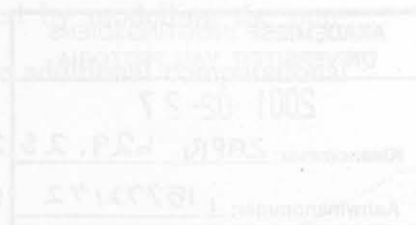
MASTER IN ENGINEERING

in the Department of Mechanical and Aeronautical Engineering

of the Faculty of Engineering

of the

University of Pretoria



# Abstract

This thesis forms part of an existing research programme to further improve the QanTiM time domain service load simulation system. Service load simulation is the reproduction of actual service responses in full scale laboratory tests, on dynamically loaded multiple axis computer controlled servo-hydraulic test rigs. A well-developed science in the frequency domain contrasts with the relatively new time domain service load simulation techniques. It is thus necessary to gain a better understanding of this time domain simulation technique and operation thereof. Furthermore, the existing time domain techniques use linear modelling techniques, which may be a limitation when simulating practical non-linear systems. The improvement of time domain simulation is addressed in two parts, firstly the effect of varying input parameters and operating procedures for the existing linear techniques, and secondly the development and implementation of non-linear time domain based system identification routines for use within service load simulation.

- The investigation into improved performance of the existing linear techniques was based on practical test rig experience and empirical research. Numerous simulations were conducted internationally using both single and multiple axis test rigs. This research resulted in a set of rules and guidelines for improved and simplified simulation. Some of these rules have been implemented in revisions of the existing simulation package and various guidelines for further research into improved and simplified simulation practices were established.
- Investigation into possible non-linear simulation was preceded by literature survey into appropriate modelling techniques. The Non-linear Auto Regressive with eXogenous input [NARX] - model description was adapted and implemented for general non-linear modelling and system identification, and subsequently applied in service load simulation. The NARX non-linear modelling technique proved ideal for general non-linear modelling and system identification problems, even for non-square systems with severe geometrical non-linearity. It does however demand immense computational power, and is plagued by potential numerical instability. The increased accuracy gained by modelling the non-linearity in practical simulations does presently not warrant the additional computational effort and possible instability problems.

# Acknowledgements

I would like to express my gratitude to the following people for their involvement in this study:

- Anton Raath, who initiated the research and encouragingly assisted the progress thereof
- Michiel Heyns, who on a short notice agreed to take over the responsibilities of research promoter
- Herman Booysen and Waldo von Fintel who were always available at a moments notice, with expert technical solutions
- Jan Eksteen, Henk van der Bijl and Rudi Siegling for their thorough research contributions
- My colleagues at LGI Structural Mechanics & Dynamics, for their unparalleled contributions and friendship
- My parents for their unfailing support
- and finally Tania, who became my wife during the course of this work.

C.R.C.

November 1997

# Contents

## CHAPTER 1

<b>INTRODUCTION .....</b>	<b>1</b>
1.1. OVERVIEW.....	2
1.2. HISTORICAL PROFILE .....	2
1.3. PRINCIPLES OF STRUCTURAL DYNAMIC RESPONSE RECONSTRUCTION.....	4
1.4. FREQUENCY VS. TIME DOMAIN .....	5
1.5. DYNAMIC SYSTEM IDENTIFICATION .....	6
1.6. THE INVERSE DYNAMIC MODEL.....	6
1.7. OPERATIONAL RESEARCH INTO TIME DOMAIN APPLICATION .....	7
1.8. NON-LINEAR IMPLEMENTATION .....	8
1.9. DOCUMENT OVERVIEW.....	10

## CHAPTER 2

<b>RESEARCH TASK.....</b>	<b>11</b>
2.1. TYPICAL SIMULATION PROBLEMS.....	12
2.2. ORIGINS OF POOR SIMULATION.....	13
2.3. PROPOSED INVESTIGATION FOR IMPROVED TIME DOMAIN SIMULATION .....	14
2.3.1. <i>Test rig integrity</i> .....	14
2.3.2. <i>Physically unrealisable desired response data</i> .....	16
2.3.3. <i>Analogue to digital conversion</i> .....	17
2.3.4. <i>Synthetic identification signals</i> .....	17
2.3.5. <i>Non-linear modelling capabilities</i> .....	18
2.4. RESEARCH SUMMARY.....	19



## PART I: EMPIRICAL RESEARCH INTO IMPROVED LINEAR SIMULATION

## CHAPTER 3

<b>EMPIRICAL RESEARCH INTO IMPROVED LINEAR SIMULATION .....</b>	<b>21</b>
3.1. RIG REPEATABILITY .....	22
3.1.1. <i>Repeatability function application 1: Electro-dynamic shaker.....</i>	<i>24</i>
3.1.2. <i>Repeatability function application 2: Vehicle damper test rig.....</i>	<i>25</i>
3.1.3. <i>Repeatability function application 3: Motorcycle road simulator.....</i>	<i>27</i>
3.1.4. <i>Repeatability function application 4: Radiator test rig.....</i>	<i>28</i>
3.1.5. <i>General discussion of repeatability test procedure and results.....</i>	<i>31</i>
3.2. SPLIT SPECTRA MODELLING AND SIMULATION .....	32
3.2.1. <i>Application of split spectra simulation on a fuel tank test rig.....</i>	<i>34</i>
3.2.2. <i>Application of split spectra simulation on motorcycle simulator.....</i>	<i>37</i>
3.3. OPTIMAL EXCITATION CHARACTERISTICS .....	42
3.3.1. <i>Application on a seven channel fuel tank test rig.....</i>	<i>44</i>
3.4. THE EFFECT OF FILTER FREQUENCIES ON MODELLING AND SIMULATION RESULTS.....	47
3.4.1. <i>Normal modelling.....</i>	<i>48</i>
3.4.2. <i>The effect of bandwidth on simulation.....</i>	<i>50</i>
3.4.3. <i>Wide spectrum simulation.....</i>	<i>51</i>
3.5. CONCLUSION AND RECOMMENDATIONS FOR FURTHER RESEARCH - PART I.....	54
5.3. MODELLED NARX SYSTEMS .....	78
5.3.1. <i>Purely Quadratic NARX.....</i>	<i>78</i>
5.3.2. <i>Quasi-Static NARX.....</i>	<i>79</i>
5.3.3. <i>Split spectra linear-non-linear modelling.....</i>	<i>80</i>
5.3.4. <i>Non-linear error signal modelling.....</i>	<i>81</i>
5.6. SYSTEMIC NON-LINEAR SYSTEMS .....	82
5.6.1. <i>State space modelling of nonlinear systems.....</i>	<i>82</i>
5.6.2. <i>Random non-linear input/output data.....</i>	<i>83</i>
5.7. ERROR FUNCTIONS .....	84
5.8. DETECTING NON-LINEARITY .....	85
<b>CHAPTER 6</b>	
<b>APPLICATION OF NON-LINEAR SYSTEM IDENTIFICATION .....</b>	<b>86</b>
6.1. CASE STUDY 1: NON-LINEAR ELASTOMERIC DAMPER .....	89
6.1.1. <i>Reconstruction of elastomeric damper field load response.....</i>	<i>89</i>
6.1.2. <i>Non-linear error signal modelling of an elastomeric damper.....</i>	<i>90</i>
6.2. CASE STUDY 2: PNEUMATIC INDEPENDENT TRAILER SUSPENSION.....	93
6.3. CASE STUDY 3: LIGHT TRUCK FRONT SUSPENSION.....	97

<b>PART II: INVESTIGATION INTO THE POSSIBLE IMPLEMENTATION OF NON-LINEAR RESPONSE RECONSTRUCTION .....</b>	<b>56</b>
<b>CHAPTER 4</b>	
<b>LINEAR TIME DOMAIN SYSTEM IDENTIFICATION: ARX.....</b>	<b>57</b>
4.1. ARX MODEL STRUCTURE.....	58
4.2. ARX STRUCTURE SELECTION.....	61
<b>CHAPTER 5</b>	
<b>NON-LINEAR TIME DOMAIN SYSTEM IDENTIFICATION: NARX .....</b>	<b>62</b>
5.1. THE NARX MODEL.....	63
5.1.1. MISO-NARX formulation.....	63
5.1.2. Non-linearity in the NARX model.....	65
5.1.3. Coefficients in the NARX model.....	67
5.2. NARX REGRESSION .....	68
5.3. NARX PARAMETER ESTIMATION .....	69
5.3.1. The least squares problem .....	70
5.3.2. Full vs. reduced parameter modelling .....	73
5.4. SIMULATION OF NARX SYSTEMS .....	74
5.4.1. Condensed NARX model structure.....	75
5.5. MODIFIED NARX SYSTEMS.....	78
5.5.1. Purely Quadratic NARX.....	78
5.5.2. Quasi-Static NARX.....	79
5.5.3. Split spectra linear-non-linear modelling.....	80
5.5.4. Non-linear error signal modelling.....	81
5.6. SYNTHETIC NON-LINEAR SYSTEMS .....	82
5.6.1. State space modelling of non-linear systems .....	82
5.6.2. Random non-linear input/output data.....	83
5.7. ERROR FUNCTIONS .....	84
5.8. DETECTING NON-LINEARITY .....	85
<b>CHAPTER 6</b>	
<b>APPLICATION OF NON-LINEAR SYSTEM IDENTIFICATION .....</b>	<b>86</b>
6.1. CASE STUDY 1: NON-LINEAR ELASTOMERIC DAMPER .....	87
6.1.1. Reconstruction of elastomeric damper field load response .....	88
6.1.2. Non-linear error signal modelling of an elastomeric damper .....	90
6.2. CASE STUDY 2: PNEUMATIC INDEPENDENT TRAILER SUSPENSION .....	93
6.3. CASE STUDY 3: LIGHT TRUCK FRONT SUSPENSION.....	97

6.3.1.	<i>Light truck suspension: Wheel <math>\Rightarrow</math> upper ball joint forces</i> .....	98
6.3.2.	<i>Light truck suspension: Wheel <math>\Rightarrow</math> ball joints</i> .....	101
6.4.	CASE STUDY 4: RADIATOR TEST RIG .....	105
6.4.1.	<i>Reconstruction of radiator top tank field acceleration response</i> .....	106
6.4.2.	<i>Radiator sine sweep tests</i> .....	108
6.5.	CASE STUDY 5: VEHICLE DAMPER TEST RIG.....	111
<b>CHAPTER 7</b> <i>Modified Gram Schmidt</i> .....		145
<b>CONCLUSIONS AND RECOMMENDATIONS FOR FURTHER RESEARCH - PART II</b> .....		113
7.1.	NON-LINEAR SYSTEM IDENTIFICATION: THE CONDENSED NARX MODEL FORMULATION.....	114
7.2.	NARX AS A GENERAL NON-LINEAR MODELLING TOOL.....	114
7.3.	NARX STRUCTURAL RESPONSE RECONSTRUCTION .....	115
7.4.	RECOMMENDATIONS FOR FURTHER RESEARCH .....	116
7.4.1.	<i>Alternative non-linear modelling capabilities</i> .....	116
7.4.2.	<i>Non-square modelling and simulation</i> .....	116
7.4.3.	<i>Modified NARX model structures</i> .....	117
<b>REFERENCES</b> .....		118
<b>APPENDIX A</b>		
<b>SURVEY OF NON-LINEAR SYSTEM IDENTIFICATION MODELS</b> .....		124
A.1.	FUNCTIONAL SERIES METHODS .....	124
A.1.1.	<i>Weiner methods</i> .....	125
A.1.2.	<i>Volterra-series methods</i> .....	125
A.2.	BLOCK-ORIENTATED SYSTEMS .....	126
A.3.	INPUT - OUTPUT MODEL DESCRIPTIONS .....	127
A.3.1.	<i>The NARMAX model</i> .....	127
A.3.2.	<i>Bilinear model</i> .....	128
A.3.3.	<i>Output-Affine and rational models</i> .....	129
A.3.4.	<i>The NARX-model</i> .....	129
<b>APPENDIX B</b>		
<b>NARX REGRESSION TECHNIQUES</b> .....		130
B.1.	GENERAL SAMPLE POINT LOOP APPROACH .....	130
B.2.	COLUMN-WISE LINEAR REGRESSION OF THE NARX DIFFERENCE EQUATION .....	132
B.3.	NON-LINEAR REGRESSION.....	132
B.3.1.	<i>Loop methods:</i> .....	133
B.3.2.	<i>Matrix manipulation methods</i> .....	133
B.3.3.	<i>Indexed matrix manipulation methods</i> .....	135



**APPENDIX C**

<b>NARX PARAMETER ESTIMATION: FULL PARAMETER SET SOLUTIONS.....</b>	<b>137</b>
C.1. SOLVING THE NORMAL LEAST SQUARES EQUATION .....	137
C.2. SINGULAR VALUE DECOMPOSITION .....	140
C.3. ORTHOGONAL DECOMPOSITION .....	141
C.3.1. <i>Gram Schmidt</i> .....	143
C.3.2. <i>Modified Gram Schmidt</i> .....	145
C.3.3. <i>Householder</i> .....	148

**APPENDIX D**

<b>NARX PARAMETER ESTIMATION: REDUCED PARAMETER SET SOLUTIONS .....</b>	<b>150</b>
---	------------

**APPENDIX E**

<b>POLYNOMIAL EXPANSION OF EXAMPLE 5.1.....</b>	<b>152</b>
---	------------

**APPENDIX F**

<b>SUMMARY OF FUNCTIONS .....</b>	<b>153</b>
-----------------------------------	------------

**APPENDIX G**

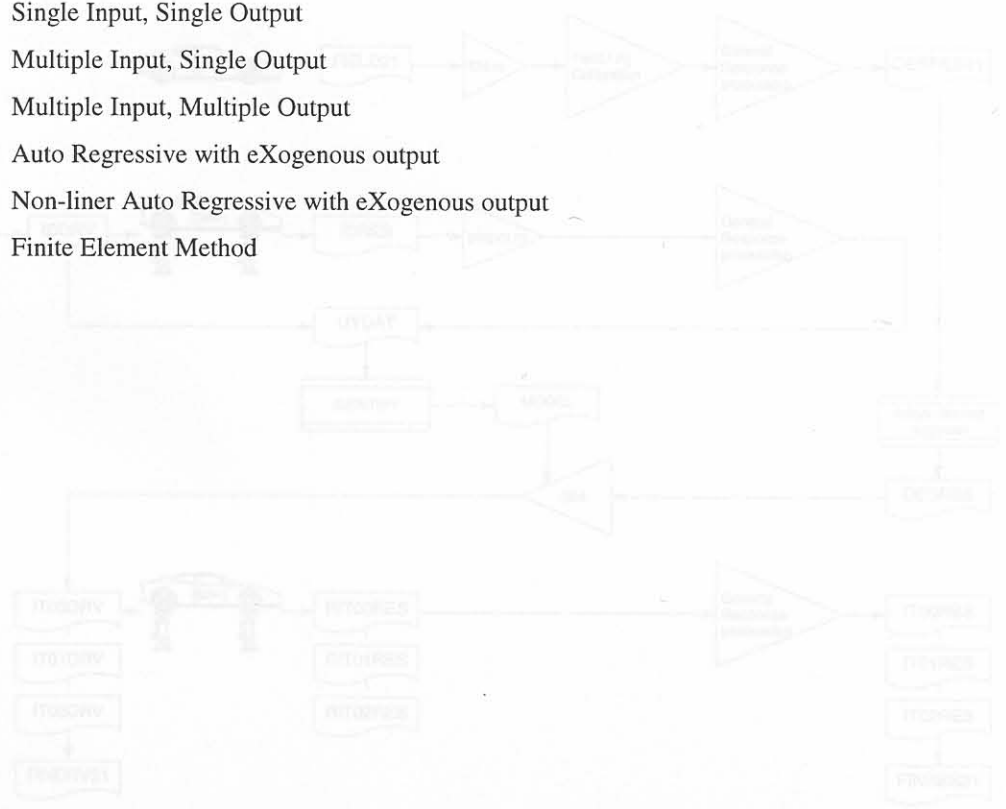
<b>QANTIM: A PRACTICAL SOLUTION TO RESPONSE RECONSTRUCTION .....</b>	<b>154</b>
--	------------

<i>SISO</i>	<i>Single Input, Single Output</i>
<i>MISO</i>	<i>Multiple Input, Single Output</i>
<i>MIMO</i>	<i>Multiple Input, Multiple Output</i>
<i>ARX</i>	<i>Auto Regressive with eXogenous output</i>
<i>NARX</i>	<i>Non-linear Auto Regressive with eXogenous output</i>
<i>FEM</i>	<i>Finite Element Method</i>



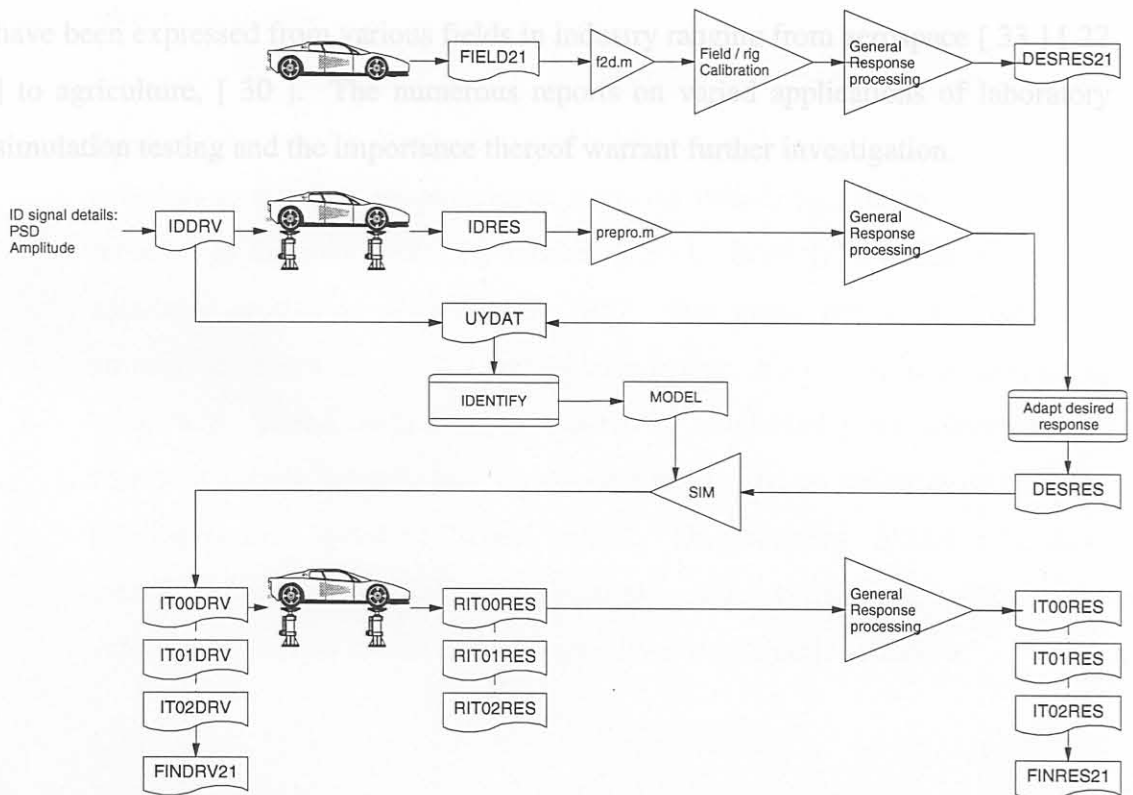
# Nomenclature

$t$	Time
$u(t)$	Dynamic input signal
$y(t)$	Dynamic response signal
$\hat{y}(t)$	Predicted dynamic response signal
$e(t)$	Error signal
$X$	Regression matrix
$\Theta, a, b, p$	Model parameters
$m$	Number of model parameters
$na$	Dynamic model order for output $y(t)$
$nb$	Dynamic model order for input $u(t)$
$nk$	Time delay
$n_k$	Model order for output channel $k$ (ARX "full order")
$nu$	Number of input channels
$ny$	Number of output channels
$L$	Degree of non-linearity
$PSD$	Power spectral density
$SISO$	Single Input, Single Output
$MISO$	Multiple Input, Single Output
$MIMO$	Multiple Input, Multiple Output
$ARX$	Auto Regressive with eXogenous output
$NARX$	Non-linear Auto Regressive with eXogenous output
$FEM$	Finite Element Method



A standard set of terminology exists within the QanTiM test and simulation software package. Terminology regarding time history data sets and data processing will, where possible, follow the standards set within QanTiM. Standard file names and processes are presented below, together with a simplified diagram of the QanTiM simulation process.

- IDDRV* Identification drive time history data
- IDRES* Identification response time history data
- FIELD* Measured field response time history data. During simulation, an identifying number is usually appended to the file name, e.g. FIELD21. This number is applied to all subsequent files that relate to this field file
- DESRES* Desired response time history data (DESR21)
- RITRES* 'Raw' iteration response file. Normally used as RIT01RES where the number 01 indicates the first iteration
- ITRES* Iteration response file, subsequent to general response processing (IT01RES)
- FINDRV* Final drive time history data, for use in laboratory simulation (FINDRV21)
- FINRES* Final response time history data, as measured during laboratory simulation (FINRES21)
- F2D* FIELD to DESRES - User definable function for processing field data
- PREPRO* User definable function to pre-process IDRES prior to inclusion into UYDAT
- GPREPRO* General response pre-processing function, applies bandwidth filtering, de-trending
- UYDAT* Combined IDDRV and IDRES, subsequent to processing by PREPRO and GPREPRO



# Chapter 1

## Introduction

Mechanical design engineers are being presented with ever more powerful and capable analytical design tools. This is principally driven by continuous improvement in the price-performance ratio of digital computer systems and the strive for optimised designs with lower safety factors and increased reliability. The competitive market of today however demands these optimised designs to be backed by extensive product development and testing. Lund and Donaldson [ 42 ] recognised the important role of testing in design, especially laboratory testing of full scale prototypes or components. The same authors stated: "The most rapid advances in testing technology in recent years have occurred in the area of service history simulation." The importance of this ability to reproduce actual measured service conditions in a controlled laboratory environment is further stressed by Zomotor, Schwarz and Weiler [ 63 ] for evaluating passenger car ride comfort and fatigue strength of vehicle components. Similar views have been expressed from various fields in industry ranging from aerospace [ 33 ] [ 27 ] to agriculture, [ 30 ]. The numerous reports on varied applications of laboratory simulation testing and the importance thereof warrant further investigation.



## 1.1. Overview

Dynamic response reconstruction, also termed service load simulation testing, or service history simulation [ 42 ], enables the replication of actual service response data on a dynamically loaded test structure in a laboratory environment using multiple axis computer controlled servo-hydraulic actuators. Service load simulation testing offers the only method of reliably conducting interactive multiple-axial fatigue tests.

This thesis forms part of a research programme to further improve a time domain service load simulation system developed by Raath [ 52 ] and implemented into a multi-axis test and control package (QanTiM) [ 34 ]. Two global aspects are addressed, firstly the effect of varying input parameters and operating procedures for the existing linear techniques, and secondly the inclusion of non-linear modelling elements within the existing linear package.

## 1.2. Historical profile

The field of simulation testing is relatively new, driven mostly by the automotive industry since the early 1960's. The use of servo-hydraulic actuators to simulate dynamic input loads for vehicle suspension systems was reported in the mid 1960's by Hodkin [ 31 ]. Scott [ 57 ] reported a road simulator erected in Coventry in 1967 that made use of an open-loop simulation system similar to a gramophone player. A six-foot diameter rotating table was "paved with bits of shattered, toughened-glass windshield to represent cobble stones", four transducers positioned on radial arms over the rotating surface measured "wheel inputs". Displacements recorded by these transducers were amplified by an electronic control system and applied to the vehicle's wheels by means of four vertical servo-hydraulic actuators.



A positive step towards simulation was reported in 1968 by Barrowcliff and Ehlert [ 3 ] in the paper: "Full Scale Road Simulated Endurance Test". The authors recorded the vehicle's wheel acceleration responses during normal driving conditions. In the laboratory these measured accelerations were integrated twice to obtain displacement drive signals for the servo-hydraulic actuators of the road simulator. A more direct method for finding displacement drive signals for road simulators involved road profile measurements, typical examples were documented by Engels [ 25 ] and Whittemore [ 62 ]. The geodetic road profile measurement apparatus presented in 1968 by Engels proved accurate, but extremely time consuming. The "General Motors Road Profilometer" as presented by Whittemore in 1972 measured the relative displacement between the road surface and the moving vehicle. These dynamic displacement responses were used, along with an analytical model of the vehicle, to calculate drive signals for a servo-hydraulic road simulator.

In 1972 Dodds [ 23 ] proposed a technique in which a dynamic mathematical model of the test system (test specimen and rig) is used to calculate actuator drive signals from service measured responses. Dodds made use of frequency domain characterisation techniques to derive a Frequency Response Function (FRF) of the test system. This model was capable of predicting actuator displacements as a function of measured road responses [ 21 ][ 22 ]. This frequency domain analysis, later also proposed by Craig [ 19 ], paved the way for development of advanced service load simulation systems such as the "Remote Parameter Control" (RPC) by MTS Systems Corporation (USA) and the "Iterative Transfer Function Compensation" (ITFC) method by Schenck AG (Germany). These systems set the standard for simulation testing and are employed world-wide in various sectors of industry.

A recent development in simulation testing was introduced in the PhD dissertation by Raath [ 52 ] in 1992 titled "Structural Dynamic Response Reconstruction in the Time Domain". This method was implemented into the QanTiM [ 34 ] multi-axis time domain based test and control package. The

time domain promises various advantages over the frequency domain techniques, which will be briefly discussed in Section 1.4, yet the principal operation proved similar to that of methods developed in the frequency domain. This basic operation and philosophy is discussed in the next Section.

### 1.3. Principles of structural dynamic response reconstruction

Over the past two and a half decades the accuracy of simulations has improved greatly due to the use of closed loop computer controlled simulation systems and an understanding of the dynamic relationship between the actuator input and the response transducer output signals [ 23 ][ 19 ][ 51 ]. Present response reconstruction techniques are generally governed by the following four steps.

- 1 Measurement:** The structure to be tested is instrumented with suitable transducers, and the response under operational conditions recorded.
- 2 Identification:** The instrumented structure is transferred to the test laboratory and placed on a servo-hydraulic test rig. Synthetic drive signals are used to drive the rig and subsequent responses are recorded from the same transducers used for the operational response measurement. The known input-output data is used to calculate a dynamic model for the complete system. ( i.e. rig, controllers, test structure, etc.)
- 3 Linear drive :** The measured field responses are passed through the dynamic model to find actuator drive signals, which when applied to the test rig should force the same measured responses.
- 4 Iteration:** Due to inherent rig non-linearity, an iterative procedure around this first approximation finally yields accurate simulation results.

#### 1.4. Frequency vs. time domain

The operation of systems in the frequency and time domain is, from a user point of view, very similar. The frequency domain however boasts a set of well-developed modelling techniques applicable to dynamic response reconstruction. This poses the question why a time domain simulation system was developed considering the long standing standards set by its frequency domain counterparts? Various discussions on the advantages, and disadvantages, of time domain modelling are found [ 28 ][ 49 ], most relevant is the one presented by Raath [ 52 ].

In general it has been shown that the newly developed time domain techniques have some principal advantages over its frequency domain predecessors. These advantages include shorter identification time [ 28 ], fewer iterations to convergence and, more important, the time domain techniques are capable of handling offsets and low frequency trends with ease. Frequency domain methods on the other hand have difficulty simulating offsets, and low frequency, high amplitude behaviour of the test specimen. Offsets in the desired response data coincide with non-zero mean structural stresses, whereas low frequency, high amplitude loading causes high peak stress levels within the structure. Inaccurate simulation of these mean stresses and low frequency, high amplitude stress conditions is detrimental from a fatigue analysis point of view. On the other hand, the main disadvantage of the time domain is the requirement of having to specify the structure and order of the dynamic system prior to the identification process. This problem has been overcome by using a generalised parametric time domain model description combined with a state-space formulation.



### 1.5. Dynamic system identification

The identification, more correctly, dynamic system identification, is the most significant phase within the response reconstruction framework. It is the platform on which response reconstruction techniques have been built and facilitated the quantum leap from the open loop gramophone system to present-day sophisticated commercial simulation systems. Dynamic system identification involves constructing a mathematical model of a dynamic system using measured input and output data from the system. System identification has found application in an extremely wide field covering engineering, socio-economics, ecology and medicine, to name but a few.

### 1.6. The inverse dynamic model

Most applications of dynamic system identification are conducted so that the system outputs are modelled as a function of the system inputs. An inverse dynamic model is however a requisite for response reconstruction. Here the system inputs (actuator drive signals) must be dynamically modelled as a function of system outputs (transducer responses from field measurements). Inversion of the dynamic model is however not trivial since the inverse model is frequently found to be unstable. Various inversion methods are presented for both the frequency and time domain [ 23 ][ 19 ][ 34 ][ 51 ].



### 1.7. Operational research into time domain application

Frequency domain methods have been in use and under development for more than two decades. In this period a wealth of knowledge and experience has been gained from its use on many service load simulation test rigs throughout the world. On the other hand, the time domain state space methods to date not have had this exposure simply because of its recent development.

Because of the limited application experience of time domain methods, operating procedures and optimisation of input parameters for the existing linear QanTiM system were researched empirically using various practical single and multiple-axis test rigs. The first aspect investigated was the effect of various band limiting filter operations on simulation results. This was followed by research into the optimal frequency content of the synthetic identification excitation signals. The concept of split spectra modelling was also investigated, where the broad spectrum dynamic behaviour of the system is split and modelled by a combination of narrow frequency bandwidth time domain models.

The experience gained during this research paved the way for further experiments and produced a set of guidelines for the practical implementation of QanTiM for various test systems. These guidelines include filter specifications for desired response data as well as synthetic identification data. Guidelines for creating optimal synthetic identification signals have proved valuable in multiple-axis test applications. Similarly split spectra modelling showed potential in rigs with dominant resonant behaviour.

A literature survey revealed various non-linear modelling techniques which showed potential for implementation into dynamic response reconstruction. Several of these methods were implemented, and in certain cases adapted by the author. The applied system identification techniques were verified through

## 1.8. Non-linear implementation

The linear time domain QanTiM techniques proved successful in simulating the dynamic response of most practical test systems. In a few isolated cases however the response of a system could not be simulated. Various possible reasons for poor simulation results were suggested including, static and dynamic non-linear system elements, rig resonance problems, numerical instability due to model inversion, orthogonal load paths between actuators and transducers, physically unrealisable response data (PUD), poor rig coherence, etc. Non-linear elements within the test system (springs, dampers, friction, servo-hydraulics, etc.) may be a likely cause of poor modelling and simulation results.

It was thus proposed to complement the linear time domain techniques by implementing non-linear modelling capabilities within the existing time domain techniques. A non-linear system identification technique well suited to response reconstruction, yet capable of seamless integration with the existing linear package was needed. An emphasis was placed on finding a black-box type model which is easy to use and requires minimal structure definition prior to identification.

The field of non-linear system identification, although relatively new, has been well researched, especially under the guidance of Billings [ 5 ][ 6 ][ 7 ][ 8 ] [ 14 ][ 38 ]. Yet a coherent body of economical, well tried and widely applicable non-linear identification techniques does not exist. Furthermore, to the author's knowledge no attempt has been made at identifying a non-linear inverse model, as required by response reconstruction.

A literature survey revealed various non-linear modelling techniques which showed potential for implementation into dynamic response reconstruction. Several of these methods were implemented, and in certain cases adapted by the author. The applied system identification techniques were verified through

testing, firstly in a normal sense to evaluate non-linear modelling capabilities and secondly for application in response reconstruction where an inverse model was required. This process showed a group of polynomial non-linear autoregressive exogenous input (NARX) model formulations as presented by Billings [ 5 ] to be ideally suited. The author subsequently developed non-linear simulation algorithms and an associated condensed non-linear model description for multiple-input-multiple-output (MIMO) systems.

The result was a set of system identification routines capable of modelling severely non-linear dynamic systems, and yet requiring minimal user input or knowledge of the system. However, the non-linear structure (that is linear, quadratic, cubic, etc.) within the system must be estimated prior to identification. The developed NARX routines are capable of both normal, and inverse dynamic non-linear modelling. Evaluation of the NARX system is presented for both synthetic and practical systems, revealing certain limitations:

- No procedure capable of practically detecting non-linearity within a servo-hydraulic test system could be found. The only indication of non-linear behaviour was thus a comparison of linear and non-linear simulation results.
- In the case of large MIMO systems the algorithms proved taxing for current computational capabilities.
- Application proved limited since the implemented non-linear algorithms showed some inherent stability problems, which were accentuated in the inverse model.
- Polynomial non-linear techniques proved ideal to facilitate ease of use and convenient integration with existing software, but may not be completely relevant for modelling vehicle dynamics. (A typical suspension element such as a jounce bump can only be modelled using a discontinuous non-linear technique.)

The NARX formulation showed potential as a general modelling and simulation tool, especially if combined with frequency splitting techniques.



## Chapter 2

### 1.9. Document overview

Only the most relevant theory is included in the body of the thesis, with more detail contained in the appendices. The thesis is presented in two parts, the first part covering empirical research into improved response reconstruction. Aspects such as rig repeatability, simulation bandwidth and split spectra modelling are introduced. The investigation into application of non-linear time domain techniques is presented in part two. As part of the literature survey, system identification theory is introduced in chapter 4 for linear systems, and expanded to non-linear systems in chapter 5. Chapter 6 shows various case studies of implementation of non-linear techniques. Appendices A through D contains the detail of the literature survey as presented in chapters 4 and 5. A summary of condensed NARX Matlab 'toolbox' of functions is presented in Appendix F. A brief description of QanTiM is presented in Appendix G.



## Chapter 2

### 2.1. Typical simulation

### Research task

The state-space time domain computation technique proved effective in modelling and subsequently simulating service responses for most structural systems. Application experience with the recently developed QanTiM time domain based simulation package is limited if compared with its frequency domain counterparts. Considering a development span of less than half a decade, the achievements in the field of time domain based service load simulation is most definitely laudable, yet little has been published on the industrial application thereof. This is simply due to the very recent development of time domain simulation techniques. On the other hand, for more than two decades operational experience using frequency domain simulation techniques have been documented and published by both users and manufactures of these systems. [ 63 ][ 25 ][ 19 ][ 20 ]. RPC and ITFC user group meetings, of typically 100 delegates, where application experience is shared amongst other users are not uncommon. It was thus proposed to embark on a research program that would attempt to improve the general application of the QanTiM system and partly alleviate this information backlog. The research was aimed directly at improving the existing QanTiM package and will regularly refer to associated aspects. Details on the functioning and operation of QanTiM are presented in Appendix G.

Most of these problems are simply due to limited experience in time domain modelling, more specifically, a lack of knowledge on input parameters and operating procedures for QanTiM. Possible causes and solutions to these problems were sought and are presented in the following sections.

## 2.1. Typical simulation problems

The state-space time domain compensation technique proved effective in modelling and subsequently simulating service responses for most structural test rigs [ 45 ][ 50 ][ 61 ]. There are however rigs for which a good dynamic model could not be found, resulting in poor simulation results. Typical examples of simulation problems include:

- Difficulty in recreating high response amplitudes.
- Inaccurate simulation of high frequency responses.
- A large number of iterations is required before accurate simulation results are achieved.
- Failure of iterations to converge to desired response.
- Divergent linear solutions.
- Difficulty in handling structural resonance within the normal operating spectrum,
- and in extreme cases a general inability to model the dynamic behaviour of the system.

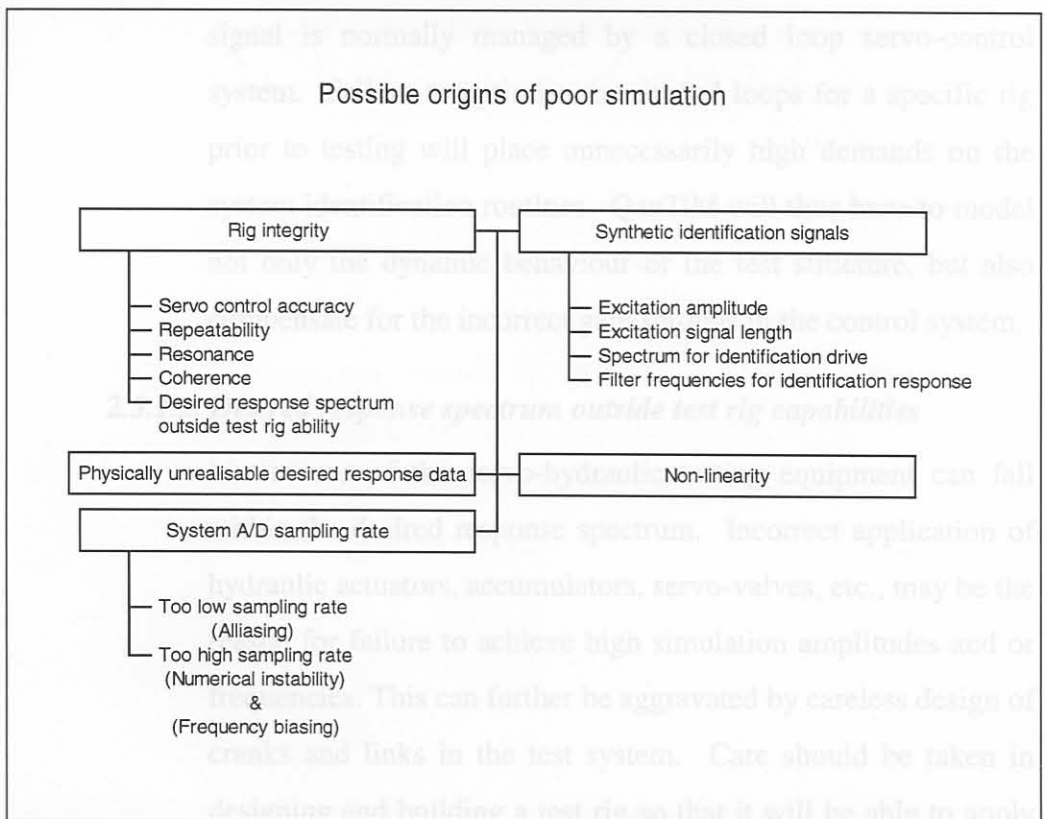
Most of these problems are simply due to limited experience in time domain modelling, more specifically, a lack of knowledge on input parameters and operating procedures for QanTiM. Possible causes and solutions to these problems were sought and are presented in the following Sections.

Figure 2.1: Possible causes of inaccurate simulation

The origins of poor simulation as suggested in Figure 2.1 were derived from practical experience on various single and multi-axial servo-hydraulic test rigs. Although not all of these problems are addressed in this study, proposed research as to their solutions are detailed in Section 2.3.

## 2.2. Origins of poor simulation

The success of system identification for response reconstruction, or more specifically QanTiM, is to a certain extent governed by user definable input parameters. There are unfortunately also parameters that are rig specific and can not easily be modified by the system identification engineer. On the other hand, certain test rig integrity factors such as servo-control accuracy, mechanical backlash in links, incorrect instrumentation settings, etc. are usually easy to trace and rectify, but often confused for modelling problems. Some of the aspects that could adversely affect simulation results are presented in Figure 2.1.



**Figure 2.1: Possible causes of inaccurate simulation**

The origins of poor simulation as suggested in Figure 2.1 were derived from practical experience on various single and multi-axial servo-hydraulic test rigs. Although not all of these problems are addressed in this study, proposed research as to their solutions are detailed in Section 2.3.



## 2.3. Proposed investigation for improved time domain simulation

The reasons for poor simulation are discussed and where applicable, a line of research into the improvement thereof suggested. The framework presented in Figure 2.1 is maintained for this discussion.

### 2.3.1. Test rig integrity

Poor modelling and simulation are often related to problems concerning the test rig configuration. The most obvious problem, servo-control loop accuracy, is normally easy to rectify. More intricate problems include poor coherence, non-repeatable rig behaviour, etc.

#### 2.3.1.1. Servo-control accuracy

The accuracy with which the actuator can maintain a drive signal is normally managed by a closed loop servo-control system. Failure to optimise the control loops for a specific rig prior to testing will place unnecessarily high demands on the system identification routines. QanTiM will thus have to model not only the dynamic behaviour of the test structure, but also compensate for the incorrect gain settings in the control system.

#### 2.3.1.2. Desired response spectrum outside test rig capabilities

Limitations of the servo-hydraulic testing equipment can fall within the desired response spectrum. Incorrect application of hydraulic actuators, accumulators, servo-valves, etc., may be the reason for failure to achieve high simulation amplitudes and or frequencies. This can further be aggravated by careless design of cranks and links in the test system. Care should be taken in designing and building a test rig so that it will be able to apply the required loading.

### 2.3.1.3. *Repeatability*

The time domain modelling routines within QanTiM are not capable of describing, chaotic or stochastic system behaviour. It was thus proposed to develop a method of quantifying rig repeatability prior to system identification. A scheme for finding a repeatability number applicable to response reconstruction with servo-hydraulic test rigs is presented in Section 3.1.

### 2.3.1.4. *Resonance*

QanTiM has difficulty in simulating data over areas of system resonance [ 15 ][ 45 ]. If the resonance is rig related, that is a function of the rig fixtures, actuators, links, cranks, etc., a redesign of the rig is necessary. If however the test specimen shows resonant frequencies within the desired response data, careful modelling is needed to correctly simulate this behaviour. Two methods were proposed to deal with rig resonance namely: split spectra modelling (Section 3.2) and anti-resonance identification (Section 3.3) both these methods attempt to model only the forced response of the rig, thus ignoring the free, or resonant, system behaviour.

### 2.3.1.5. Coherence

Coherence describes the extent to which the system response is linearly related to the excitation [ 60 ]. A high level of coherence between a system's individual input - output pairs simplifies the modelling process. A good design policy implies designing test rigs in which each response transducer is closely correlated to its corresponding actuator. Coherence, as such, is fundamentally applicable to the frequency domain. Accurate coherence calculations are not possible using the short Sections of data common to time domain modelling. A time domain equivalent to coherence may shed some light on many modelling problems.

### 2.3.2. Physically unrealisable desired response data

For the purpose of service history simulation testing all desired response data should ideally be taken from field measurements done with the same test structure to be used in the laboratory, using exactly the same transducers. This implies that all data will be physically realisable. Some sort of signal processing will however invariably be performed on the field data prior to response reconstruction. This pre-processing of field data may include: low-pass filtering to remove system noise, de-glitching to remove spikes, scaling, removing of DC-offsets, etc. If care is not taken when pre-processing field data, the data could be modified to such an extent that it is no longer characteristic of the response of the system.



### 2.3.3. Analogue to digital conversion

Computer analysis of measured data invariably requires the use of some analogue to digital conversion system. This step from continuous to discrete time presents the test engineer yet another obstacle: the correct sampling rate. Selecting a too low sampling rate may result in aliasing, and an inaccurate representation of the system responses, which is particularly problematic for fatigue testing where accurate achievement of load cycle turning points is imperative. On the other hand, a too high sampling rate can have detrimental effects on the numerical stability of system identification algorithms. It is hypothesised that an optimum relationship exists between the system sampling rate, the simulation bandwidth and the dynamic model order.

### 2.3.4. Synthetic identification signals

Synthetic excitation signals are generated from a prescribed power spectral density (PSD) function and conceptually constitute pseudo random, shaped white noise. These signals are sent simultaneously to all actuators, thereby exciting the entire test rig, while at the same time recording the responses from the same transducers used during field measurements. This input - output data is then used to calculate a time domain model for the entire test system.

#### 2.3.4.1. Identification drive spectrum

The shape of the PSD function from which the identification drive signals are generated adversely influences the accuracy of the model. Investigation into an optimum excitation spectrum for a specific rig would prove of immense value. A method was devised to calculate an excitation PSD, which would minimise the effect of system resonance and optimise coherence for MIMO systems. This automatic PSD generation function is described in Section 3.3.

#### 2.3.4.2. Identification signal length

The length of the identification signal proved relatively insignificant to the simulation results. Identification signals in the region of 15 ~ 30 seconds are typically used. It is however proposed that an optimal signal length be calculated automatically. Such an optimal identification signal length is likely to be a function of the system sampling rate, the simulation bandwidth and the number of channels.

#### 2.3.4.3. Filter frequencies for identification responses

The identification response signal is invariably filtered in a pre-processing routine prior to system modelling. The effect of filtering and filter frequencies of the identification response signal is addressed in Section 3.4.

#### 2.3.5. Non-linear modelling capabilities

All commercially available response reconstruction packages, including QanTiM are limited to linear modelling techniques. The ability to model non-linear system behaviour could have a notable effect on accuracy and general applicability of the package. Non-linear behaviour in the system could be due to geometrical non-linearity, tyre characteristics, leaf springs, rubber and other synthetic elements, friction, backlash, etc. A comprehensive investigation into implementation of non-linear modelling techniques to complement the existing linear software package is included in Part II of this study.

## 2.4. Research summary

Simulation results are not always as accurate as desired, examples of typical simulation problems were presented, and possible solutions suggested. The research into implementation of these solutions can be divided into three categories:

1. Problems that can be solved by accurate engineering decisions concerning test rig design, servo-control accuracy, transducer type and placement, etc.
2. Problems to which solutions can be found empirically through research on various practical test rigs. These include identification parameters, pre-processing of desired response data, repeatability quantification and sampling rates for optimal numerical stability and modelling sensitivity.
3. Non-linear modelling: Investigation concerning the implementation and application of non-linear modelling capabilities within the existing system.

Not all the solutions suggested in Section 2.3 are addressed in this thesis. The issues, which are addressed, correspond to Categories 2 and 3 above, and are discussed according to Table 2.1.

**Table 2.1: Research summary**

PART I Empirical research for improved linear simulation		PART II Investigation into the possible implementation of non-linear response reconstruction	
	Section:		Chapter:
Repeatability quantification	3.1	Linear background	4
Split spectra modelling	3.2	Non-linear system identification	5
Optimal identification drive	3.3	Application of non-linear system identification and response reconstruction	6
Pre-processing of identification data. (filtering, de-trending, etc.)	3.4		



## Chapter 3

## Empirical research into improved linear simulation

## PART I: Empirical research into improved linear simulation

Due to the relatively short development span of time domain simulation techniques, in particular the Q-ETM software suite, a large amount of empirical research is needed to offset the resultant lack of application expertise and simulation experience. This lack of application experience is presently a handicap, considering that frequency domain simulation techniques can boast with decades of experience and applications at major testing installations worldwide. The work presented in this Section attempts to clarify some of the uncertainties surrounding time domain simulation, more specifically it addresses input parameters to, and general simulation techniques for, improved time domain response reconstruction. Section 3.1 introduces a procedure to quantify a test rig's input - output repeatability. To the author's knowledge, these repeatability functions are novel. Split-spectra modelling and simulation techniques are introduced in Section 3.2. These functions were developed over a time span of years at LCH Structural Mechanics and Dynamics, by amongst others, the author. Optimal excitation characteristics are briefly discussed in Section 3.3. The procedures developed by the author are based on principles introduced by Barnard [ 2 ]. Some of the effects of filter frequencies and bandwidth selections on simulation and modelling results are discussed in Section 3.4. Part I is concluded in Section 3.5 with recommendations for future research.

## Chapter 3

### Empirical research into improved linear simulation

The most fundamental assumption made prior to modelling and simulating field responses on a test rig is dynamic input-output repeatability. The linear

Due to the relatively short development span of time domain simulation techniques, in particular the QanTiM software suite, a large research effort was engaged to alleviate the resultant lack of application expertise and simulation experience. This lack of application experience is presently a handicap, considering that frequency domain simulation techniques can boast with decades of experience and applications at major testing installations worldwide. The work presented in this Section attempts to clarify some of the uncertainties surrounding time domain simulation, more specifically it addresses input parameters to, and general simulation techniques for, improved time domain response reconstruction. Section 3.1 introduces a procedure to quantify a test rig's input – output repeatability. To the author's knowledge, these repeatability functions are novel. Split-spectra modelling and simulation techniques are introduced in Section 3.2. These functions were developed over a time span of years at LGI Structural Mechanics and Dynamics, by amongst others, the author. Optimal excitation characteristics are briefly discussed in Section 3.3. The procedures developed by the author are based on principles introduced by Barnard [ 2 ]. Some of the effects of filter frequencies and bandwidth selections on simulation and modelling results are discussed in Section 3.4. Part I is concluded in Section 3.5 with recommendations for future research.

The performance of the proposed repeatability functions is demonstrated at the hand of four application examples, namely:

- Electro-dynamic linear actuator with an accelerometer mounted directly on the output shaft.
- Vehicle dragger unit in a servo hydraulic test rig
- Motorcycle rear wheel road simulator
- Radiator vibration test rig

### 3.1. Rig repeatability

The most fundamental assumption made prior to modelling and simulating field responses on a test rig, is dynamic input-output repeatability. The linear system identification techniques used within QanTiM are not capable of modelling chaotic or stochastic rig behaviour. It is thus important for the simulation engineer to evaluate rig repeatability prior to modelling and simulation. Two methods are proposed, the first deals with repeatability as a function of excitation frequency, the second attempts to calculate a general repeatability number (scalar).

The test, described in Figure 3.1 makes use of random drive signals created with a prescribed PSD function. The rig is driven five times with the same drive signal while subsequent responses are recorded. A mean response is then calculated from the five response signals. The frequency related repeatability number  $R_f$  is defined so that perfect repeatability is achieved at  $R_f = 100$ . The repeatability vs. frequency plot is useful to identify frequencies that should be avoided while modelling. The repeatability number should provide the engineer with a quick indication of the system's repeatability, and subsequently modelability.

The performance of the proposed repeatability functions is demonstrated at the hand of four application examples, namely:

- Electro-dynamic linear actuator with an accelerometer mounted directly on the output shaft.
- Vehicle damper unit in a servo hydraulic test rig
- Motorcycle rear wheel road simulator
- Radiator vibration test rig



## 3.1.1. Repeatability function application II Electro-dynamic shaker

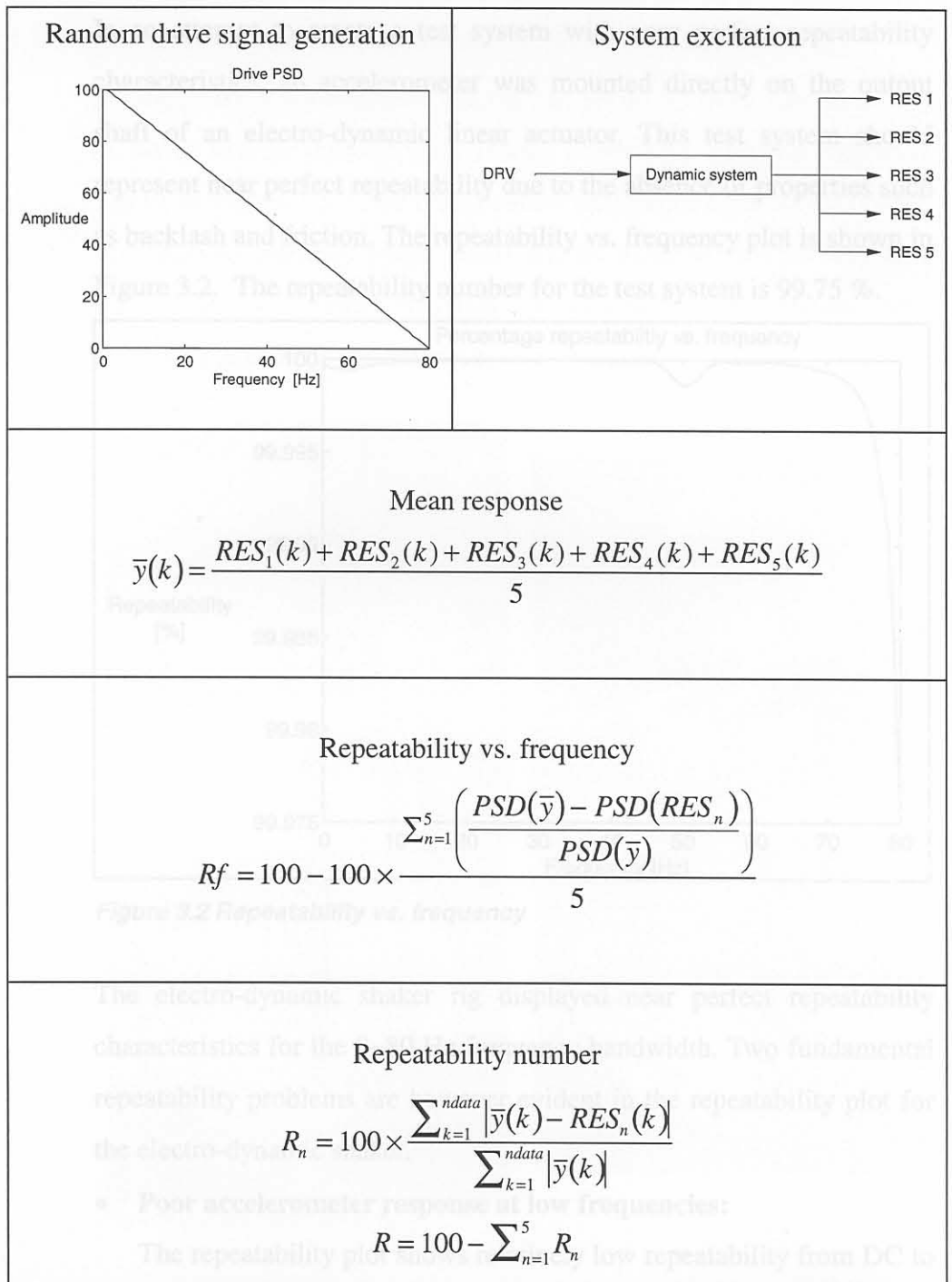
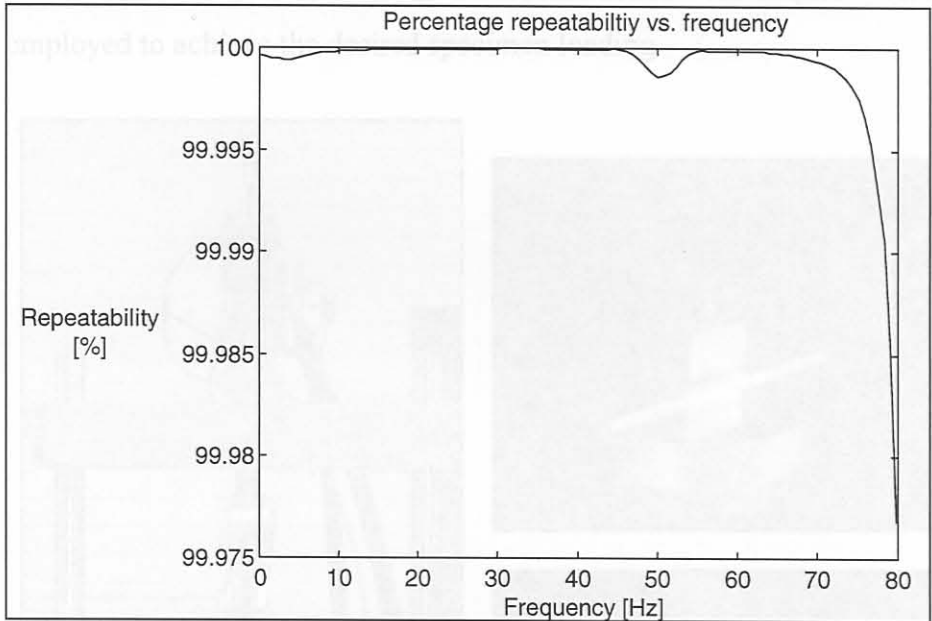


Figure 3.1: Repeatability test procedure

### 3.1.1. Repeatability function application 1: Electro-dynamic shaker

In an attempt to create a test system with near perfect repeatability characteristics, an accelerometer was mounted directly on the output shaft of an electro-dynamic linear actuator. This test system should represent near perfect repeatability due to the absence of properties such as backlash and friction. The repeatability vs. frequency plot is shown in Figure 3.2. The repeatability number for the test system is 99.75 %.



**Figure 3.2 Repeatability vs. frequency**

The electro-dynamic shaker rig displayed near perfect repeatability characteristics for the 0~80 Hz frequency bandwidth. Two fundamental repeatability problems are however evident in the repeatability plot for the electro-dynamic shaker.

- **Poor accelerometer response at low frequencies:**

The repeatability plot shows relatively low repeatability from DC to 10 Hz. This can be attributed to transducer insensitivity at low frequencies.

- **Power line noise:**

The repeatability plot further shows a decline in the region of 50 Hz. This can be attributed the 50 Hz alternating current power supply.

### 3.1.2. Repeatability function application 2: Vehicle damper test rig

A single axis servo-hydraulic test rig was set up for qualification testing of heavy vehicle damper units (shock absorbers). The test system is shown in Figure 3.3. The qualification tests required accurate control of specimen loading, which could not be achieved by the analogue servo control system. Response reconstruction techniques were employed to achieve the desired specimen loading.

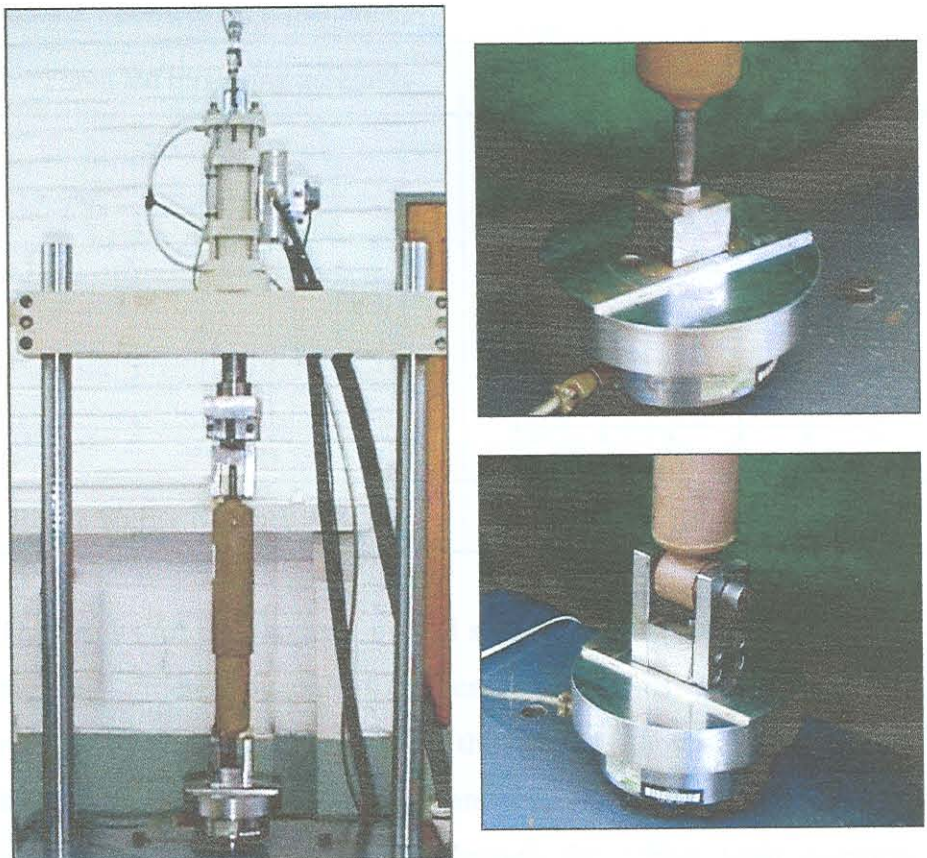


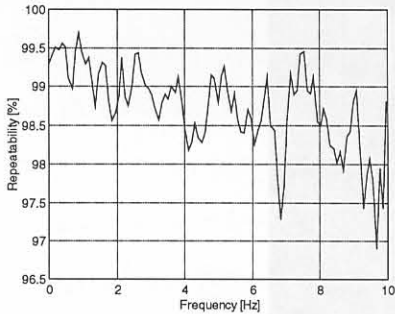
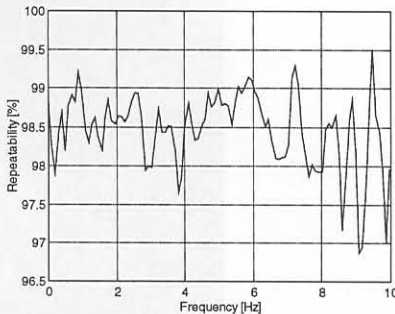
*Figure 3.3 Damper test rig*

Two damper attachment systems were used (Figure 3.3). The first made use of a threaded connector that rigidly locked the damper to the actuator shaft and the load cell. The second method attached the damper via two rubber bushes. This rubber bush mounting assembly resulted in mechanical play and backlash in the load path.



proposed that the backlash associated with the rubber mounting bushes might be the cause of the unsatisfactory simulation results. The repeatability for each of the two damper mounting methods was assessed with the defined repeatability functions. The damper qualification test prescribed a simulation bandwidth between 0 Hz and 10 Hz. Subsequently the repeatability drive file was randomly generated from 0 to 10 Hz, with a triangular PSD. The repeatability results are presented in Table 3.1 below.

**Table 3.1 Damper rig repeatability**

Threaded mounting assembly	Rubber bush mounting assembly
	
Repeatability Number = 98.49 %	Repeatability Number = 98.45%

The results for the two tests proved similar, the calculated repeatability numbers differed by only 0.04 percentage points. Furthermore, the repeatability vs. frequency plots for the two tests show similar trends for the 0Hz to 10 Hz simulation bandwidth. The repeatability results indicate that the load response through the rubber bush assembly, including the backlash behaviour, is indeed repeatable. These responses may however be non-linear. Non-linear modelling of the damper unit is presented in Part II of this thesis.

### 3.1.3. Repeatability function application 3: Motorcycle road simulator

A single axis test rig was set up to simulate road inputs to the rear suspension of a motorcycle. The test rig is shown in Figure 3.4. Input to the system was the actuator displacement drive signals, system responses were recorded from an accelerometer on the wheel spindle, and strain gauges applied to the coil spring.

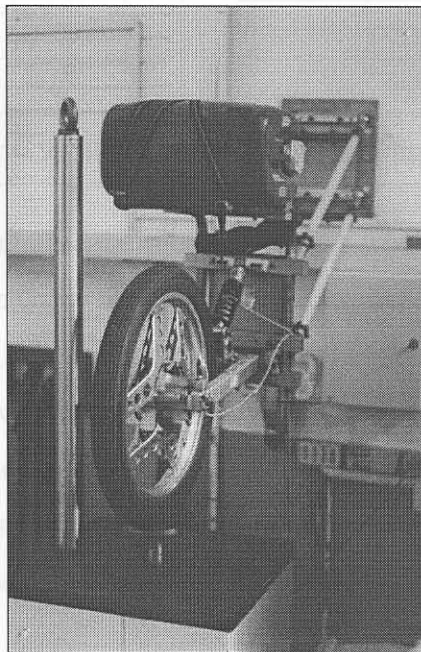


**Figure 3.4 Motorcycle rear wheel road simulator**

The repeatability drive file was created under a triangular PSD with a bandwidth of 0 Hz to 30 Hz. The repeatability results for the acceleration and strain responses are compared in Table 3.2.

The mounts were fitted to the rigid mounting frame. Play between the mounting pins and the rubber mounts allowed some free movement of the radiator, both vertically and horizontally.

Acceleration responses were recorded on the base of the mounting frame, and on the top tank of the radiator. The repeatability of the base and top tank accelerations are compared in Table 3.3 for a simulation bandwidth of 0 Hz to 25 Hz.

Table 3.2 Radiator test rig repeatability results

**Table 3.2 Motorcycle rear wheel simulator repeatability results**

Acceleration response	Strain response
Repeatability number = 97.80 %	Repeatability number = 98.15 %

The repeatability results for the motorcycle rear wheel road simulator show the distinct differences between the characteristics of acceleration and strain responses. Accelerometers, and acceleration as such, exhibit poor sensitivity at low frequencies. Strain responses on the other hand show good low frequency response, with less sensitivity at increasing frequencies. Poor sensitivity gives rise to poor signal to noise ratios and subsequently poor repeatability.

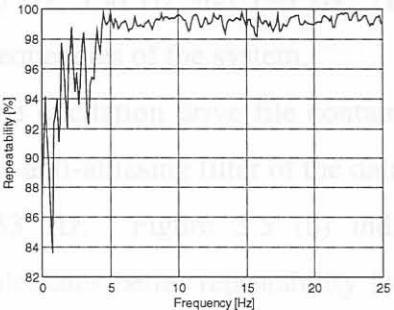
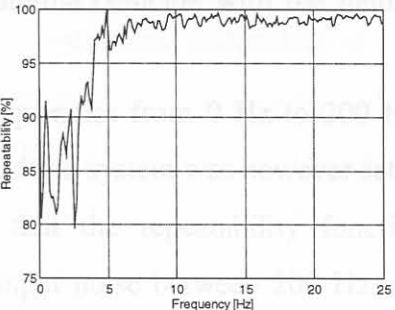
#### 3.1.4. Repeatability function application 4: Radiator test rig

Vibration tests were conducted on a vehicle radiator assembly. The test rig made use of a rigid mounting frame, installed vertically on a servo-hydraulic actuator. Mounting pins on the top and bottom radiator tanks fitted into doughnut shaped rubber mounts. These rubber mounts were fitted to the rigid mounting frame. Play between the mounting pins and the rubber mounts allowed some free movement of the radiator, both vertically and horizontally.

Acceleration responses were recorded on the base of the mounting frame, and on the top tank of the radiator. The repeatability of the base and top tank accelerations are compared in Table 3.3 for a simulation bandwidth of 0 Hz to 25 Hz.

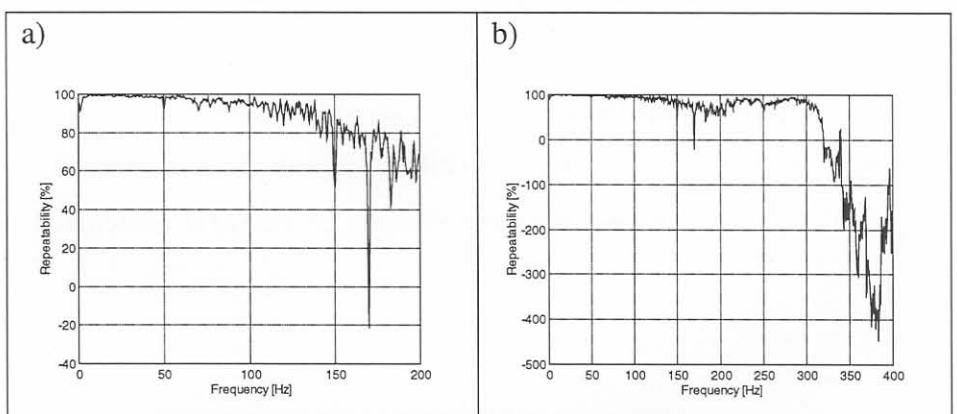


**Table 3.3 Radiator test rig repeatability results**

Mounting base acceleration	Radiator top tank acceleration
	
Repeatability number = 97.76 %	Repeatability number = 96.95 %

The repeatability results are similar for both transducer locations. The repeatability numbers differ with only 0.81 percentage points.

A second frequency related repeatability test was conducted on the top tank accelerometer response. A 0 Hz to 200 Hz drive signal was used to excite the tests system. The results for this wide-band test are shown in Figure 3.5. Figure 3.5(a) shows the repeatability vs. frequency graph for the 0Hz to 200 Hz excitation bandwidth. Figure 3.5(b) is the same set of results, presented over a wider 0 Hz to 400 Hz frequency band.

**Figure 3.5 Radiator top tank repeatability, 0Hz – 200 Hz**

The repeatability of the radiator top tank acceleration response is relatively constant between 5 Hz and  $\pm 60$  Hz, except for a slight decline at 50 Hz (alternating current power supply). Globally, the

repeatability graphs decreases from frequencies above 100 Hz, which coincides with the frequency response of the hydraulic servo control valve. Some distinct minima are evident from the repeatability plot at 70 Hz, 150 Hz and 170 Hz. These minima coincide with the natural frequencies of the system.

The excitation drive file contained frequencies from 0 Hz to 200 Hz, the anti-aliasing filter of the data acquisition system was however set at 333 Hz. Figure 3.5 (b) indicates that the repeatability function calculates better repeatability for the input noise between 200 Hz and 333 Hz, than for large sections of the 0 Hz to 200 Hz signal.

- The validity of comparing PSD amplitudes to determine frequency related repeatability is questionable. The radiator test rig example showed better repeatability for frequencies above the test bandwidth (i.e. system noise), than for sections of the driven system response.
- Typical scalar repeatability numbers are in the region of 98% - 99.9%. The linear percentage scale is not sensitive enough to clearly show the effect of repeatability on simulation. A more sensitive parameter is needed to quantify test rig repeatability.

### 3.1.5. General discussion of repeatability test procedure and results

The scalar and frequency related repeatability functions defined in Section 3.1 provide the test engineer with some indication on the repeatability of the test system's input/output behaviour. These functions do however require further refinement, as both are not ideally suited for application in time domain modelling and simulation.

- Accurate frequency analysis, such as PSD calculations, requires long sections of time data. One of the drives behind time domain simulation is the capability of using short excitation data for model identification. The advantages of short identification signals would become irrelevant considering the lengthy sections of data needed to compute such a frequency related repeatability function. Further investigations into accurate frequency analysis using shorter sections of data could place a new perspective on a function of repeatability vs. excitation frequency.
- The validity of comparing PSD amplitudes to determine frequency related repeatability is questionable. The radiator test rig example showed better repeatability for frequencies above the test bandwidth (i.e. system noise), than for sections of the driven system response.
- Typical scalar repeatability numbers are in the region of 98% ~ 99.9%. The linear percentage scale is not sensitive enough to clearly show the effect of repeatability on simulation. A more sensitive parameter is needed to quantify test rig repeatability.

Figure 3.6: Spill spectra modeling



### 3.2. Split spectra modelling and simulation

The concept of split spectra time domain modelling was initially proposed to reduce the effect of resonant peaks in the system response on simulation results. The philosophy is to model the broad-spectrum behaviour of a system with two or more narrow bandwidth time domain models. The procedure is illustrated in Figure 3.6 for a two-way split of 0 ~ 80 Hz data.

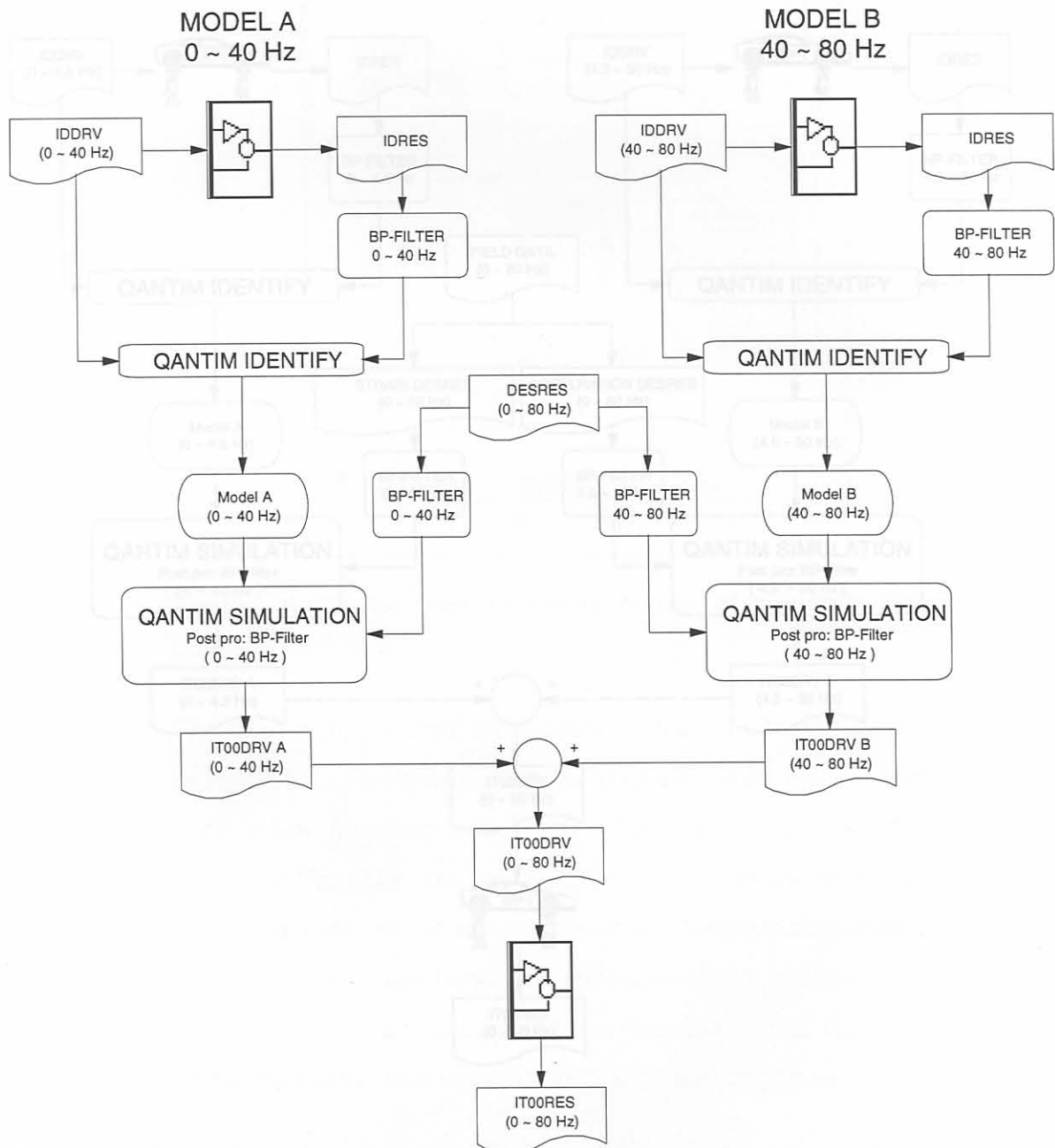


Figure 3.6: Split spectra modelling

The concept of split spectra modelling was further extended by using separate transducers for different frequency bandwidths. This was done to optimally utilise each transducer frequency response. A typical example being the measurement of wheel movements of a motorcycle as presented in Section 3.2.2. A flow diagram illustrating split spectra modelling and simulation with separate transducers is shown in Figure 3.7.

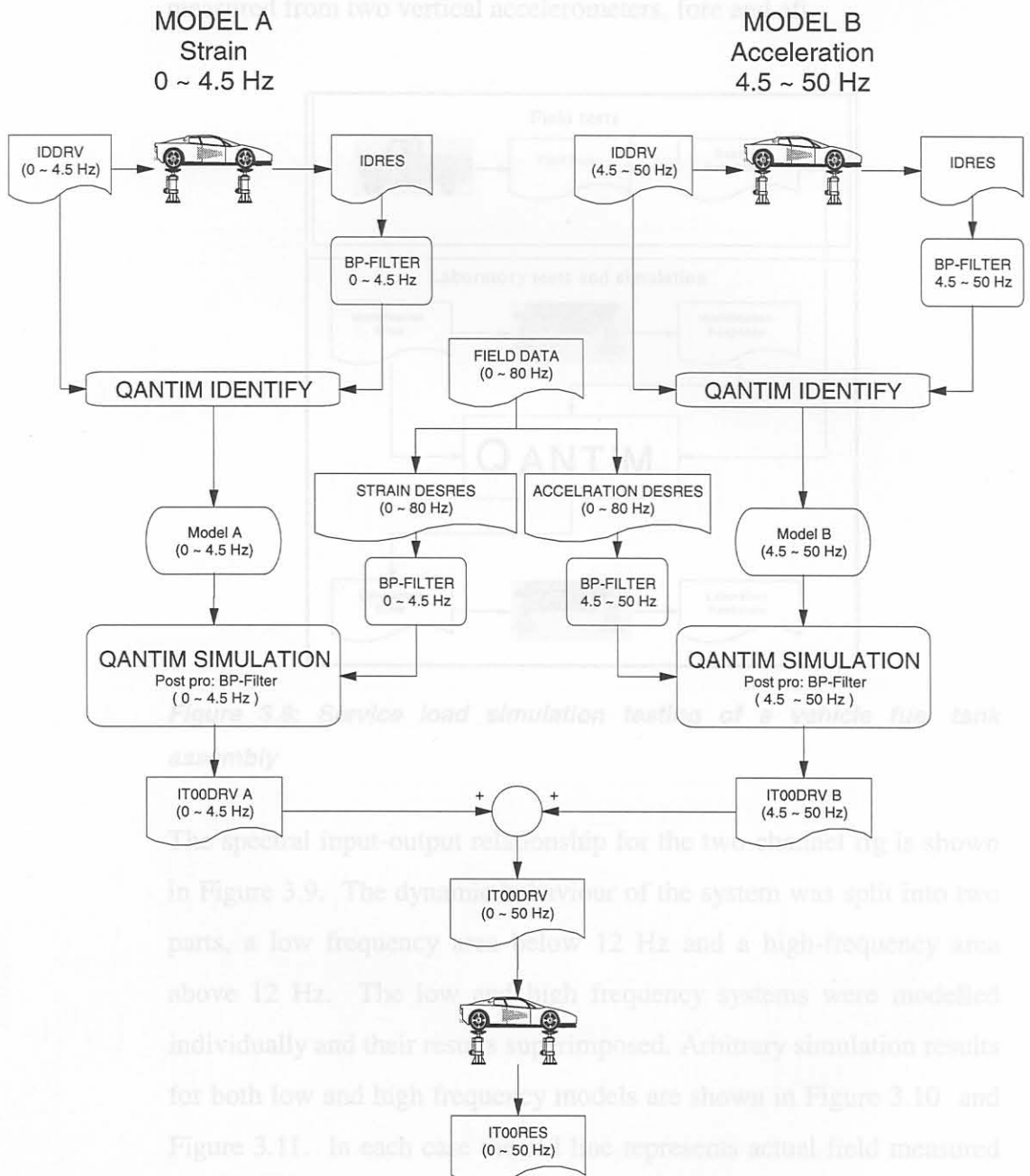


Figure 3.7 Split spectra modelling, using separate transducers

### 3.2.1. Application of split spectra simulation on a fuel tank test rig

A simulation test on a delivery vehicle fuel tank assembly is discussed as an example of the implementation of split spectra modelling. The basic steps of service load simulation testing, as introduced in chapter 1.3 is again presented in Figure 3.8 for the fuel tank test rig [ 50 ]. The fuel tank assembly was mounted on two vertical actuators, and response measured from two vertical accelerometers, fore and aft.

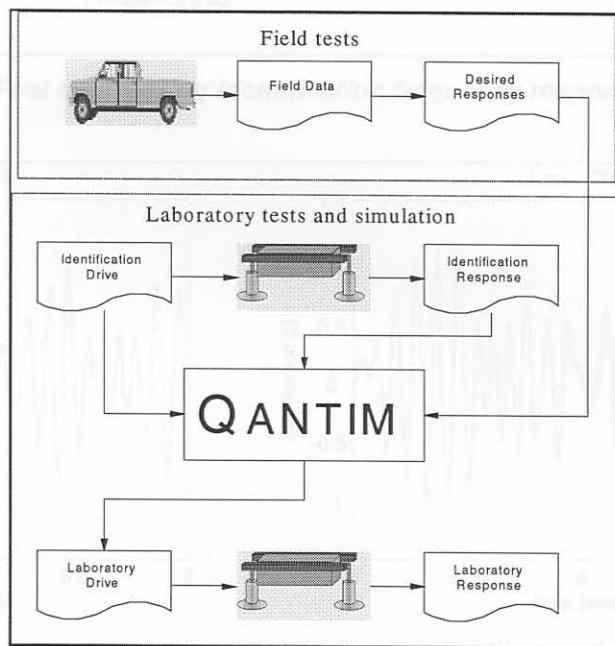


Figure 3.8: Service load simulation testing of a vehicle fuel tank assembly

The spectral input-output relationship for the two-channel rig is shown in Figure 3.9. The dynamic behaviour of the system was split into two parts, a low frequency area below 12 Hz and a high-frequency area above 12 Hz. The low and high frequency systems were modelled individually and their results superimposed. Arbitrary simulation results for both low and high frequency models are shown in Figure 3.10 and Figure 3.11. In each case the red line represents actual field measured responses and the blue line laboratory simulated responses.

Figure 3.11: High frequency simulation results



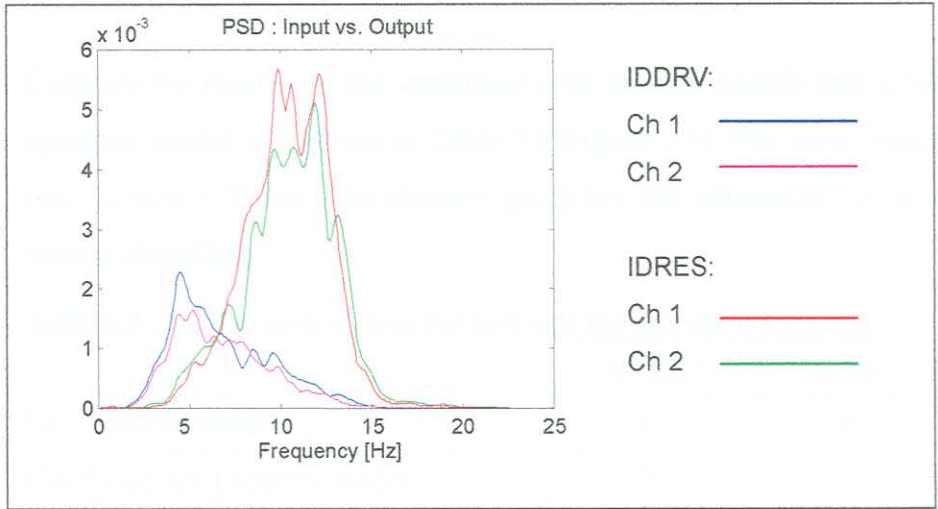


Figure 3.9: Fuel tank test rig identification frequency response

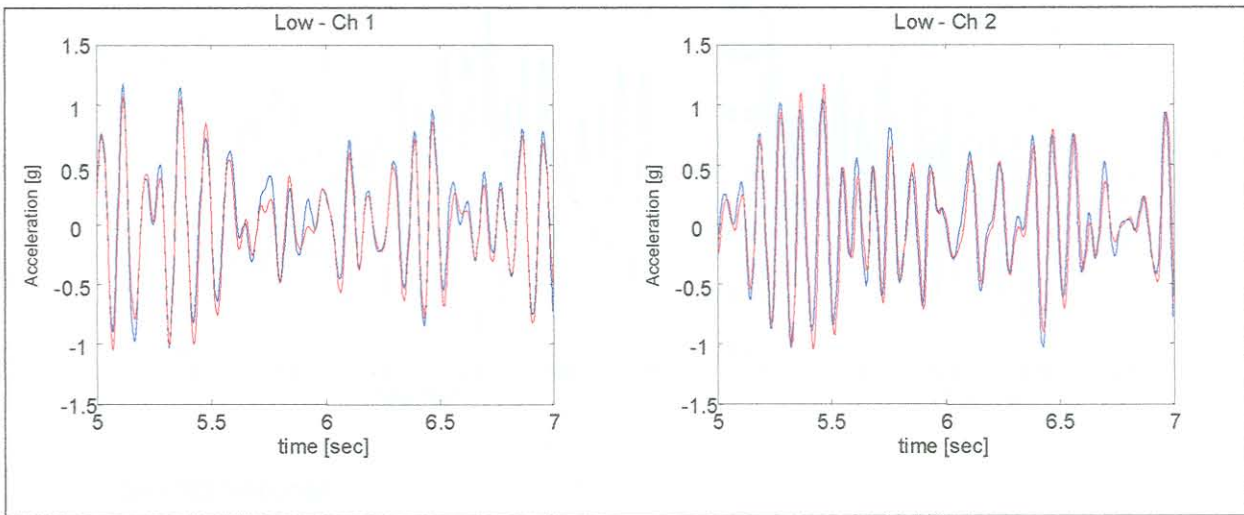


Figure 3.10: Low frequency simulation results

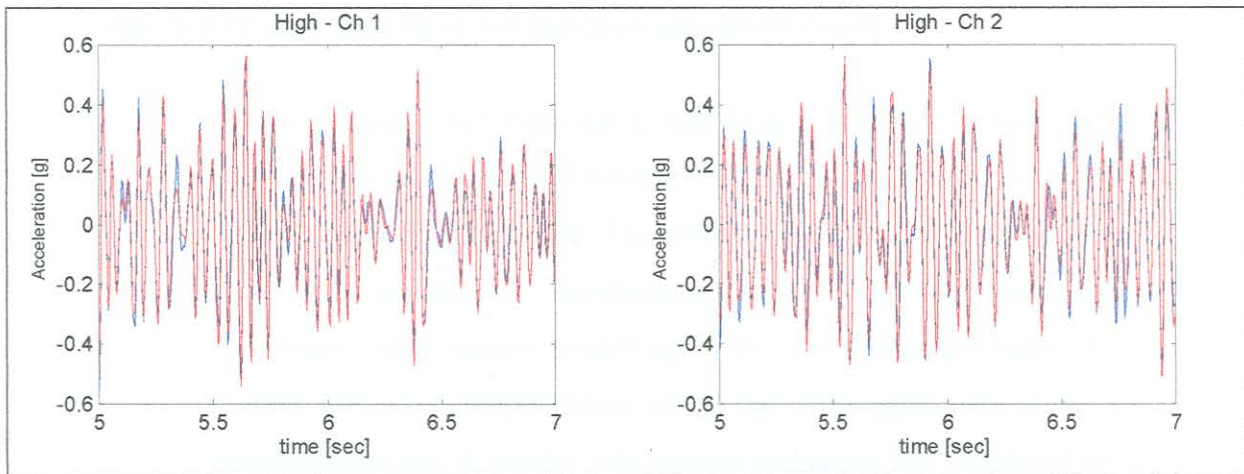
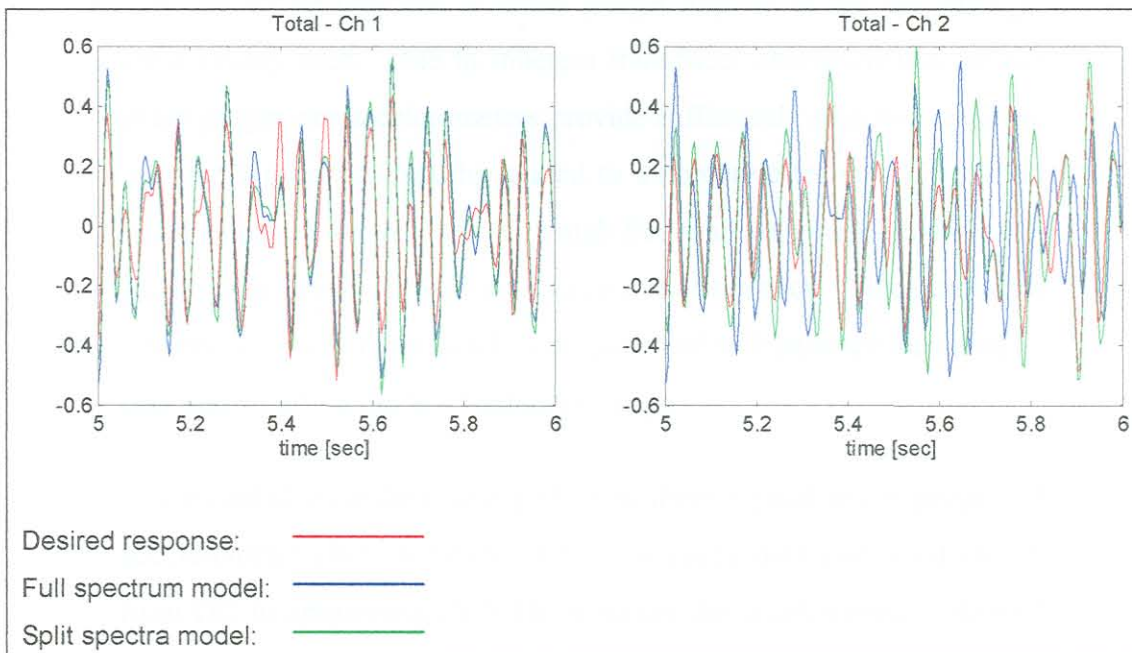


Figure 3.11: High frequency simulation results

Comparative results for the combined split spectra models and a full spectrum model are shown in Table 3.4 Figure 3.12 The error values (see Section 5.7) for each channel quantifies the advantages of split spectra modelling.

**Table 3.4: QanTiM error values for split and full spectra simulation**

	Channel 1	Channel 2
Full spectra model	46	46
Combined split spectra model	20	19



**Figure 3.12: Split spectra vs. full spectrum simulation results**

The two channel fuel tank test system clearly exhibits the potential of split spectra modelling and simulation to improve results for systems with resonant field response. The resonant peak within the simulation bandwidth resulted in unsatisfactory modelling and subsequent simulation. Split spectra modelling of the two frequency bands does involve increased computational effort, but is rewarded with improved simulation results. A similar split spectra technique was employed on a three-axis heavy vehicle chassis simulator with equally favourable results. [ 45 ]

### 3.2.2. Application of split spectra simulation on motorcycle simulator

A simulation example using multiple transducer split-spectra modelling is presented for the rear suspension of a motorcycle on a single axis road simulator. The motorcycle rear suspension road simulator was presented in Section 3.1.3. Typical simulation of field response data is normally conducted using a single remote parameter transducer for each simulation channel. In the case of vehicle simulations, spindle mounted accelerometers, or strain gauges applied to the coil springs, are normally used. Due to inherent transducer characteristics neither strain gauges nor accelerometers provide sufficiently sensitive response over the typical bandwidths related to automotive testing. The small strain amplitudes associated with high frequency responses make strain gauges less sensitive with an increase in frequency. Accelerometer sensitivity, on the other hand, is proportional to frequency, resulting in poor sensitivity in the low frequency ranges.

The recorded field data clearly showed these typical strain gauge and accelerometer characteristics. The strain gauge data contained energy from DC to approximately 8 Hz, whereas the accelerometers showed energy from approximately 8 Hz to 30 Hz.

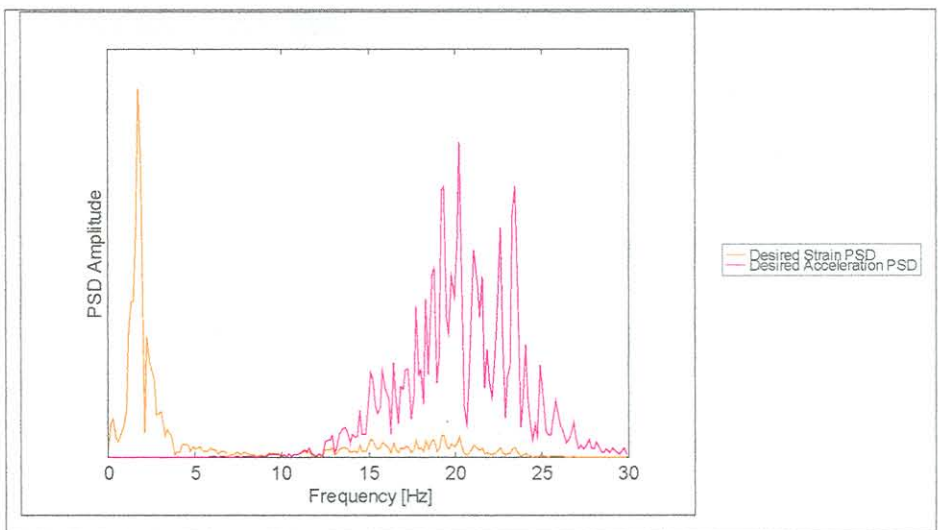


**Figure 3.13** Motorcycle rear suspension desired response PSD



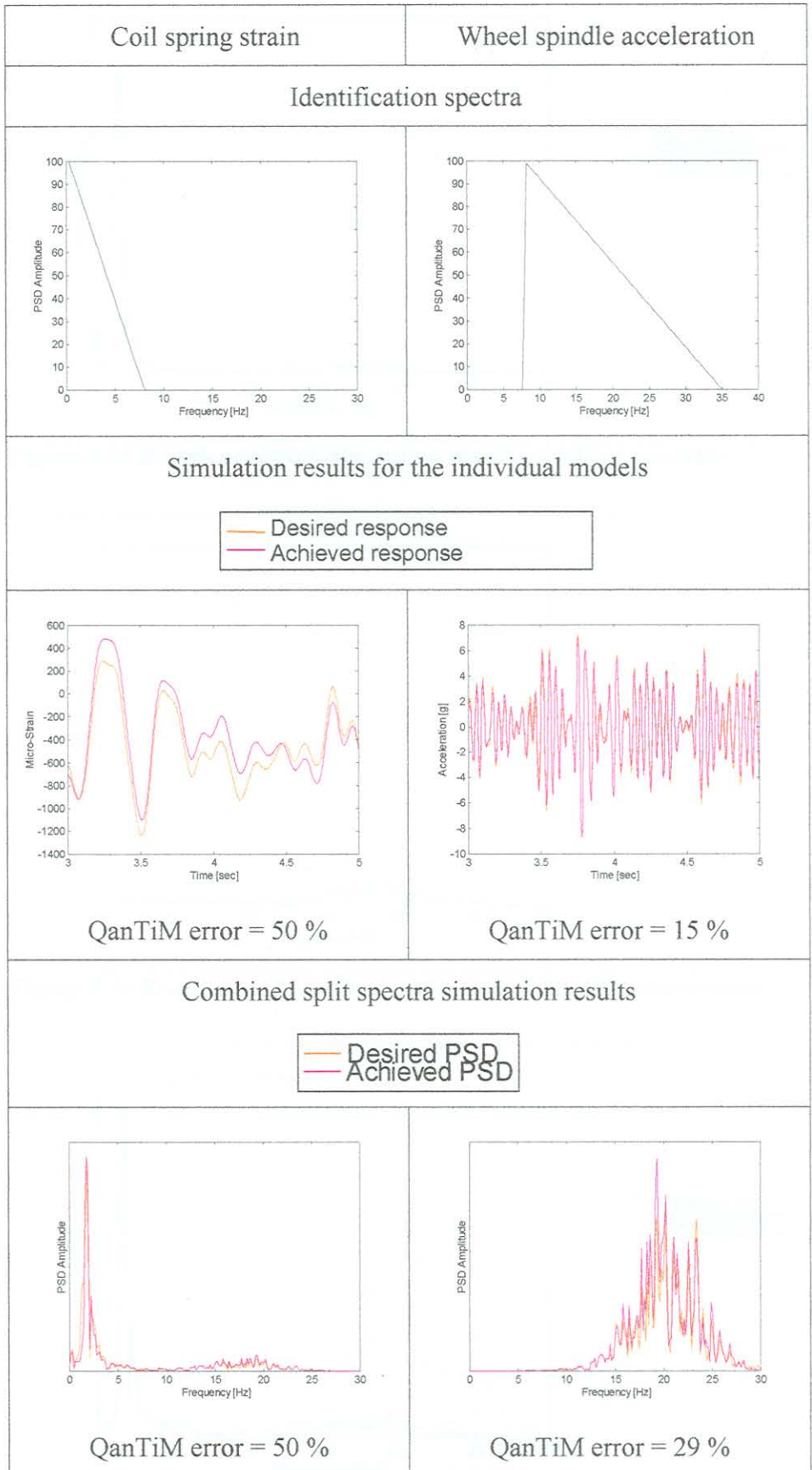
From the spectral plots in Figure 3.13 it was decided to split the responses at 8 Hz. The upper limit for simulation was chosen at 30Hz. Subsequently the strain responses were low-pass filtered at 8 Hz and the acceleration responses band-pass filtered between 8 Hz and 30Hz. The simulation results for the multiple transducer split spectra procedure are presented in Figure 3.14. The split spectra results are subsequently compared to results obtained with broad spectrum, single transducer simulations. In order to compare the effect of the modelling techniques, only the linear solution results are presented i.e. no iterations are performed subsequent to simulation.

Figure 3.15, Figure 3.16 and Figure 3.17 compare the simulation results of the conventional single transducer, broad-spectrum QanTiM simulations, with that of the split spectra, multiple transducer technique.

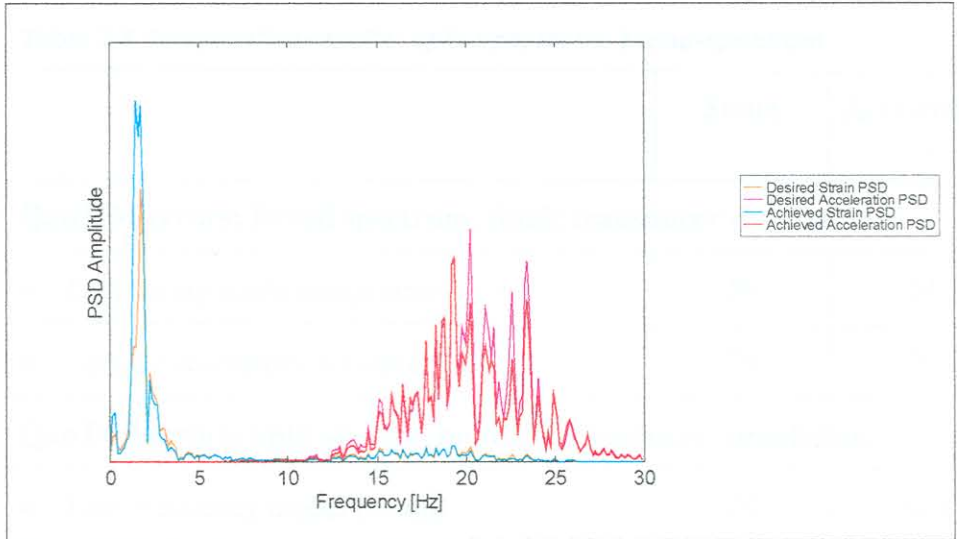
- The broad spectrum strain simulation results in a generally good simulation of both strain and acceleration response. The strain simulation does however produce too large amplitudes at low frequencies, and small amplitudes at higher frequencies.
- The broad-spectrum acceleration simulation provides good high frequency results, but poor simulation of the low frequency strains.
- The split spectra model results in improved simulation over the full simulation bandwidth.



Figure 3.14 Multiple transducer split spectra simulation results



**Figure 3.14 Multiple transducer split spectra simulation results**



**Figure 3.15 Broad- spectrum simulation results: Coil spring strain**

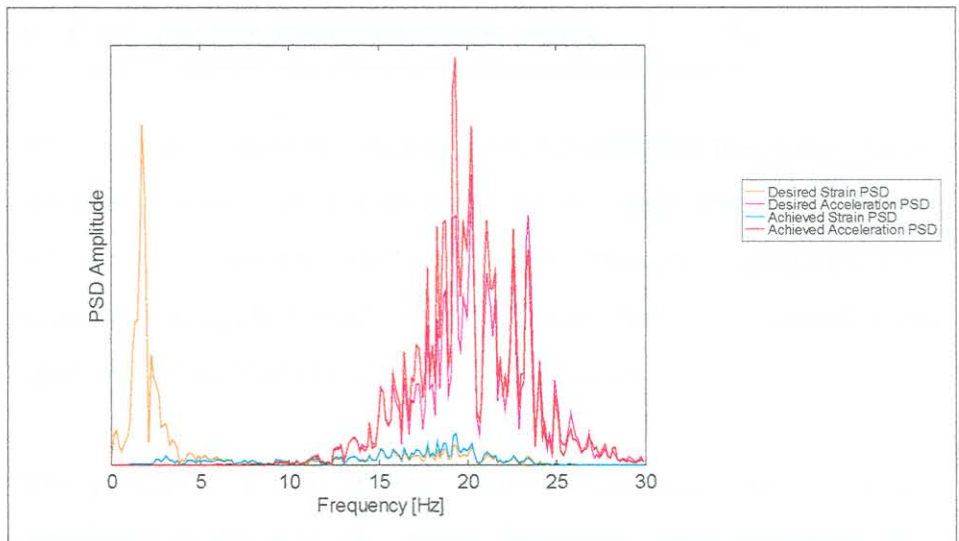


**Figure 3.16 Broad- spectrum simulation results: Spindle acceleration**

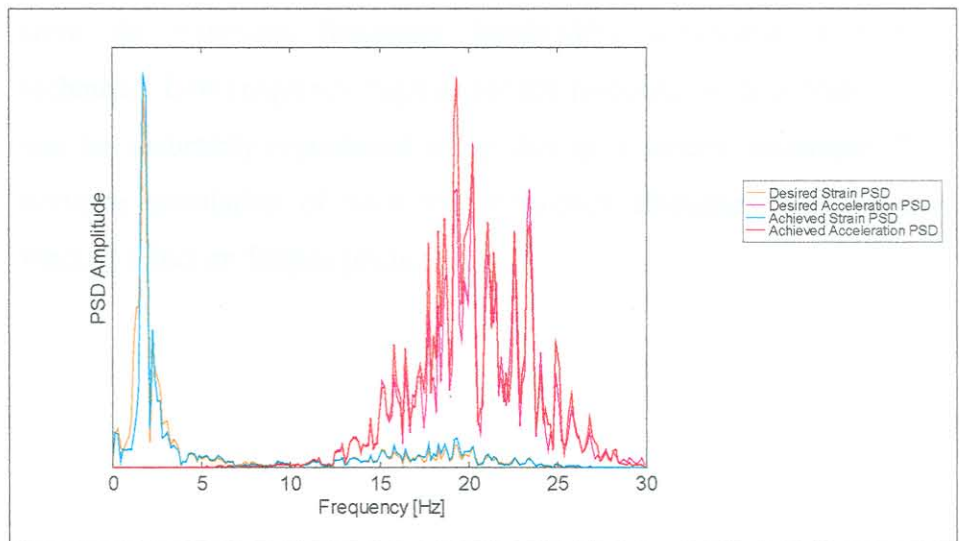


**Figure 3.17 Split spectra simulation results**



**Table 3.5 Comparative results: split-spectra vs. broad-spectrum**

	Strain	Acceleration
<b>QanTiM errors: Broad spectrum, single transducer simulation</b>		
• Coil spring strain gauge simulation	56	51
• Spindle accelerometer simulation	78	31
<b>QanTiM errors: Split spectra, multiple transducer simulation</b>		
• Low frequency model (strain)	50	N/A
• High frequency model (acceleration)	N/A	15
• Combined split spectra simulation results	50	29

The result summary presented in Table 3.5 indicates that strain gauges are more effective than accelerometers as single transducer, remote simulation parameters. More important, multiple transducer, split-spectra simulation proved more accurate than conventional broad spectrum, single transducer QanTiM simulations.

The principle of split-spectra, multiple transducer simulation was introduced at the hand of a relatively simple, single-axis application example. Vehicle simulation tests on four post road simulators benefit from the extended frequency bandwidths achievable with this technique. Low frequency, high amplitude response, such as body twist, can be accurately reproduced using this split spectra technique. The accurate simulation of such low frequency responses may have a marked effect on fatigue predictions.

### 3.3. Optimal excitation characteristics

The PSD function from which the identification drive signals are generated can have notable effect on the simulation outcome. Frequency domain simulation systems usually make use of a  $1/f^n$  PSD function to create identification drive signals. The  $1/f$  PSD, as shown in Figure 3.18a, is normally representative of a servo hydraulic actuator's dynamic capabilities. A similar approach is generally followed for time domain identification, although a triangular PSD function is found to give better results [ 15 ], [ 13 ], [ 24 ].

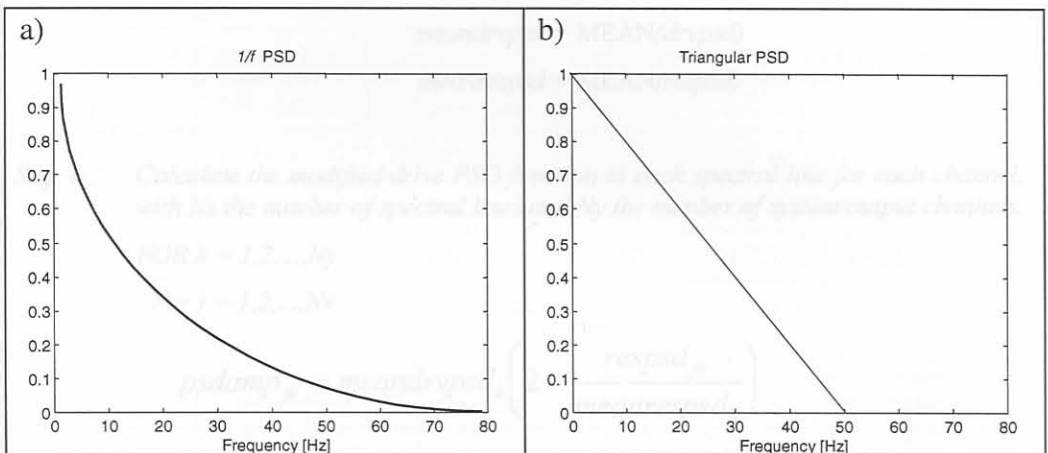


**Figure 3.18:  $1/f$  and triangular PSD functions for identification drive signals.**

The  $1/f^n$  and triangular PSD functions proved limited for systems with intricate dynamic behaviour [ 17 ]. A method for finding an optimised PSD function is needed, especially for multi-axial test rigs. Based on the work by Barnard [ 2 ], the author devised a simple method of anti-resonant excitation to create an identification drive signal well suited to a specific test rig. This purely intuitive method limits the excitation PSD function in the areas of system resonance. The procedure for finding a set of rig specific identification drive PSD's is described briefly in Algorithm 3.1 and an application example is given. The example in Figure 3.19 shows the sine sweep drive and response PSD functions as well as the modified rig specific PSD function for a single axis test rig. A detailed application example is presented in Section 3.3.1 for a seven-channel fuel tank test rig.

**Algorithm 3.1: Rig specific identification PSD's**

Step 1: Excite all channels of the rig with a low amplitude linear sine sweep within the typical frequency bandwidth of the system. Simultaneously record the responses from the relevant transducers.

Step 2: For each channel calculate the PSD functions of both the drive and response signals so that:

$$drvpsd = \text{PSD}(\text{sweepdrive})$$

$$respsd = \text{PSD}(\text{sweepres})$$

Where *drvpsd* and *respsd* are matrices with row entries containing the PSD amplitudes at each specified spectral line for all the input and output channels of the system.

Step 3: Calculate the mean value of the PSD amplitudes in *drvpsd* and *respsd* for each channel:

$$\text{meandrvpsd} = \text{MEAN}(\text{drvpsd})$$

$$\text{meanrespsd} = \text{MEAN}(\text{respsd})$$

Step 4: Calculate the modified drive PSD function at each spectral line for each channel, with *Ns* the number of spectral lines and *Ny* the number of system output channels.

FOR  $k = 1, 2, \dots, Ny$

For  $j = 1, 2, \dots, Ns$

$$\text{psdamp}_{jk} = \text{meandrvpsd}_k \left( 2 - \frac{\text{respsd}_{jk}}{\text{meanrespsd}_k} \right)$$

Step 5: Create a random identification drive signal using the modified PSD function.

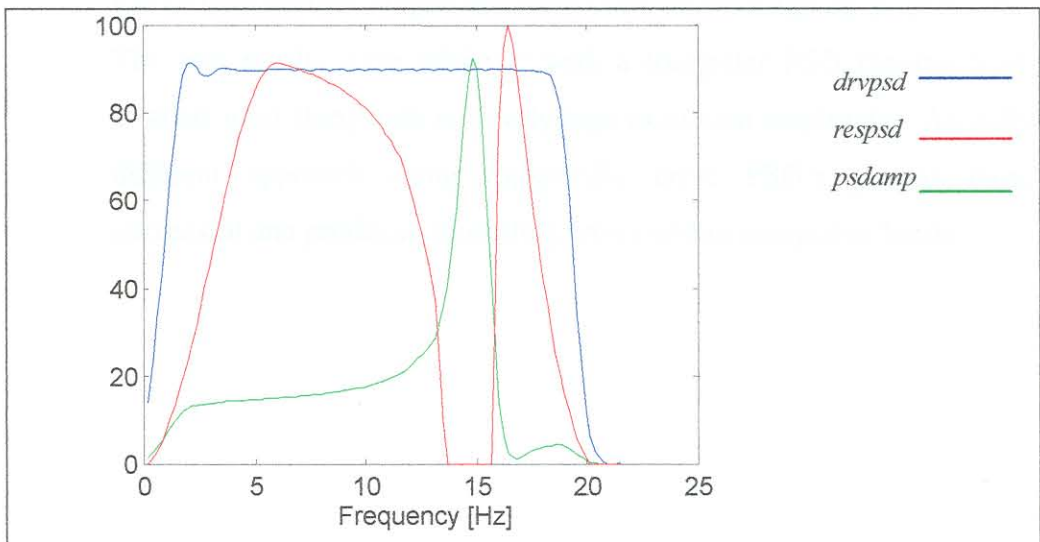


**Figure 3.19: Rig specific PSD calculation**



### 3.3.1. Application on a seven channel fuel tank test rig

QanTiM was used to drive a MTS 498 seven-channel full chassis fuel tank test rig [ 17 ] (courtesy of Ford motor co. Dearborn). The inputs to the rig consisted of vertical displacements at the four corners, as well as two lateral displacements, and a longitudinal displacement. The responses were measured from accelerometers mounted near the actuator connecting points.

**Table 3.6: Test rig summary**

Ch #	Test rig drive characteristics			Model response
	Description	Control mode	Full scale	Description
1	L/F vertical	Displacement	3"	L/F vertical acceleration
2	R/F vertical	Displacement	3"	R/F vertical acceleration
3	L/R vertical	Displacement	3"	L/R vertical acceleration
4	R/R vertical	Displacement	3"	R/R vertical acceleration
5	Front lateral	Displacement	3"	Front lateral acceleration
6	Rear lateral	Displacement	3"	Rear lateral acceleration
7	Longitudinal	Displacement	3"	Longitudinal acceleration

Despite the rig's apparent simplicity, numerous modelling iterations were performed without any success. Typical triangular and  $1/f$  drive PSD's with various amplitudes were used, all with equally poor results. The best results were achieved with a triangular PSD ranging from 1~40Hz used along with relatively high excitation amplitudes. A totally different approach using rig-specific drive PSD's proved more successful and produced modelling errors within acceptable limits.

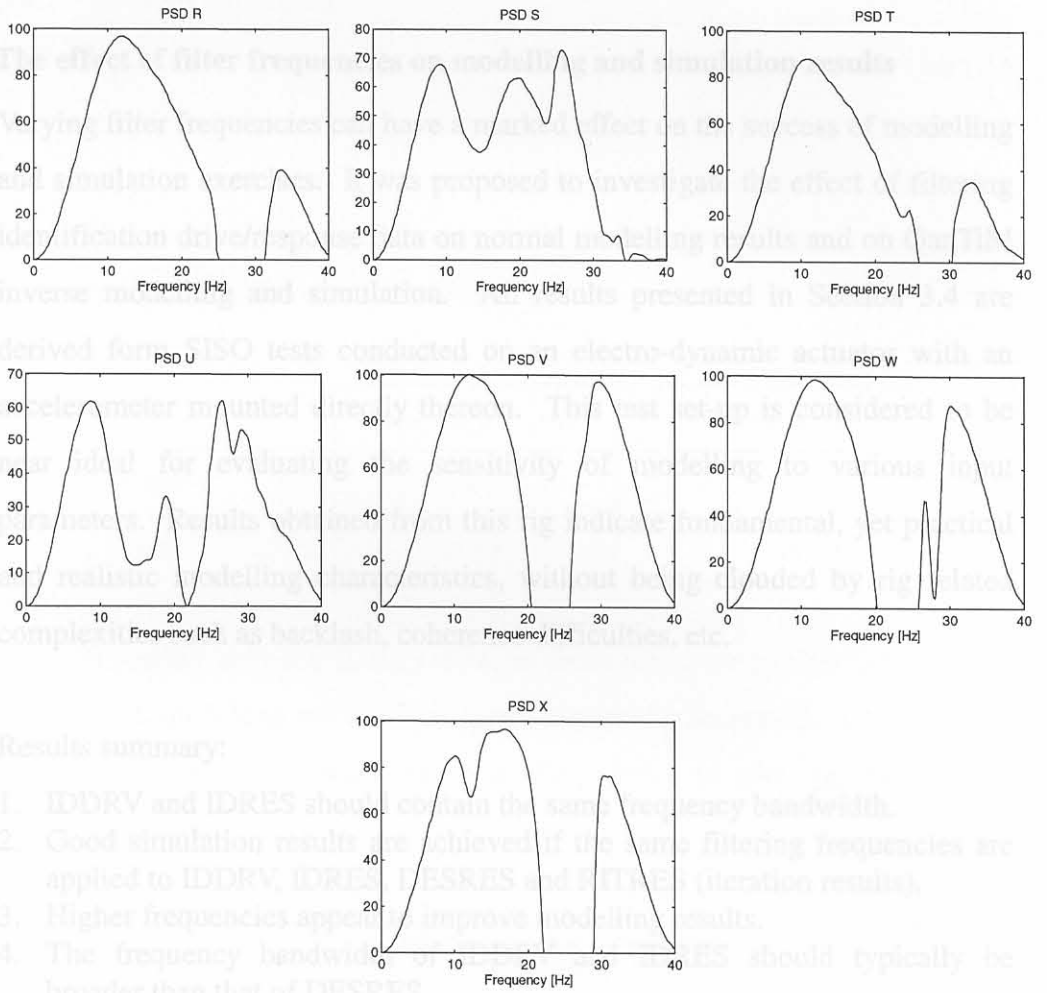
In order to gain some knowledge of the rig characteristics, a 0~40Hz linear, small amplitude, (0.015") sine sweep was driven through the four vertical actuators. The PSD's of the sweep input / output data were used to create a drive PSD that would minimise energy in the rig's regions of resonance. This proved effective for the vertical channels and the process was repeated for all seven actuators. The result was a set of seven unique PSD's from which the identification drive signals were generated. The modelling results improved drastically and showed some potential for rig-specific PSD's. The models created with the rig-specific PSD's seemed inherently stable, as is shown in a typical model order selection plot. (The concept of QanTiM model orders are discussed in Section 4.2) The modelling error tended to decrease with order without signs of instability; this seemed to be the case for all channels.

**Table 3.7: MISO rig specific modelling results**

Ch	Description	IDDRV Parameters		GPREPRO Filter cut-off frequencies		Modelling results	
		PSD	Amp	Low	High	order	error
1	L/F vertical	R	1"	1 Hz.	40 Hz.	4	20
2	R/F vertical	S	1"	1 Hz.	40 Hz.	9	22
3	L/R vertical	T	1"	1 Hz.	40 Hz.	6	19
4	R/R vertical	U	1"	1 Hz.	40 Hz.	7	29
5	Front lateral	V	0.2"	1 Hz.	40 Hz.	5	23
6	Rear lateral	W	0.2"	1 Hz.	40 Hz.	7	19
7	Longitudinal	X	0.2"	1 Hz.	40 Hz.	6	37



*Figure 3.21: Model error vs. order for channel 1*



Results summary:

1. IDDRV and IDRES show good results within the same frequency bandwidth.
2. Good simulation results are achieved if the same filtering frequencies are applied to IDDRV, IDRI, IDRESSES and FITRES (iteration results).
3. Higher frequencies appear to improve modelling results.
4. The frequency bandwidth of the simulation should typically be broader than that of DESRES.
5. Models identified from broad spectrum data showed good iteration results.

**Figure 3.20: Rig specific PSD functions**

Points number 1 and 2 led to the implementation of general simulation bandwidths for the various models. Points number 4 and 5 suggest that a simulation bandwidth broader than that of the desired response may have a limited effect on simulation accuracy, especially during the iteration process.

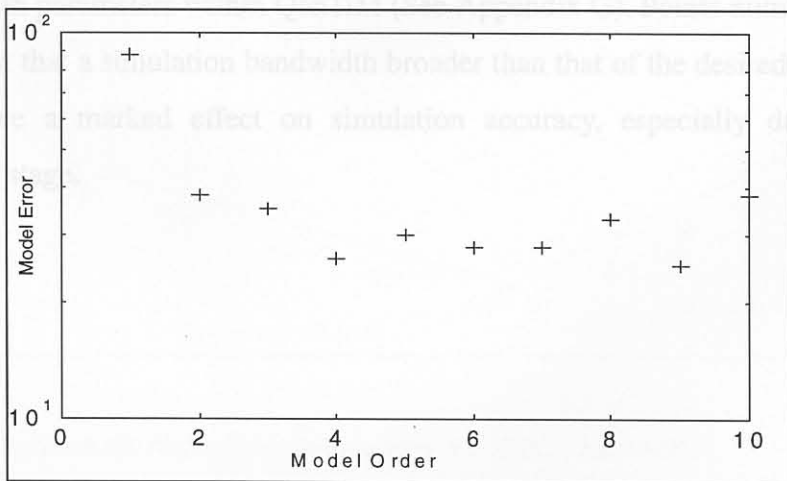


**Figure 3.21: Model error vs. order for channel 1**



## 3.4.1. Normal modelling

## 3.4. The effect of filter frequencies on modelling and simulation results

Varying filter frequencies can have a marked effect on the success of modelling and simulation exercises. It was proposed to investigate the effect of filtering identification drive/response data on normal modelling results and on QanTiM inverse modelling and simulation. All results presented in Section 3.4 are derived from SISO tests conducted on an electro-dynamic actuator with an accelerometer mounted directly thereon. This test set-up is considered to be near ideal for evaluating the sensitivity of modelling to various input parameters. Results obtained from this rig indicate fundamental, yet practical and realistic modelling characteristics, without being clouded by rig related complexities such as backlash, coherence difficulties, etc.

Results summary:

1. IDDRV and IDRES should contain the same frequency bandwidth.
2. Good simulation results are achieved if the same filtering frequencies are applied to IDDRV, IDRES, DESRES and RITRES (iteration results).
3. Higher frequencies appear to improve modelling results.
4. The frequency bandwidth of IDDRV and IDRES should typically be broader than that of DESRES.
5. Models identified from broad spectrum data showed good iteration characteristics

Points number 1 and 2 led to the implementation of general simulation bandwidth parameters within QanTiM (See Appendix G). Points number 4 and 5 suggest that a simulation bandwidth broader than that of the desired response may have a marked effect on simulation accuracy, especially during the iteration stage.

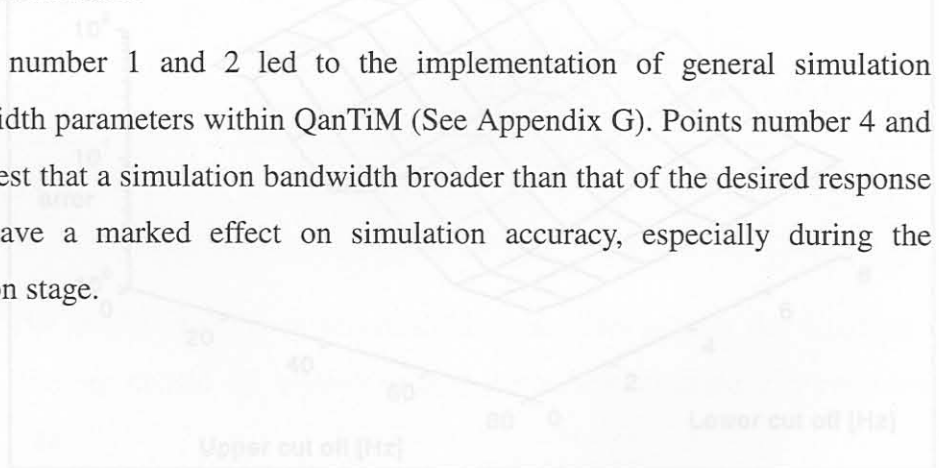


Figure 3.22: Normal modelling error vs. IDRES bandwidth

### 3.4.1. Normal modelling

Two sets of filtering exercises were conducted using normal QanTiM (ARX)-models. Firstly models were calculated for a system excited with a broad-spectrum random signal and band filtered responses. Thereafter both identification drive and response signals were band pass filtered prior to modelling.

	lower cut off [Hz]	Upper cut off [Hz]
IDDRV	0	80
IDRES	0 ~ 8	16 ~ 80

Filtering only the IDRES data, as presently done in QanTiM, showed high modelling errors as the signal bandwidth decreased. This is shown in Figure 3.22 where the modelling error is plot against IDRES bandwidth.

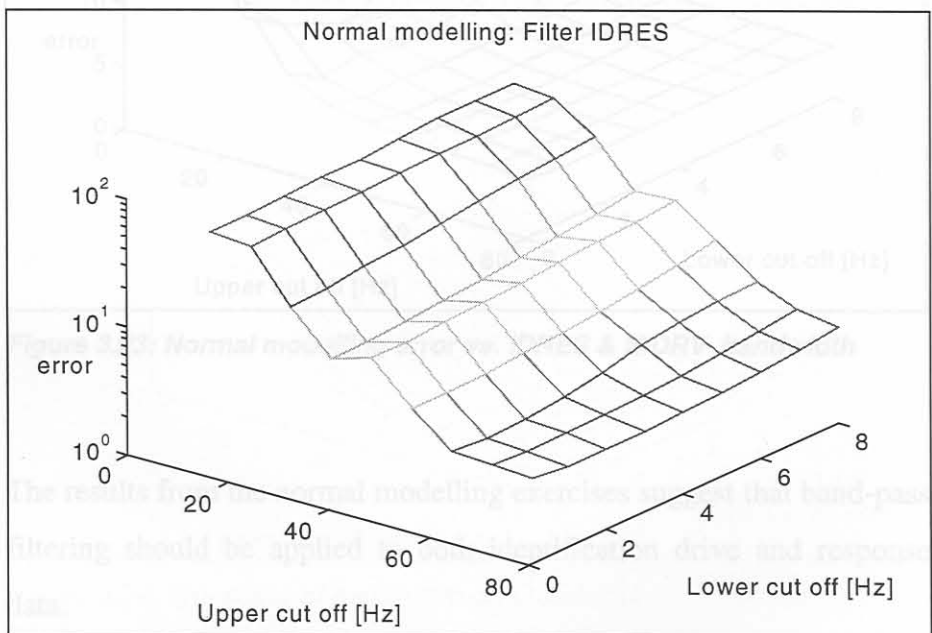


**Figure 3.22: Normal modelling error vs. IDRES bandwidth**

Using a band-pass filter on both IDDRV and IDRES prior to modelling greatly improved results. Modelling errors were generally reduced by a factor ten and showed good results for all frequency bandwidths wider than 20 Hz.

	lower cut off frequency [Hz]	Upper cut off frequency [Hz]
IDDRV	0 ~ 8	16 ~ 80
IDRES	0 ~ 8	16 ~ 80

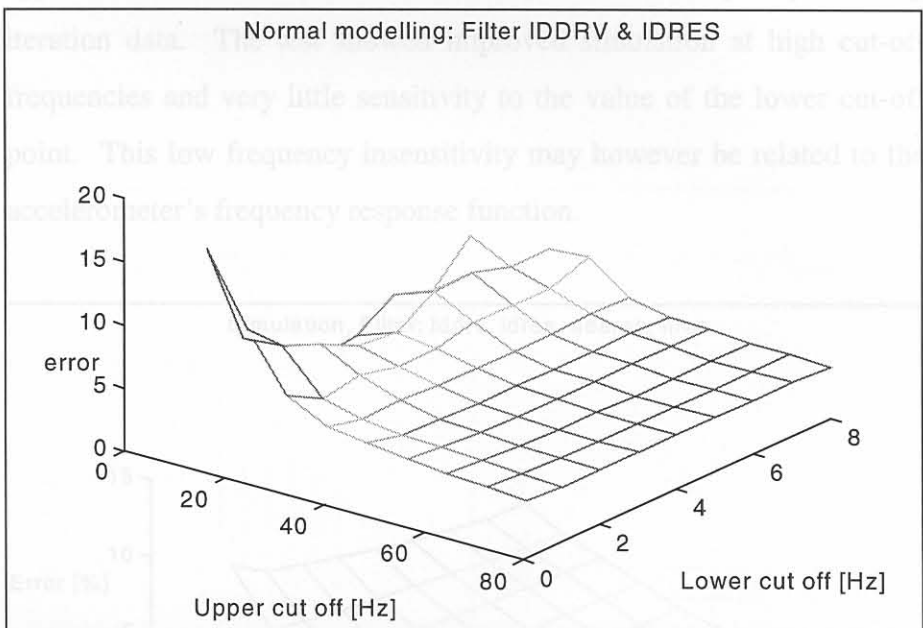


**Figure 3.23: Normal modelling error vs. IDRES & IDDRV bandwidth**

The results from the normal modelling exercises suggest that band-pass filtering should be applied to both identification drive and response data.



### 3.4.2. The effect of bandwidth on simulation

3.4.3. Tests were conducted to investigate the effects of modelling bandwidths on simulation results. The tests were conducted using desired response data recorded from the electro-dynamic test system while driving with either a 0 ~ 50 Hz or a 0 ~ 80 Hz random drive.

The results from the normal modelling exercise suggested that band-pass filtering should be applied to both identification drive and response data prior to modelling. This concept was further investigated for inverse QanTiM type models. The same band-pass criteria were applied to identification data, desired response data and post-processing iteration data. The test showed improved simulation at high cut-off frequencies and very little sensitivity to the value of the lower cut-off point. This low frequency insensitivity may however be related to the accelerometer's frequency response function.

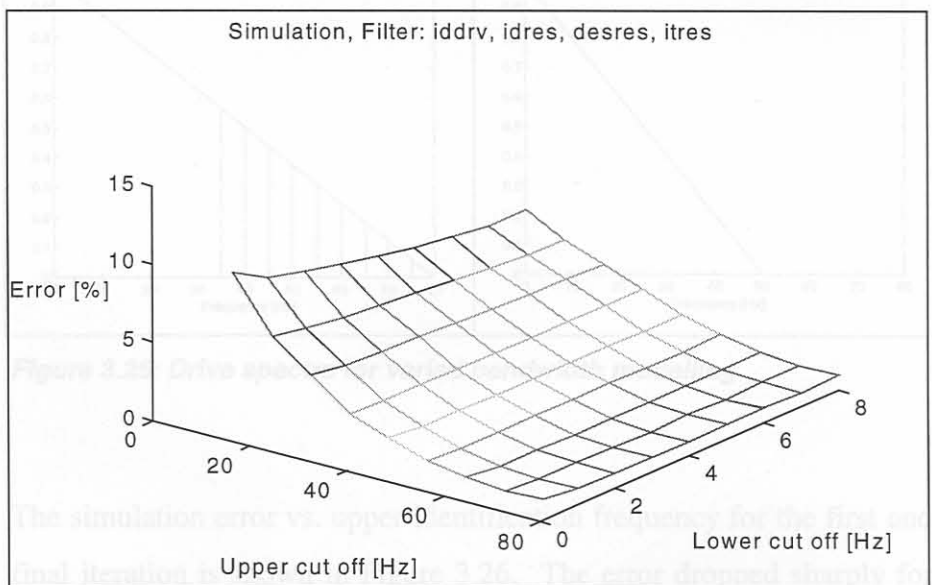


**Figure 3.24: The effect of bandwidth on simulation**

The simulation error vs. upper cut-off frequency for the first and final iteration is shown in Figure 3.26. The error decreased sharply for the first iteration and then remained stable up to 80 Hz (which returned the most accurate results after 4 iterations). Simulations using models identified with sub 50 Hz data tended to diverge during iteration, whereas the broader bandwidth models converged to a small error value (Figure 3.27).

### 3.4.3. Wide spectrum simulation

A series of tests were conducted to investigate the effect of identification bandwidth on simulation of a fixed desired response signal. Identification drive/response data was generated using a triangular full spectrum (0~80 Hz) PSD. Subsequently ten narrower bandwidth signals were generated by low-pass filtering according to Figure 3.25a. The desired response data was recorded from the system driven with the 0~50 Hz triangular PSD drive in Figure 3.25b. Prior to modelling a 2 Hz high-pass filter was used to compensate for low accelerometer sensitivity in the low frequency regions. No post-processing filtering operations were performed on the iteration response data

Figure 3.25: Simulation errors for iteration 0 and iteration 4

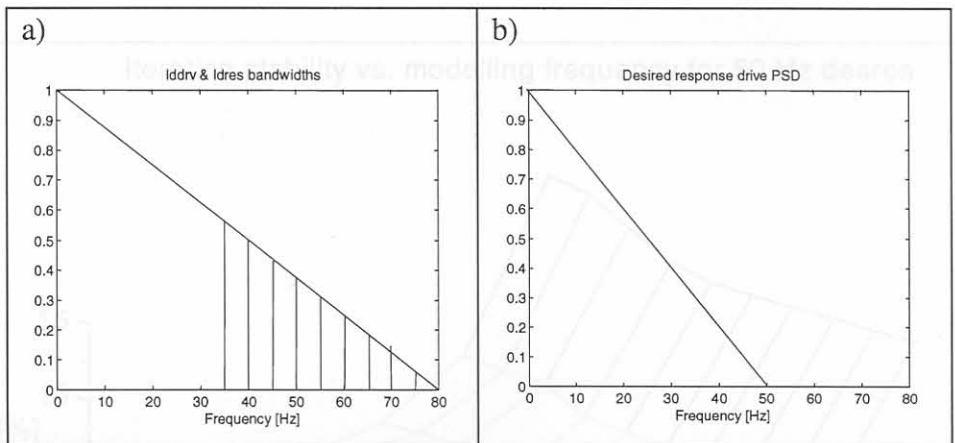


Figure 3.25: Drive spectra for varied bandwidth modelling

The simulation error vs. upper identification frequency for the first and final iteration is shown in Figure 3.26. The error dropped sharply for identification frequencies above 50 Hz, and remained stable up to 80 Hz (which returned the most accurate results after 4 iterations). Simulations using models identified with sub 50 Hz data tended to diverge during iteration, whereas the broader bandwidth models converged to a small error value. (Figure 3.27).

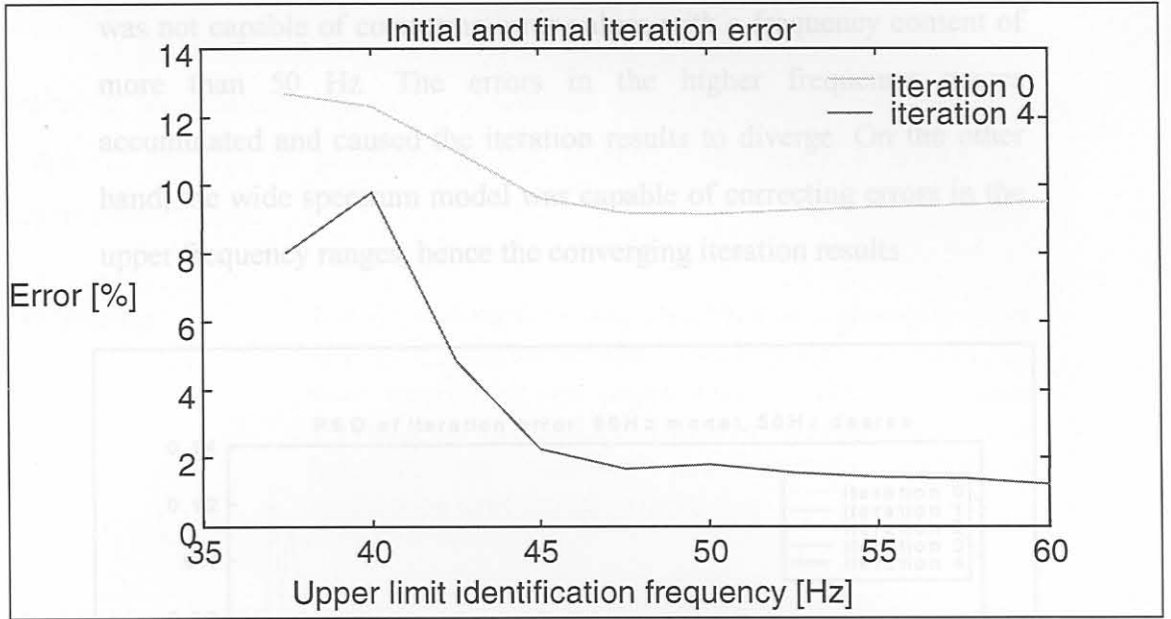


Figure 3.26: Simulation errors for iteration 0 and iteration 4

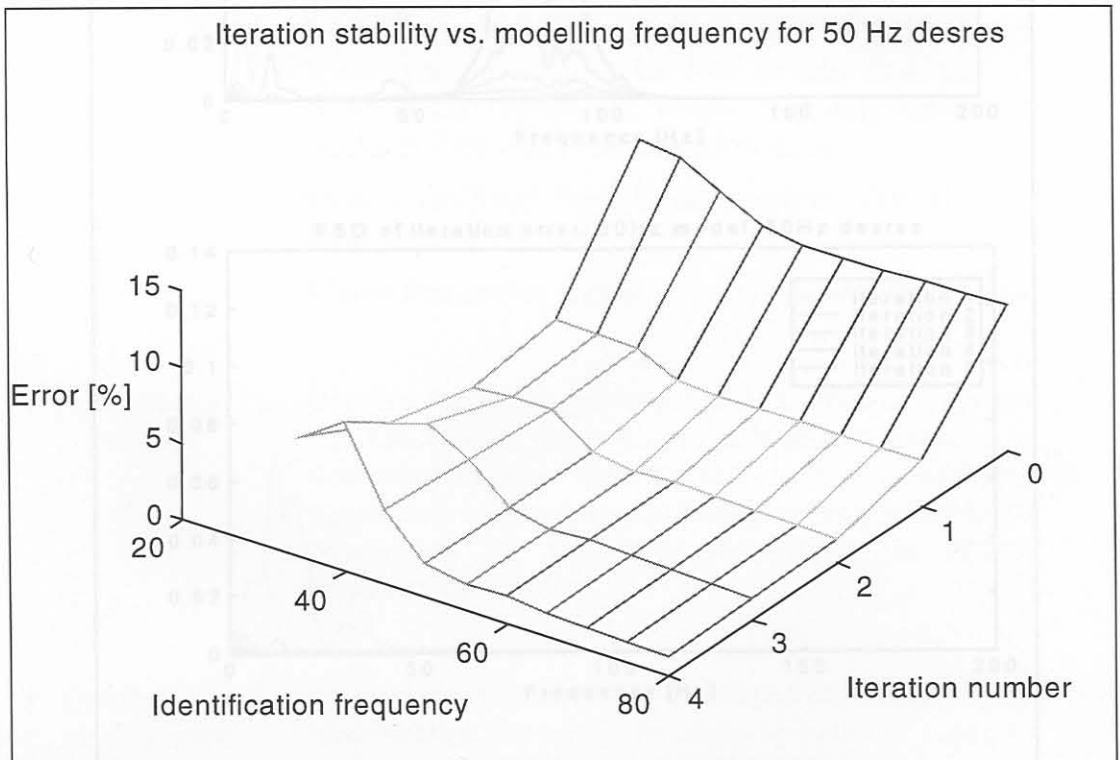
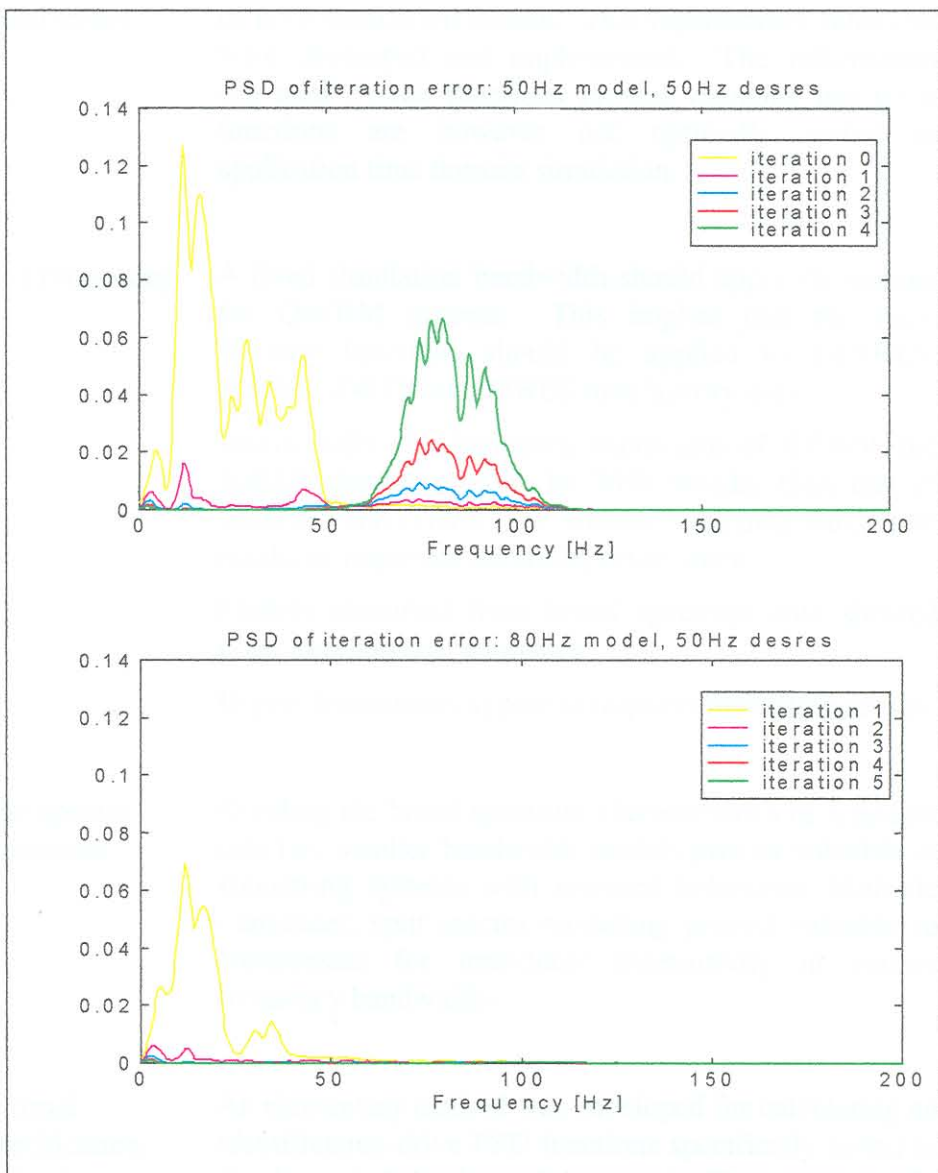


Figure 3.27: Iteration errors for various ID upper frequencies



PSD's of the iteration error signals are shown in Figure 3.28 for a 0 ~ 50 Hz model and a 0 ~ 80 Hz model. The narrower bandwidth model was not capable of correcting error values with a frequency content of more than 50 Hz. The errors in the higher frequency ranges accumulated and caused the iteration results to diverge. On the other hand, the wide spectrum model was capable of correcting errors in the upper frequency ranges, hence the converging iteration results.



**Figure 3.28: Iteration error frequency content**

### 3.5. Conclusion and recommendations for further research - Part I

Valuable information concerning simulation accuracy was gained from the empirical research as presented in this chapter. The research results are summarised below.

- **Test rig repeatability** Test rig repeatability was identified as a potential cause of poor simulation results. Two repeatability functions were developed and implemented. The information provided by the functions proved valuable, but these functions are however not optimally suited to application time domain simulation.
- **Data processing** A fixed simulation bandwidth should apply throughout the QanTiM process. This implies that the same filtering functions should be applied to DESRES, IDDRV, IDRES, and ITRES time history data.

Additionally, the frequency bandwidth of IDDRV and IDRES should typically be 20% broader than that of DESRES and ITRES. The broader modelling bandwidth results in improved iteration performance.

Models identified from broad spectrum data showed good iteration characteristics

Higher frequencies appear to improve modelling results.
- **Split spectra simulation** Dividing the broad-spectrum characteristics of a system into two smaller bandwidth models proved valuable in simulating systems with resonant behaviour. Multiple transducer, split-spectra modelling proved valuable to compensate for transducer insensitivity in certain frequency bandwidths.
- **Optimal identification excitation** An elementary method was developed for calculating an identification drive PSD functions specifically suited to the dynamic behaviour of the test rig. These rig specific identification drive signal PSD functions improve model accuracy and model stability.

Further research in QanTiM specific repeatability functions will provide the simulation engineer with valuable information with which to assess test rig integrity prior to modelling.

A field that poses potential for further investigation concerns the system analogue to digital sampling rate. The use of a localised sampling rate is suggested. This implies a constant ratio between sampling rate and signal frequency. It is however not possible to sample at various rates, a high sampling rate would thus be used and the signals then decimated prior to modelling and simulation. As a first implementation, a scheme similar to that presented for split spectra modelling is suggested. Each separate model will however utilise a different sampling rate. It is proposed that the use of such localised sampling rates would improve model accuracy and eliminate errors related to numerical instability.

Further research into optimal identification excitation signals is most definitely necessary. The effect of excitation signal characteristics proved extremely significant and yet it is the part of the simulation procedure, which involves the most *black magic*. An automated excitation routine would greatly improve the versatility and ease of use of the existing QanTiM package.

The concept of a fixed simulation bandwidth has been implemented within QanTiM, but additional research is required into modelling and simulating with a bandwidth broader than that of the desired response data.

At present it appears that non-linear modelling capabilities are however the most likely to have a significant effect on simulation results. Research into non-linear system identification and response reconstruction is presented formally in part II of this thesis.



## PART II: Investigation into the possible implementation of non-linear response reconstruction

---

This second part of the thesis presents an investigation into the possible implementation of polynomial non-linear system identification routines in response reconstruction. Non-linear system identification has been well researched from a mathematical formulation point of view – see Billings *et al.* [ 5 ][ 6 ][ 7 ] Chen [ 18 ], Fasol [ 26 ], Korenberg [ 36 ], etc. To the author's knowledge, non-linear dynamic system identification has not previously been applied to the field of response reconstruction.

The development of a non-linear response reconstruction technique is presented in a concise, almost chronological manner. Only the most relevant theory is included in the body of the thesis, with more detail included in the appendices. Linear system identification is introduced in Chapter 4, at the hand of the ARX [ 40 ][ 41 ] time domain model formulation. The ARX fundamentals are extended to accommodate polynomial non-linear modelling capabilities with the NARX [ 9 ][ 46 ] model structure in Chapter 5. Application of the developed NARX modelling and response reconstruction techniques is presented in Chapter 6. Finally some conclusions and recommendations for future research are made in Chapter 7.

## Chapter 4

### 4.1. ARX model structure

## Linear time domain system identification: ARX

Dynamic response reconstruction for fatigue tests has the global aim to reproduce operational measured response stresses in the test structure as accurately as possible using servo-hydraulic actuators. To calculate actuator drive signals from knowledge of operational measured responses a dynamic model that describes the complete system is required. Such a dynamic model is found by using some system identification formulation. In choosing from the multitude of different system identification model types and structures, two factors are of prime importance: accuracy and ease of operation. System identification for use in response reconstruction is predominantly frequency based, and linear. Accuracy, ease of use, low calculation time, and minimal computing requirements prompted investigation into a time domain approach. More specifically the ARX model format, as presented by Ljung [ 40 ][ 41 ] combined with a time domain state space description was indicated by Raath [ 51 ] to be ideal for use in response reconstruction. The characteristics of the ARX model structure and the modifications thereof are briefly discussed.

In ( 4-1 )  $v(t)$  is an additional, unmeasurable disturbance (noise). Its properties can be expressed in terms of its spectrum  $\Phi_v(\omega)$ , which is defined as:

$$\Phi_v(\omega) = \sum_{\tau} R_v(\tau) e^{-j\omega\tau} \quad (4-3)$$

where  $R_v(\tau)$  is the covariance function of  $v(t)$  with  $E$  the mathematical expectation.

$$R_v(\tau) = E\{v(t)v(t-\tau)\} \quad (4-4)$$

Alternatively, the disturbance  $v(t)$  can be described as filtered white noise:

$$v(t) = H(v) \epsilon(t) \quad (4-5)$$

#### 4.1. ARX model structure

A basic single input, single output (SISO) dynamic system is presented in Figure 4.1, with a system input  $u(t)$ , output  $y(t)$  and a disturbance signal  $e(t)$ ;  $t = 1, 2, \dots, N$ . The development of the ARX model from the generalise time-invariant model structure is adapted from the work presented by Ljung [ 40 ].

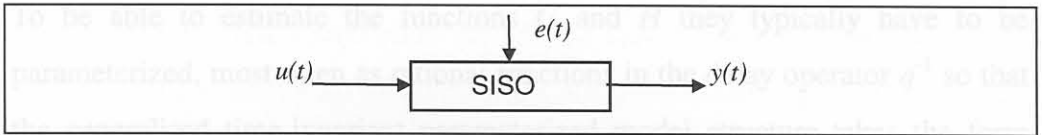


**Figure 4.1: Basic SISO configuration**

Assuming the signals are related by a linear system, we can write:

$$y(t) = G(q)u(t) + v(t) \quad (4-1)$$

where  $q$  is the shift operator and  $G(q)u(t)$  is short for

$$G(q)u(t) = \sum_{k=1}^{\infty} g(k)u(t-k) \quad (4-2)$$

In ( 4-1 )  $v(t)$  is an additional, unmeasurable disturbance (noise). Its properties can be expressed in terms of its spectrum  $\Phi_v(\omega)$ , which is defined as:

$$\Phi_v(\omega) = \sum_{\tau=-\infty}^{\infty} R_v(\tau)e^{-i\omega\tau} \quad (4-3)$$

where  $R_v(t)$  is the covariance function of  $v(t)$  with  $E$  the mathematical expectation.

$$R_v(\tau) = E v(t)v(t-\tau) \quad (4-4)$$

Alternatively, the disturbance  $v(t)$  can be described as filtered white noise:

$$v(t) = H(t) e(t) \quad (4-5)$$



Substitution into ( 4-1 ) gives the complete time domain description for the system of Figure 4.1.

$$y(t) = a_1 y(t-1) + \dots + a_{na} y(t-na) + b_0 u(t-nk) + b_1 u(t-nk-1) + \dots + b_{nb} u(t-nk-nb) + e(t) \quad (4-6)$$

To be able to estimate the functions  $G$  and  $H$  they typically have to be parameterized, most often as rational functions in the delay operator  $q^{-1}$  so that the generalised time-invariant parameterized model structure takes the form (Ljung [ 40 ]):

$$A(q)y(t) = \frac{B(q)}{F(q)}u(t) + \frac{C(q)}{D(q)}e(t) \quad (4-7)$$

where  $A(q)$ ,  $B(q)$ ,  $C(q)$ ,  $D(q)$  and  $F(q)$  are polynomials in the delay operator  $q^{-1}$ . Various simplifications can be applied, one of which leads to the ARX-model (Auto Regressive with eXogenous input).

$$A(q)y(t) = B(q)u(t) + e(t) \quad (4-8)$$

with:

$$A(q) = 1 + a_1 q^{-1} + a_2 q^{-2} + \dots + a_{na} q^{-na} \quad (4-9)$$

$$B(q) = b_0 + b_1 q^{-1} + b_2 q^{-2} + \dots + b_{nb} q^{-nb} \quad (4-10)$$

If  $nk$  is the number of delays from input to output the model is usually written as:

$$A(q)y(t) = B(q)u(t-nk) + e(t) \quad (4-11)$$

## 4.2. ARX Structure selection

If expanded, the ARX's polynomial structure may be written as a linear difference equation of the form:

$$y(t) = a_1 \cdot y(t-1) + \dots + a_{na} \cdot y(t-na) + \dots + b_0 \cdot u(t-nk) + b_1 \cdot u(t-nk-1) + \dots + b_{nb} \cdot u(t-nk-nb) \quad (4-12)$$

This is the one-step-ahead predictor for a SISO system. A novel method of expanding the ARX formulation for MIMO systems was proposed by Raath [ 52 ]. For a system with  $ny$  outputs, the ARX difference equation of ( 4-12 ) is expanded to  $ny$  multiple input, single output (MISO) one step ahead predictors, so that for each output channel  $k$ :

$$y_k(t) = y_1(t-1), \dots, y_1(t-na_1), y_2(t-1), \dots, y_2(t-na_2), \dots, y_{ny}(t-1), \dots, y_{ny}(t-na_{ny}), \dots + u_1(t-nk_1), \dots, u_1(t-nk_1-nb_1), u_2(t-nk_2), \dots, u_2(t-nk_2-nb_2), \dots, \dots, u_{nu}(t-nk_{nu}), \dots, u_{nu}(t-nk_{nu}-nb_{nu}) \quad (4-13)$$

These MISO models are combined into a MIMO discrete state space model description where:

$$\begin{aligned} x_{k+1} &= \Phi x_k + \Gamma u_k \\ y_k &= \mathbf{C} x_k + \mathbf{D} u_k \end{aligned} \quad (4-14)$$

and:  $x_k$  = state vector

$u_k$  = input vector

$y_k$  = output vector

$\Phi$  = state matrix

$\Gamma$  = input matrix

$\mathbf{C}$  = output matrix

$\mathbf{D}$  = direct transmission matrix

For brevity the combination of MISO models into a single MIMO model description is not included in this thesis, it is however presented in detail by Raath [ 51 ][ 52 ]. To further simplify the model description the "full order" approach to structure detection is presented in the next Section.

## 4.2. ARX Structure selection

For application in response reconstruction a black box model, which requires minimal information about the system prior to modelling is needed. The ARX formulation in ( 4-13 ) is a general black-box type model capable of accurately describing the dynamic behaviour of most linear engineering structures. It is however required to estimate the model structure prior to modelling, which for each output channel  $k$  involves:

- Selection of the number of  $a$  parameters,  $na_k$
- Selection of the number of  $b$  parameters,  $nb_k$
- Selection of the number of delays,  $nk_k$

For MIMO systems the number of model structure parameters to be estimated explodes for increasing numbers of channels. This problem is solved by utilisation of the “full order” approach, presented by Raath [ 51 ], which defines that for each output channel  $y_k(t)$  only the dynamic model order,  $n$ , must be selected. Equation ( 4-15 ) presents the relation between the parameters  $na$ ,  $nb$ , and  $nk$  and the dynamic model order  $n$  for each output channel  $k$ :

$$\begin{array}{l}
 na_i = n_k \\
 : \\
 nb_j = n_k + 1 \\
 nk_j = 0
 \end{array}
 \left. \begin{array}{l}
 \\
 \\
 \\
 \end{array} \right\}
 \begin{array}{l}
 i = 1, 2, \dots, ny \\
 j = 1, 2, \dots, nu
 \end{array}
 \quad (4-15)$$

Each MISO model is identified for increasing model orders to detect the optimal model structure, a relatively simple procedure, even for MIMO systems with large numbers of channels.

This full order MIMO-ARX model is the basis of the linear QanTiM package, and showed potential to be extended to include non-linear modelling terms. This expansion of the linear ARX model to the non-linear NARX model is presented in the next chapter.



## Chapter 5

### Non-linear time domain system identification: NARX

Successful implementation of linear ARX - state-space algorithms presented a further challenge: Non-linear system identification for use in response reconstruction. This could greatly improve simulation results, and eradicate the need for iterative linearization of the non-linear system. Investigation into inclusion of non-linear modelling in the QanTiM simulation system started with a survey of applicable modelling techniques. This survey is presented in Appendix A. Non-linear model requirements facilitating inclusion into response reconstruction are similar to that presented by Raath [ 51 ] for the linear case:

#### 5.1.1. MISO-NARX formulation

- Discrete.
- Multivariable.
- Time invariant.
- Black-box.
- Allow stable inversion.
- Allow use of model for simulation purposes.
- Accommodate simultaneous multiple-actuator identification.

Furthermore the model would be required to:

- Model highly non-linear systems (cubic polynomials).
- Include non-linear capabilities with minimal extra user input.
- Allow inclusion into existing QanTiM software.

This study investigates the NARX formulation, a polynomial non-linear extension of the ARX model used by QanTiM. Raath and Verwey [ 54 ], showed that the NARX model formulation satisfied all the above requirements, especially so for ease of use and possible compatibility with existing linear software. Detailed descriptions of the NARX model formulation, as well as the application thereof are given. Non-linear simulation and its limitations are discussed as well as modifications to the NARX structure for improved performance and QanTiM compatibility.

## 5.1. The NARX model

NARX (Non-linear Auto Regressive with eXogenous input) is a parametric difference equation that forms a convenient linear-in-the-parameters set of equations capable of describing systems with severe non-linearity. It is a special case of the general NARMAX [ 18 ] model in which only the system dynamics are taken into account. The NARMAX model is reduced to NARX by removal of the noise model and moving average terms, presented by Billings *et al.* [ 5 ] [ 9 ] and Peyton Jones [ 46 ] [ 47 ] .

$$y(t) = F^L[y(k-1), \dots, y(k-na), u(t-nk), \dots, u(t-nk-nb)] \quad (5-1)$$

With  $F^L[\bullet]$  some non-linear polynomial function.

### 5.1.1. MISO-NARX formulation

Consider the MIMO non-linear dynamic system presented in Figure 5.1. As with the linear ARX model, the MIMO-NARX consists of a combination of MISO models. Combining the NARX MISO models could however not be done as elegantly as for the ARX models. A system is identified for each output channel and the MISO NARX models are then combined in a one-step-ahead simulation routine as described in Section 5.4. The most general form of the MISO-NARX model [ 56 ] as shown in equation ( 5-2 ) describes each output  $y_k(t)$  as a function of inputs  $u_i(t)$  and outputs  $y_j(t)$ . With  $F^L[\bullet]$  some non-linear function.

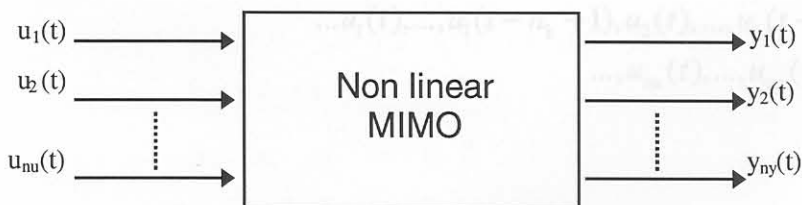


**Figure 5.1. Non-linear MIMO system**

$$y_k(t) = F^{L_k} [y_1(t-1), \dots, y_1(t-na_1), y_2(t-1), \dots, y_2(t-na_2), \dots, y_{ny}(t-1), \dots, y_{ny}(t-na_{ny}), \dots, \dots, u_1(t-nk_1), \dots, u_1(t-nk_1-nb_1), u_2(t-nk_2), \dots, u_2(t-nk_2-nb_2), \dots, \dots, u_{nu}(t-nk_{nu}), \dots, u_{nu}(t-nk_{nu}-nb_{nu})] \quad (5-2)$$

5.1.2. Non-linearity in the NARX model

- where for channel  $k$ :  $L_k$  = The degree of non-linearity within  $F$
- $na_k$  = dynamic model order for output  $y(t)$
- $nb_k$  = dynamic model order for input  $u(t)$
- $nk_k$  = time delay

The full order approach as proposed by Raath [ 53 ] is, as with the linear ARX model, used to greatly simplify modelling. Using this approach the model format is predicted with only two parameters per output channel namely:  $n$ , the dynamic model order, and  $L$ , the degree of non-linearity. Thus for each channel  $y_k(t)$  the following applies:

$$\begin{matrix} na_i = n_k \\ nb_j = n_k + 1 \\ nk_j = 0 \\ L_k = L_k \end{matrix} \left\{ \begin{matrix} i = 1, 2, \dots, ny \\ j = 1, 2, \dots, nu \end{matrix} \right. \quad (5-3)$$

By substituting the full order model parameters ( 5-3 ) into equation ( 5-2 ) the NARX formulation is reduced as shown in equation ( 5-4 ):

$$y_k(t) = F^{L_k} [y_1(t-1), \dots, y_1(t-n_k), y_2(t-1), \dots, y_2(t-n_k), \dots, y_{ny}(t-1), \dots, y_{ny}(t-n_k), \dots, \dots, u_1(t), \dots, u_1(t-n_k+1), u_2(t), \dots, u_2(t-n_k+1), \dots, \dots, u_{nu}(t), \dots, u_{nu}(t-n_k+1)] \quad (5-4)$$

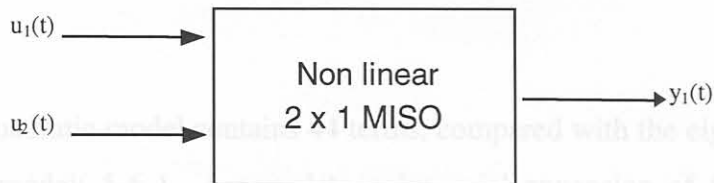


For a value of  $L_k = 1$ , the NARX model is identical to the linear ARX so that  $F^{L_k}[\text{ARX}] \Rightarrow \text{NARX}$ . NARX is thus a non-linear extension of the linear ARX as shown in the next Section.

### 5.1.2. Non-linearity in the NARX model

The NARX-model of ( 5-4 ) is described in terms of some non-linear function  $F^L[\bullet]$ . This function finds all unique combinations of  $L_k$ -degree multiples of the linear model terms. The non-linear structure is introduced in Example 5.1 for a specific MISO system to precede the more general formulation [ 12 ].

Example 5.1: NARX formulation for a simple MISO system



The second order linear ARX difference equation for a two-input single output system is:

$$\begin{aligned}
 y_1(t) = & y_1(t-1) \cdot a_{1_1} + y_1(t-2) \cdot a_{1_2} + \\
 & u_1(t) \cdot b_{1_1} + u_1(t-1) \cdot b_{1_2} + u_1(t-2) \cdot b_{1_3} + \\
 & u_2(t) \cdot b_{1_4} + u_2(t-1) \cdot b_{1_5} + u_2(t-2) \cdot b_{1_6}
 \end{aligned} \quad (5-5)$$

Using vector notation, we may further reduce it to:

$$\begin{aligned}
 X_{L_1}(t) &= [y_1(t-1) \quad y_1(t-2) \quad u_1(t) \quad \cdots \quad u_2(t-2)] \quad \text{and} \\
 \Theta_1 &= [a_{1_1} \quad a_{1_2} \quad b_{1_1} \quad \cdots \quad b_{1_6}]^T \\
 &= [\theta_{1_1} \quad \theta_{1_2} \quad \theta_{1_3} \quad \cdots \quad \theta_{1_8}]^T \\
 &\Rightarrow \\
 y_1(t) &= \sum_{i=1}^8 X_{L_1}(t,i) \cdot \theta_{1_i}
 \end{aligned} \quad (5-6)$$

Now extend this model to the non-linear second order quadratic NARX-formulation by adding all quadratic combinations of the linear regression vector  $X_{L1}(t)$ .

$$\begin{aligned}
 y_1(t) &= \sum_{i=1}^8 X_{L1}(t, i) \cdot \theta_{1i} + \sum_{R_1=1}^8 \sum_{R_2=1}^{R_1} \overbrace{X_{L1}(t, R_1) \cdot X_{L1}(t, R_2)}^{j=(9,10,\dots,44)} \cdot \theta_{1j} \\
 &= \sum_{i=1}^{44} \mathbf{X}_1(t, i) \cdot \theta_{1i} \\
 &= \mathbf{X}_1(t) \cdot \Theta_1
 \end{aligned} \tag{5-7}$$

where

$$\mathbf{X}_1(t) = \begin{bmatrix} \underbrace{X_{L1}(t)}_{\text{Linear}} & \underbrace{X_{L2}(t)}_{\text{Quadratic}} \end{bmatrix}, \text{ and}$$

$$X_{L2}(t) = \begin{bmatrix} y_1(t-1)^2 & y_1(t-1) \times y_1(t-2) & \dots & u_2(t-2)^2 \end{bmatrix}$$

This quadratic model contains 44 terms, compared with the eight of the linear model (5-6). A complete polynomial expansion of (5-7) is given in Appendix E.

The general form of the non-linear model is shown below for cubic ( $L=3$ ) non-linearity [14][56]:

$$\begin{aligned}
 y_k(t) &= \underbrace{\sum_{i=1}^R X_{L1}(t, i) \cdot \theta_{ki}}_{\substack{\text{Linear part} \\ L=1 \\ R=ny \cdot n + nu \cdot (n+1)}} + \underbrace{\sum_{R_1=1}^R \sum_{R_2=1}^{R_1} X_{L1}(t, R_1) \cdot X_{L1}(t, R_2) \cdot \theta_{kj}}_{\substack{\text{Quadratic part} \\ L=2 \\ j=(M_{L1}+1, M_{L1}+2, \dots, M_{L2})}} + \underbrace{\sum_{R_1=1}^R \sum_{R_2=1}^{R_1} \sum_{R_3=1}^{R_2} X_{L1}(t, R_1) \cdot X_{L1}(t, R_2) \cdot X_{L1}(t, R_3) \cdot \theta_{kj}}_{\substack{\text{Cubic part} \\ L=3 \\ j=(M_{L2}+1, M_{L2}+2, \dots, M_{L3})}} + \dots \\
 &= \sum_{i=1}^M \mathbf{X}_k(t, i) \cdot \theta_{ki}
 \end{aligned} \tag{5-8}$$

The variable  $M$  represents the maximum number of coefficients in the NARX-equation. In Equation( 5-8 ) the terms  $M_{L2}$  and  $M_{L3}$  respectively represent the number of terms for the quadratic and cubic parts of the NARX-model. The non-linear model is still linear-in-the-parameters even though it can describe systems with severe non-linearity.

### 5.1.3. Coefficients in the NARX model

For the SISO system the maximum number of coefficients is defined by Billings & Voon [ 7 ] as  $M$ :

$$M = \sum_{i=1}^L n_i$$

$$n_i = \frac{n_{i-1} \cdot (na + nb + i - 1)}{i}, \text{ where } n_0 = 1 \quad (5-9)$$

The author [ 14 ] showed that this equation does not hold for non-linear MIMO systems. Such a system's maximum number of coefficients for a specific output channel can be expressed by the following equations:

$$M_k = R + \sum_{R_1=1}^R \left[ R_1 + \sum_{R_2=1}^{R_1} \left[ R_2 + \sum_{R_3=1}^{R_2} \left[ R_3 + \dots + \sum_{R_L=1}^{R_{L-1}} R_L \right] \right] \right]$$

$$R = ny \cdot n_k + nu \cdot (n_k + 1) \quad (5-10)$$

The number of coefficients explodes with increasing degrees of non-linearity, prompting investigation into reduced parameter modelling [ 8 ] [ 38 ] [ 39 ]. Reduction of the number of model parameters can be done by structure selection prior to modelling, as discussed in Section 5.5, or by making use of a reduced parameter estimation technique, as discussed in Section 5.3



### 5.3. NARX parameter estimation

#### 5.2. NARX regression

Transformation of input-output data into the NARX formulation of Equation ( 5-4 ) and ( 5-8 ) is done in such a manner as to maintain generality at all times. Based on the work by Leontaritis [ 38] for NARMAX systems, Equation ( 5-8 ) is written in matrix formulation, with the non-linear extensions appended to the linear ARX regression matrix so as to maintain a linear-in-parameters set of equations.

$$\mathbf{Y}_k = \mathbf{X}_k \cdot \Theta_k \quad (5-11)$$

where:  $\mathbf{Y}_k^T = [y_k(1) \ y_k(2) \ \dots \ y_k(t) \ \dots \ y_k(N)]$

$$\Theta_k^T = [\theta_{k_1} \ \theta_{k_2} \ \dots \ \theta_{k_M}]$$

$$\mathbf{X}_k = [X_{L1} \ X_{L2} \ X_{L3} \ \dots]$$

$$= \begin{bmatrix} X_k(1,1) & X_k(1,2) & \dots & X_k(1,M) \\ X_k(2,1) & X_k(2,2) & \dots & X_k(2,M) \\ \vdots & \vdots & & \vdots \\ X_k(t,1) & X_k(t,2) & \dots & X_k(t,M) \\ \vdots & \vdots & & \vdots \\ X_k(N,1) & X_k(N,2) & \dots & X_k(N,M) \end{bmatrix} \quad (5-12)$$

The procedure of finding a MISO NARX regression matrix is to be repeated for each output channel of the MIMO system. A number of such regression methods were developed by the author, a summary of these algorithms is presented in Appendix B. The next step in the system identification process is to find the NARX coefficient matrix  $\Theta_k$ . Methods in which these coefficients can be estimated are the subject of the next Section.

### 5.3. NARX parameter estimation

Parameter estimation is the process of finding the unknown coefficients  $\theta_i$  for the NARX equation and thus identifying the dynamic characteristics of the system. A number of well-studied methods are available for parameter estimation, most of which are well suited to the NARX model.

The majority of the parameter estimation techniques can be placed into two categories: Prediction error methods and Correlation methods. [ 7 ] [ 8 ] [ 18 ] [ 36 ] The first being concerned with minimising some error function for the identification model. Correlation techniques are however concerned with finding the solution for some function. Various authors [ 1 ] [ 4 ] [ 7 ] [ 51 ] showed prediction error methods to be best suited to practical system identification. In this thesis the focus will thus remain on the prediction error methods for finding the parameter vector of the NARX-model.

A loss function  $J[\bullet]$  can be defined with the following form:

$$J = \frac{1}{N} \cdot \sum_{\tau=1}^N f(\varepsilon(\tau)) \quad (5-12)$$

With  $f(\bullet)$  some positive function of the identification error  $\varepsilon(t) = y(t) - X(t) \cdot \Theta$ .

The basis of the prediction error methods now lies with finding a set of parameters  $\Theta$  associated with minimising this loss function. Various techniques are based on this principle, including Least Squares [ 52 ] , Extended Least Squares [ 8 ], and Maximum Likelihood [ 7 ] parameter estimation. The Least Squares technique is inherently suited to the NARX-model and computationally simple to apply. According to Strejc [ 58 ] "It may be stressed that in the field of parameter estimation the Least Squares technique has reached a significant level of popularity and perfection." It is thus the only technique that will be covered in this study. Various solutions to the Least Squares problem are however given.

### 5.3.1. The Least Squares problem

Gauss defined: "the most probable value of the unknown quantities will be that one for which the sum of the squares of the differences between the actually observed and computed values multiplied by numbers that measure the degree of precision is a minimum". In a Least Squares form the loss function of Equation ( 5-12 ) is thus described with  $f(\bullet)$  a quadratic function of  $\varepsilon(t)$  which can be minimised with respect to  $\Theta$ : Equation [ 29 ]

$$J = \frac{1}{N} \cdot \sum_{\tau=1}^N (\varepsilon(\tau))^2 \quad (5-13)$$

This defines the Least Squares equation ( 5-13 ) for a specific output channel.

$$y_k(t) = X_k(t) \cdot \Theta_k + \varepsilon_k(t) :$$

Table 5.1: Obstacles in finding the inverse  $[X^T X]^{-1}$

Size	Large number of terms in the NARX regression
Ill-conditioning	Presented a problem for existing inversion processes. Most NARX regression processes showed signs of ill conditioning
Linear dependency	Incorrect sampling rates captured data with similar samples, resulting in a regression matrix with

Substitute into  $\varepsilon_k = Y_k - X_k \cdot \Theta_k$  into ( 5-14 ) and expand the expressions to obtain the following equation for the loss function.

$$\begin{aligned} J_k &= \frac{\varepsilon_k^T \cdot \varepsilon_k}{2} \\ &= \frac{(Y_k - X_k \cdot \Theta_k)^T \cdot (Y_k - X_k \cdot \Theta_k)}{2} \\ &= \frac{Y_k^T \cdot Y_k - 2 \cdot (Y_k^T \cdot X_k \cdot \Theta_k) + (X_k \cdot \Theta_k)^T X_k \cdot \Theta_k}{2} \end{aligned} \quad (5-15)$$

### 5.3.1.1. Orthogonal decomposition

The Least Squares estimation of  $\Theta_k$  is found by minimising the loss function  $J_k$  with respect to  $\Theta_k$

$$\frac{d}{d\Theta_k}(J_k) = \frac{\mathbf{X}_k^T \cdot \mathbf{X}_k \cdot \Theta_k - \mathbf{X}_k^T \cdot \mathbf{Y}_k}{2} \quad (5-16)$$

and  $J_k(\Theta_k)$  is thus a minimum for :

$$\begin{aligned} \mathbf{X}^T \cdot \mathbf{X} \cdot \Theta - \mathbf{X}^T \cdot \mathbf{Y} &= 0 \\ \Downarrow \\ \Theta &= [\mathbf{X}^T \cdot \mathbf{X}]^{-1} \cdot \mathbf{X}^T \cdot \mathbf{Y} \end{aligned} \quad (5-17)$$

This is the familiar Least Squares equation [ 8 ][ 52 ][ 58 ] which is valid only if  $[\mathbf{X}^T \cdot \mathbf{X}]^{-1}$  exists which proved not trivial for various reasons, including:

**Table 5.1: Obstacles in finding the inverse  $[\mathbf{X}^T \cdot \mathbf{X}]^{-1}$**

Size	The large number of terms in the NARX regression matrix presented a problem for existing inversion processes.
Ill-conditioning	More often than not, the NARX regression matrix showed signs of ill conditioning
Linear dependency	Incorrect sampling rates captured data with similar samples, resulting in a regression matrix with linearly dependant rows.

A survey of finding the solutions to the Least Squares equation ( 5-17 ) is presented in Appendix C and D for full, as well as condensed parameter sets. This survey of parameter estimation techniques showed that methods based on orthogonal decomposition to be the most effective for finding the inverse  $[\mathbf{X}^T \cdot \mathbf{X}]^{-1}$ . The concepts of a condensed model structure and the associated parameter estimation techniques are discussed in Section 5.3.2.



### 5.3.1.1. Orthogonal decomposition

Parameter estimation techniques based on orthogonal decomposition [ 36 ], [ 58 ] of the NARMAX and, similarly, the NARX regression matrix proved the most effective. These methods all have in common that a matrix  $\mathbf{X}$  can be transformed into an orthogonal matrix  $\mathbf{Q}$  and an upper triangular matrix  $\mathbf{R}$  so that.

$$\mathbf{X} = \mathbf{Q} \cdot \mathbf{R} \quad (5-18)$$

### 5.3.2. Full vs. reduced parameter modelling

Transform the Least Squares equation, in order to find the parameter vector  $\Theta$ .

$$\begin{aligned} \Theta &= [\mathbf{X}^T \cdot \mathbf{X}]^{-1} \cdot \mathbf{X}^T \cdot \mathbf{Y} \\ \mathbf{X}^T \cdot \mathbf{X} \cdot \Theta &= \mathbf{X}^T \cdot \mathbf{Y} \end{aligned} \quad (5-19)$$

Substitute  $\mathbf{X} = \mathbf{Q} \cdot \mathbf{R}$

$$\begin{aligned} [\mathbf{Q} \cdot \mathbf{R}]^T \cdot \mathbf{Q} \cdot \mathbf{R} \cdot \Theta &= [\mathbf{Q} \cdot \mathbf{R}]^T \cdot \mathbf{Y} \\ \mathbf{Q}^T \cdot \mathbf{R}^T \cdot \mathbf{Q} \cdot \mathbf{R} \cdot \Theta &= \mathbf{Q}^T \cdot \mathbf{R}^T \cdot \mathbf{Y} \end{aligned} \quad (5-20)$$

but  $\mathbf{Q}^T \cdot \mathbf{Q} = \mathbf{I}$

$$\mathbf{R}^T \cdot \mathbf{R} \cdot \Theta = \mathbf{Q}^T \cdot \mathbf{R}^T \cdot \mathbf{Y} \quad (5-21)$$

$$\mathbf{R} \cdot \Theta = [\mathbf{R}^T]^{-1} \cdot \mathbf{Q}^T \cdot \mathbf{R}^T \cdot \mathbf{Y}$$

thus

$$\Theta = [\mathbf{R}^T]^{-1} \cdot \mathbf{Q}^T \cdot \mathbf{Y} \quad (5-22)$$

$$\Theta = [\mathbf{R}^T]^{-1} \cdot \mathbf{Q}^T \cdot \mathbf{Y}$$

#### 5.4. Simulation of NARX systems

Methods for solving the Least Squares equation using orthogonal decomposition include:

- Classical Gram Schmidt methods [ 11 ]
- Modified Gram Schmidt methods [ 10 ], [ 32 ] and
- Householder transformations [ 32 ]

These methods are discussed in Appendix C and D

#### 5.3.2. Full vs. reduced parameter modelling

Korenberg [ 36 ] indicated that “provided the significant terms in the model can be detected, models with fewer than ten terms are usually sufficient to capture the dynamics of highly non-linear processes.” This presents the problem of structure detection for the NARX equation. Appendix D details various methods for finding a reduced set of parameters i.e. discarding terms in the NARX equation which do not contribute to the dynamic behaviour of the system. These methods all require the full set of NARX coefficients to be available for evaluation, thus an initial full set regression and parameter estimation is required prior to structure detection. Further the structure detection processes proved computationally cumbersome. More importantly simulation of the NARX models proved insensitive to the number of terms involved. The author found that the amount of effort concerned with model reduction does not warrant the implementation thereof. Full parameter set modelling proved more practical to investigate the implementation of NARX in structural response reconstruction.

#### 5.4. Simulation of NARX systems

In the linear case a state space representation of the ARX model was calculated prior to simulation. This MIMO state space system proved convenient, especially so for linear application within Matlab [ 53 ]. A non-linear equivalent of this model format conversion, that is NARX to state space, can be done in the same way for a specific system. Formulation of a general NARX to state space procedure is however not trivial and the simulation of non-linear differential state space equations is computationally taxing. The non-linear state space simulation algorithms created and implemented by the author proved too complex and mathematically expensive to warrant further investigation, application or discussion. The purpose of this study does not warrant an extensive investigation into general NARX to state space conversion algorithms. A simulation algorithm that made use of a step-ahead-predictor nested in a sample point loop proved an effective method for simulation non-linear systems. This non-linear simulation algorithm makes full use of the linear-in-the-parameters structure of the NARX model, in principle done according to Algorithm 5.1. It is a direct implementation of Equation ( 5-4 ).

##### Algorithm 5.1: NARX simulation

INPUT:	Dynamic system input data:	$u_1(t), u_2(t) \dots, u_{nu}(t)$
	NARX model coefficients for each o/p channel	$\Theta_k$
	Dynamic model order for each o/p channel:	$n_k$
	Degree of non-linearity for each o/p channel:	$L_k$
	Number of sample points to use in regression	$N$
	Number of input and output channels	$nu, ny$
OUTPUT:	Dynamic system output data:	$y_1(t), y_2(t) \dots, y_{ny}(t)$
	FOR $t = 1, 2, \dots, N$	Sample point loop
	FOR $k = 1, 2, \dots, ny$	Channel loop
	$X_k(t) = f(u, y, na, L)$	Calculate non-linear regression vector for channel $k$ at sample point $t$
	$y_k(t) = X_k(t) \cdot \Theta_k$	Calculate the value for output channel $y_k$ at sample point $t$ . Note that $\cdot$ denotes a vector product operation so that $y_k(t) = X_k(t) \cdot \Theta_k = \sum_{i=1}^M X_k(t, i) \cdot \theta_{k_i}$
		with $M$ the number of coefficients in the NARX equation.



This basic simulation loop ( Algorithm 5.1 ) however proved extremely slow due to the regression operation at each sample point. This regression includes the process of finding the appropriate combinations of linear model terms to form the non-linear extensions to the ARX format. Another limitation is the use of a sample point main loop, which implies the simulation may become slow for large data sets. Due to the one-step-ahead nature of the algorithm a more elegant method than this sample point loop could not be found. The problem of regression and NARX structure formulation at each sample point is solved by careful use of Matlab's matrix capabilities. This was done by defining a condensed NARX model structure which, once identified, could easily be passed to the simulation algorithm and thus eradicate the need to recalculate the NARX structure.

#### 5.4.1. Condensed NARX model structure

The NARX coefficient vector  $\Theta_k$  completely characterises the  $k^{th}$  channel of the system. Thus if all  $n_y$  coefficient vectors are known the system can be considered thoroughly identified. This format is however not convenient for simulation purposes since for each channel a separate set of coefficients must be stored, and passed to various functions. Furthermore, for the purpose of simulation, the NARX model structure, i.e. the non-linear combinations of linear ARX terms to be multiplied must be recalculated.

The author defined a model structure that contains the coefficient vectors for all system channels, as well as model information such as model order and degree of non-linearity for each channel. This condensed NARX structure further contained the combinations of all non-linear terms within the model. The elements contained in the condensed model structure for each channel are described in Table 5.2.



**Table 5.2. Model descriptors for output channel k**

NARX coefficient vector	$\Theta_k^T = [\theta_{k_1} \theta_{k_2} \dots \theta_{k_M}] \quad (1 \times M_k)$		
Model parameters	Model order:	$n_k$	$(1 \times 1)$
	Degree of non-linearity:	$L_k$	$(1 \times 1)$
	Number of model terms:	$M_k$	$(1 \times 1)$
	Number of quadratic terms:	$ML2_k$	$(1 \times 1)$
	Number of cubic terms:	$ML3_k$	$(1 \times 1)$
Non-linear combination vectors	Quadratic combinations:	$\Pi2_k$	$(2 \times ML2_k)$
	Cubic combinations:	$\Pi3_k$	$(3 \times ML3_k)$

The model parameters of Table 5.2 are written into a model parameter matrix  $Mpar_k$  for each channel k. These MISO models are then appended into a single model parameter matrix for all system channels, as shown in Equation ( 5-23 ) The condensed NARX model structure was implemented to accommodate, at most, cubic ( $L=3$ ) non-linear models.

$$Mpar_k = \left[ \begin{array}{c} \left[ \dots \quad \Theta_k^T \quad \dots \right] \\ \left[ n_k \quad L_k \quad M_k \quad M_{L2_k} \quad M_{L3_k} \right] \\ \left. \begin{array}{c} \left[ 1 \quad 1 \quad \dots \quad 2 \quad \dots \quad M_k \right] \\ \left[ 1 \quad 2 \quad \dots \quad 2 \quad \dots \quad M_k \right] \end{array} \right\} \Pi2_k \\ \left. \begin{array}{c} \left[ 1 \quad 1 \quad \dots \quad 1 \quad \dots \quad 2 \quad \dots \quad M_k \right] \\ \left[ 1 \quad 1 \quad \dots \quad 2 \quad \dots \quad 2 \quad \dots \quad M_k \right] \\ \left[ 1 \quad 2 \quad \dots \quad 2 \quad \dots \quad 2 \quad \dots \quad M_k \right] \end{array} \right\} \Pi3_k \end{array} \right] (7 \times M_k)$$

$$Mpar = \begin{bmatrix} Mpar_1 \\ Mpar_2 \\ \vdots \\ Mpar_{ny} \end{bmatrix}$$

( 5-23 )

The condensed NARX model structure has the capability to model so called non-square systems. That is a dynamic system of which the number of inputs differs from the number of outputs. The author developed simulation algorithms using this condensed NARX model structure that are sufficiently fast to allow implementation in general non-linear system identification and response reconstruction. The computation time of the algorithm is directly proportional to the length of the data. A linear regression operation must still be performed at each sample point, but the non-linear combinations thereof need not be done. A revised simulation procedure is presented in Algorithm 5.2

**Algorithm 5.2: NARX condensed model structure simulation**

INPUT:	Dynamic system input data:	$u_1(t), u_2(t) \dots, u_{nu}(t)$
	NARX condensed model parameter matrix	$Mpar$
OUTPUT:	Dynamic system output data:	$y_1(t), y_2(t) \dots, y_{ny}(t)$

<i>FOR</i> $k = 1, 2, \dots, ny$	<i>Channel loop</i>
$Mpar_k = f(Mpar)$	<i>Extract model parameter matrix for channel k</i>
$\Theta_k = f(Mpar_k)$	<i>Extract NARX coefficient vector for channel k</i>
$na_k = f(Mpar_k)$	<i>Extract model parameters for channel k</i>
$L_k = f(Mpar_k)$	
$M_k = f(Mpar_k)$	
$ML2_k = f(Mpar_k)$	
$ML3_k = f(Mpar_k)$	
$I\Omega_k = f(Mpar_k)$	<i>Extract non-linear combination matrices for channel k</i>
$I\beta_k = f(Mpar_k)$	
<i>FOR</i> $t = 1, 2, \dots, N$	<i>Sample point loop</i>
<i>FOR</i> $k = 1, 2, \dots, ny$	<i>Channel loop</i>
$XL1_k(t) = f(u, y, na)$	<i>Calculate linear regression vector for channel k at sample point t</i>
$XL2_k(t) = f(XL1_k(t), I\Omega_k)$	
$XL3_k(t) = f(XL1_k(t), I\beta_k)$	<i>Calculate the non-linear terms of the regression matrix using the linear ARX terms and the non-linear combination vectors.</i>
$X_k(t) = [XL1_k(t) XL2_k(t) XL3_k(t)]$	
$y_k(t) = X_k(t) \cdot \Theta_k$	<i>Calculate the value for output channel <math>y_k</math> at sample point t.</i>

## 5.5. Modified NARX systems

The number of terms in the NARX formulation tends to explode for systems with high degrees of non-linearity and large numbers of input and output channels. Furthermore, numerical techniques tend to become unstable for models with large numbers of non-linear terms. It would thus be ideal to limit the number of terms within the NARX model. The concept of reduced parameter modelling was introduced in Section 5.3.2, which concluded sub-set selection techniques to be computationally too taxing to warrant implementation. An alternative route is to select a non-linear model structure prior to identification. A number of special cases of the NARX model were defined and are presented in Sections 5.5.1. through 5.5.4.

### 5.5.1. Purely Quadratic NARX

An approach similar to the bi-linear model (Appendix A.3.2) was used to limit the number of model terms, yet maintain a high degree of non-linear modelling capability. The purely quadratic NARX, as shown in Equation ( 5-24 ) for a SISO system, includes all quadratic combinations of the linear ARX model, without any non-linear cross-coupling terms.

$$y_k(t) = a_0 + \sum_{i=1}^{n_k} a_i \cdot y(t-i) + \sum_{i=1}^{n_k+1} b_i \cdot u(t-i) + \sum_{i=1}^{2n_k+1} c_i \cdot (u(t-i))^2 + \sum_{i=1}^{2n_k+1} d_i \cdot (y(t-i))^2 \quad (5-24)$$

Parameter estimation for the purely quadratic NARX is done exactly the same as for the full parameter set NARX model.



### 5.5.3. Split spectra linear-non-linear modelling

#### 5.5.2. Quasi-Static NARX

Block orientated models (Appendix A.2) include the concept of modelling system dynamics linearly and only the static system behaviour with a non-linear model. An implementation of such a modelling approach was presented by Billings and Fakhouri [ 4 ]. Their approach utilised the first two kernels in the Volterra series expansion, which proved too complex for practical application. The author implemented a similar approach for NARX models, where only the static part of the system behaviour is modelled non-linearly. A simple method to implement this quasi-static NARX, is to include the entire linear ARX model but append only the static combinations (dynamic order = 0) in the non-linear extension. Consider again the two input single output system presented in Example 5.1 Equation ( 5-25 ) shows only the static relation between the two input channels and the output squared.

$$\begin{aligned}
 y_1(t) = & y_1(t-1) \cdot a_{1_1} + y_1(t-2) \cdot a_{1_2} + \\
 & u_1(t) \cdot b_{1_1} + u_1(t-1) \cdot b_{1_2} + u_1(t-2) \cdot b_{1_3} + \\
 & u_2(t) \cdot b_{1_4} + u_2(t-1) \cdot b_{1_5} + u_2(t-2) \cdot b_{1_6} + \\
 & (u_1(t))^2 \cdot c_{1_1} + (u_2(t))^2 \cdot c_{1_2}
 \end{aligned} \quad (5-25)$$

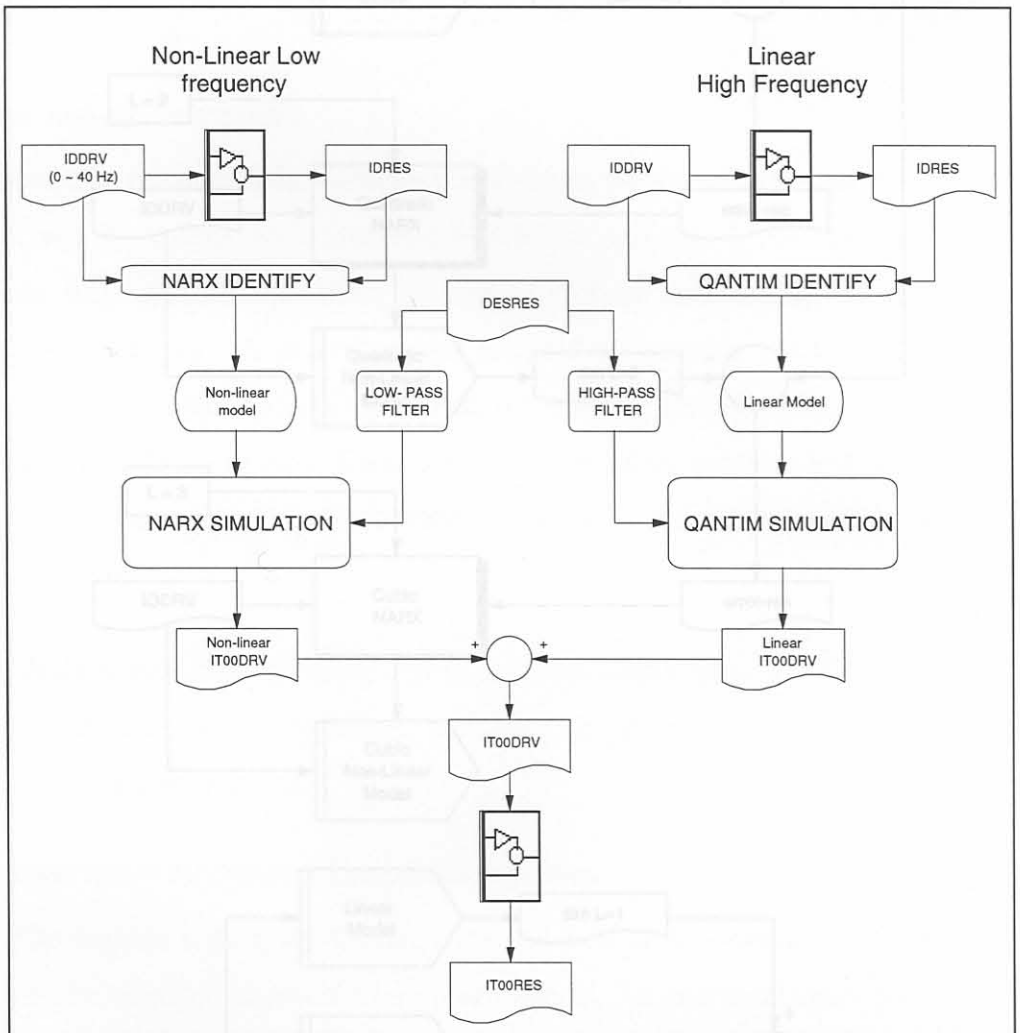
A more direct approach is to apply the split-spectra modelling concept as presented in Section 3.2 to non-linear systems.

Figure 5.2: Linear-non-linear split spectra modelling

The linear-non-linear split spectra modelling technique proved ideal to model the low frequency high amplitudes associated with non-linear response, as well as the high frequency linear dynamics of a system.

### 5.5.3. Split spectra linear-non-linear modelling

The linear-non-linear split spectra modelling procedure presented in Figure 5.2 is similar to the linear system split spectra approach, only here the low frequency part of the data is modelled with non-linear algorithms, and the high frequency dynamics with the conventional linear ARX formulation.



**Figure 5.2: Linear-non-linear split spectra modelling**

The linear-non-linear split spectra modelling technique proved ideal to model the low frequency high amplitudes associated with non-linear response, as well as the high frequency linear dynamics of a system.

*Figure 5.3: Non-linear error signal modelling*

### 5.5.4. Non-linear error signal modelling

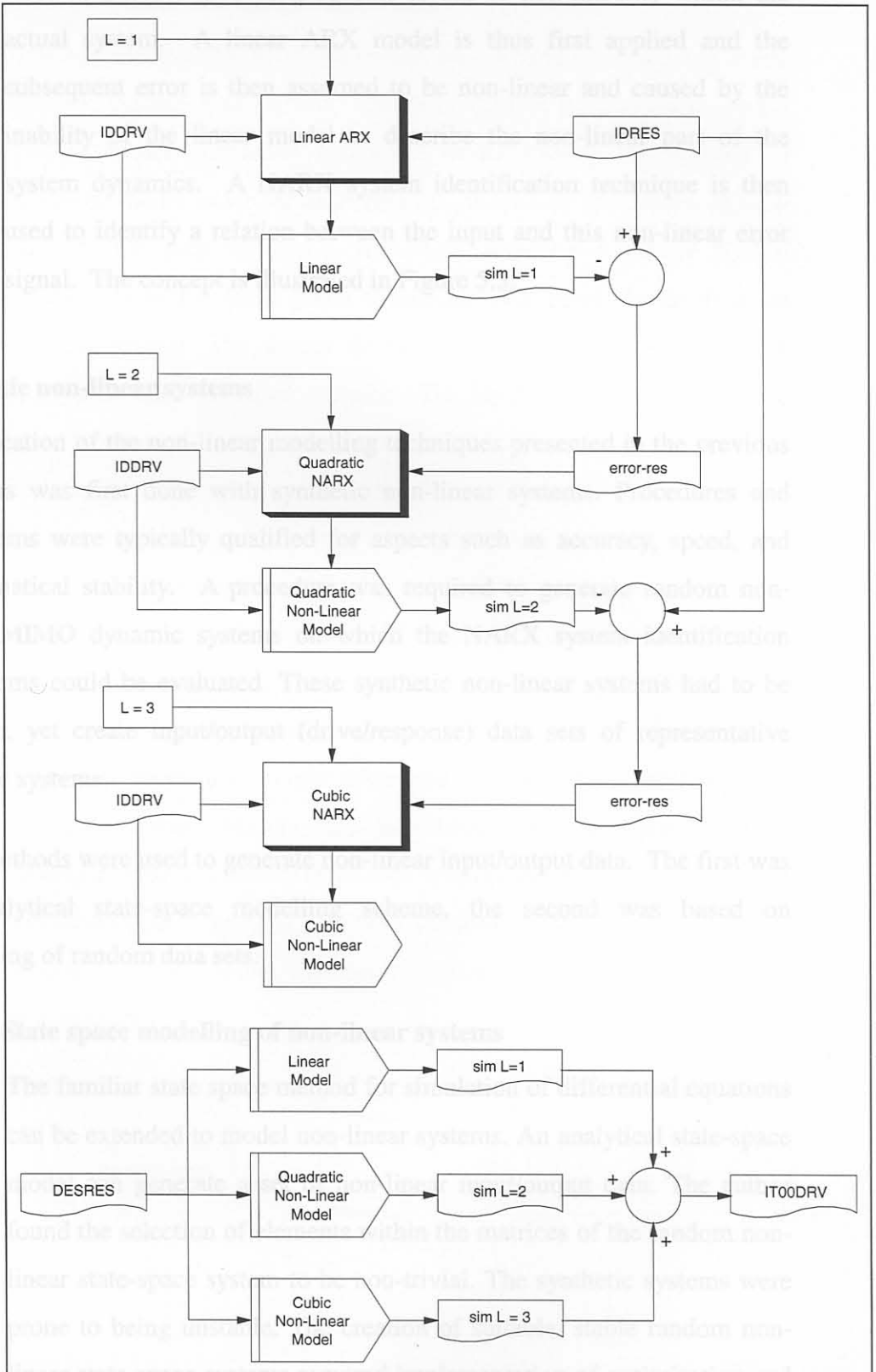


Figure 5.3: Non-linear error signal modelling

Non-linear error signal modelling is based on the assumption that the error in a linear modelling scheme is due to non-linearity within the actual system. A linear ARX model is thus first applied and the subsequent error is then assumed to be non-linear and caused by the inability of the linear model to describe the non-linear part of the system dynamics. A NARX system identification technique is then used to identify a relation between the input and this non-linear error signal. The concept is illustrated in Figure 5.3.

## 5.6. Synthetic non-linear systems

Qualification of the non-linear modelling techniques presented in the previous Sections was first done with synthetic non-linear systems. Procedures and algorithms were typically qualified for aspects such as accuracy, speed, and mathematical stability. A procedure was required to generate random non-linear MIMO dynamic systems on which the NARX system identification algorithms could be evaluated. These synthetic non-linear systems had to be random, yet create input/output (drive/response) data sets of representative real-life systems.

Two methods were used to generate non-linear input/output data. The first was an analytical state-space modelling scheme, the second was based on modelling of random data sets.

### 5.6.1. State space modelling of non-linear systems

The familiar state space method for simulation of differential equations can be extended to model non-linear systems. An analytical state-space model can generate a set of non-linear input/output data. The author found the selection of elements within the matrices of the random non-linear state-space system to be non-trivial. The synthetic systems were prone to being unstable. The creation of suitable, stable random non-linear state space systems required implementation of optimisation and non-linear control system techniques [ 48 ]. Subsequently, a more simplistic alternative approach was devised.



### 5.6.2. Random non-linear input/output data

A more general and easy to use system for creating synthetic non-linear dynamic systems was needed. The desired input parameters to such a random model generation technique would include the number of channels, model order for each channel, as well as the degree of non-linearity for each channel. Randomly selecting a set of NARX coefficients within these given parameters will generally result in an unstable system. The author devised a technique to create random stable non-linear dynamic systems. The input/output data from these systems could then be used to test the various non-linear algorithms. The random non-linear model generator as shown in Figure 5.4 makes use of a random signal generator to create two sets of random data. The first set will be used as a pseudo drive and the second as a pseudo response for the random model. These random data sets comply with the desired number of system channels. A NARX identification routine is then used to find a model parameter matrix which best describes the relation between the pseudo drive and response data, resulting in a random non-linear model. Valid non-linear input/output data can now be obtained by simulating drive data through the model and recording the subsequent responses. These random models proved ideal for evaluation of the various parameter estimation techniques as described in Appendix C.

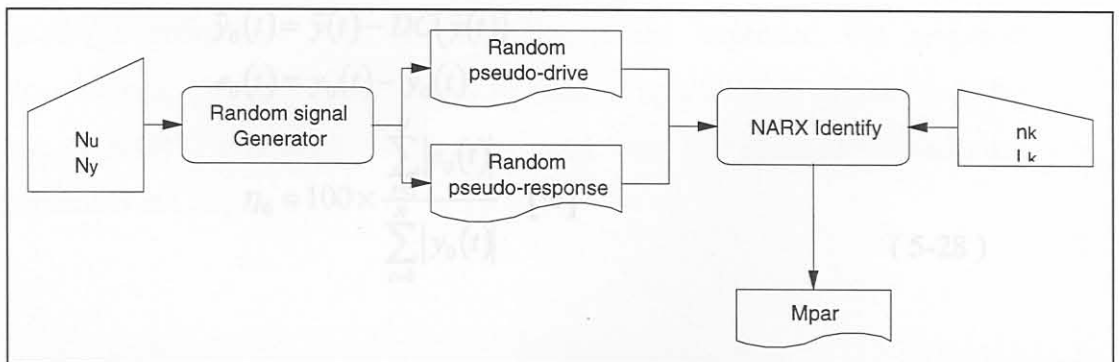


Figure 5.4: Random non-linear model generator

## 5.7. Error functions

It is important to be able to quantify the success of a simulation exercise. The QanTiM fit value [ 34 ] as used in the linear simulation package also proved ideally suited to judge non-linear simulation accuracy. An error function  $e_y$  is defined by subtracting the achieved simulation response from the desired response.

$$e_y(t) = y(t) - \hat{y}(t) \quad (5-26)$$

The QanTiM fit value is then calculated for each channel for N data points.

$$\eta_y = 100 \times \frac{\sum_{t=1}^N |e_y(t)|}{\sum_{t=1}^N |y(t)|} \quad (5-27)$$

The error function as presented in ( 5-27 ) is inappropriate for responses with high DC offsets. The error value,  $\eta_y$  for a response signal with a DC offset will be factored by the DC value and thus be lower than actually is the case. Removing all DC offsets prior error quantification can however rectify this problem. In Equation ( 5-28 ) the author revised the QanTiM fit value. This DC-corrected function is used for evaluation of all simulation results.

$$y_0(t) = y(t) - DC(y(t))$$

$$\hat{y}_0(t) = \hat{y}(t) - DC(\hat{y}(t))$$

$$e_0(t) = y_0(t) - \hat{y}_0(t)$$

$$\eta_0 = 100 \times \frac{\sum_{t=1}^N |e_0(t)|}{\sum_{t=1}^N |y_0(t)|} \quad [\%] \quad (5-28)$$

## Chapter 6

## 5.8. Detecting non-linearity

Ideally a system should be classified as linear, or non-linear prior to modelling and thus warrant the use of a non-linear model. The general problem with non-linear modelling is determining which type of non-linearity, if any, is applicable. This could be polynomial, exponential, dead bands, signum functions or any other type of non-linearity. This difficulty is not encountered in linear systems modelling, which has largely attributed to the popularity of linear modelling.

Billings and Fadzil [ 6 ] suggested to plot the system gain against amplitude for a series of step inputs of varying amplitudes. This method is however not suited to practical mechanical systems, especially so for servo-hydraulic testing applications. Another method as suggested by Billings and Voon [ 8 ] showed that whenever the input:  $u(t) + b, \bar{u}(t) = 0, b \neq 0$  is applied to a system, the system cannot be linear if  $\bar{z}_b(t) \neq \bar{z}(t)$  where  $\bar{z}_b(t)$  and  $\bar{z}(t)$  are the mean levels of the system output for the inputs  $b$  (i.e.  $u(t) = 0$ ) and  $u(t)+b$  respectively. In theory, this method based on evaluation of system mean responses is applicable to most servo-hydraulic test systems. In practice, however, comparison between linear and non-linear modelling of a system proved the best practical method of detecting non-linearity. Typically a system which proved difficult to model linearly was then identified using the NARX formulation. Generally the optimal model order as found in the linear case was then used along with a quadratic polynomial. If the modelling results improved, but remained unsatisfactory, a cubic model could be used. Application examples were the use of NARX techniques did improve modelling and simulation results are presented in Chapter 6.



## Chapter 6

### Application of non-linear system identification

The principles introduced in chapter 5 were implemented into a comprehensive toolbox of NARX related Matlab M-functions (see Appendix F). These functions include non-linear system identification and simulation tools that allow relative easy access to complex mathematical routines capable of modelling severely non-linear MIMO dynamic systems. All applications, NARX and the various modifications thereof, make use of a full parameter set estimation technique based on the orthogonal decomposition method described in Section 5.3.

In general, practical test systems did not warrant the use of the non-linear techniques. NARX techniques did not necessarily render improved simulation results on test systems for which the linear QanTiM techniques failed to accurately simulated system responses. Typical examples of such test systems are listed in Table 6.1.

**Table 6.1 Test rigs were NARX did not alleviate problems encountered with QanTiM**

No. of axis	Test specimen / configuration	Desired response
7	Commercial vehicle load body [ 13 ]	Operational acceleration response
7	Commercial vehicle load body [ 59 ]	Operational acceleration response
7	Chassis mounted fuel tank [ 17 ]	Operational acceleration response
5	Aircraft engine cradle [ 12 ]	Pre-defined flight load spectrum
4	Full vehicle road simulation [ 24 ]	Operational acceleration response
3	Heavy vehicle engine assembly [ 45 ]	Operational acceleration response
2	Commercial vehicle fuel tank assembly [ 50 ]	Operational acceleration response
1	Motorcycle rear wheel simulator (LGI)	Operational strain response

Some test systems did however render improved simulation results with NARX techniques. Furthermore, the NARX technique showed potential as a general modelling tool, capable of accurately modelling highly non-linear dynamic systems. Examples of NARX modelling and simulations are presented for five practical test systems.



### 6.1. Case study 1: Non-linear elastomeric damper

Elastomeric damper units generally show highly non-linear stiffness characteristics. The static displacement / load relationship of an elastomeric cabin mounting damper used on off-road vehicles is shown in Figure 6.1(a). The damper unit showed severe non-linearity including hysteresis.

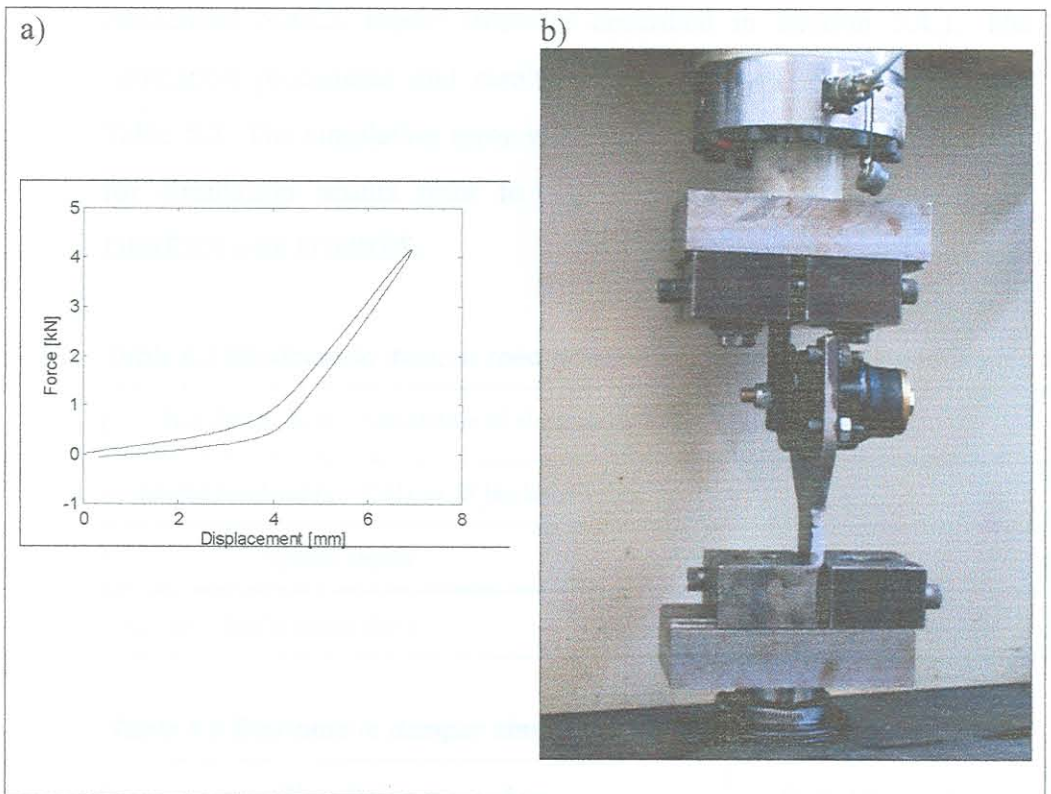


**Figure 6.1 Elastomeric damper static stiffness characteristics and test set-up**

Two application examples are presented for the elastomeric damper test system shown in Figure 6.1(b):

- Test 1: A road simulation test, reproducing damper load responses measured while travelling through an obstacle on a rough gravel road.
- Test 2: The damper test system is utilised to demonstrate the application of non-linear error signal modelling.

### 6.1.1. Reconstruction of elastomeric damper field load response

The damper unit was subjected to tests that simulate loads measured whilst negotiating a slow ditch. The dynamic response of the damper unit was simulated using linear QanTiM methods, as well as the condensed NARX model structure described in Section 5.4.1. The simulation procedures and results are summarised in Table 6.2 and Table 6.3. The simulation error values (see Section 5.7) are calculated for simulation results prior to any iteration, i.e. a comparison of DESRES with IT00RES.

**Table 6.2 Elastomeric damper road simulation test – System summary**

Test description: Simulation of elastomeric damper load response	
Model bandwidth: 0 Hz to 25 Hz Bandwidth	
System Inputs	System Outputs
Actuator displacement drive	Damper load response

**Table 6.3 Elastomeric damper simulation results**

Simulation procedure	Simulation error
QanTiM 6 <sup>th</sup> order model (inverse)	57 %
NARX 4 <sup>th</sup> order quadratic model (inverse)	24 %

A 6<sup>th</sup> order QanTiM model showed the best simulation results, with no further improvement in accuracy with an increase in model order. The 6<sup>th</sup> order QanTiM model made use of 13 polynomial terms. The full parameter set NARX description made use of 54 terms for the 4<sup>th</sup> order quadratic model. The results for both model types are shown in Figure 6.2.

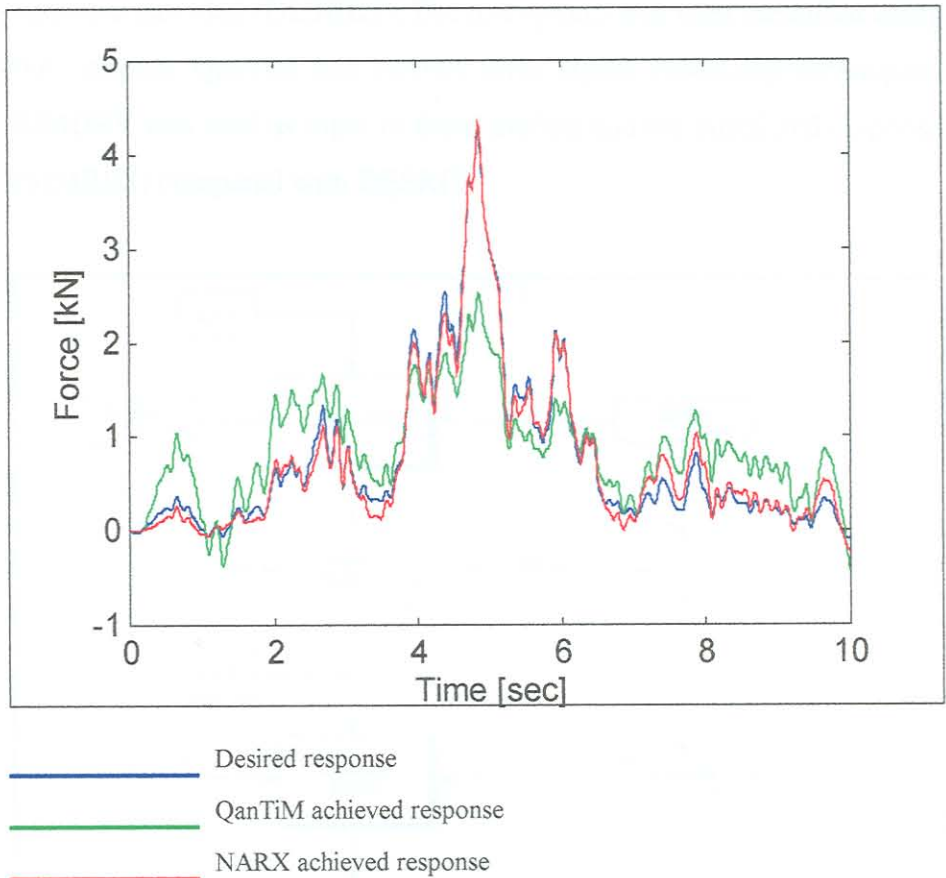


**Figure 6.2 QanTiM vs. NARX simulation results**

The NARX simulation technique shows clear advantage over the linear QanTiM technique. QanTiM failed to accurately model, and subsequently simulate the severe non-linear behaviour of the elastomeric damper unit. Simulations conducted with NARX show good reconstruction of load response over a broad amplitude range.



### 6.1.2. Non-linear error signal modelling of an elastomeric damper

The elastomeric damper test system presented in Figure 6.1 is utilised to demonstrate the potential of the non-linear error signal modelling technique presented in Section 5.5.4. The test system was excited with a random drive signal (SIMDRV) and the subsequent pseudo desired response recorded (DESRES). The test system was then identified using both normal QanTiM and NARX error signal modelling techniques. SIMDRV was used as input to these models and the simulated response (SIMRES) compared with DESRES.

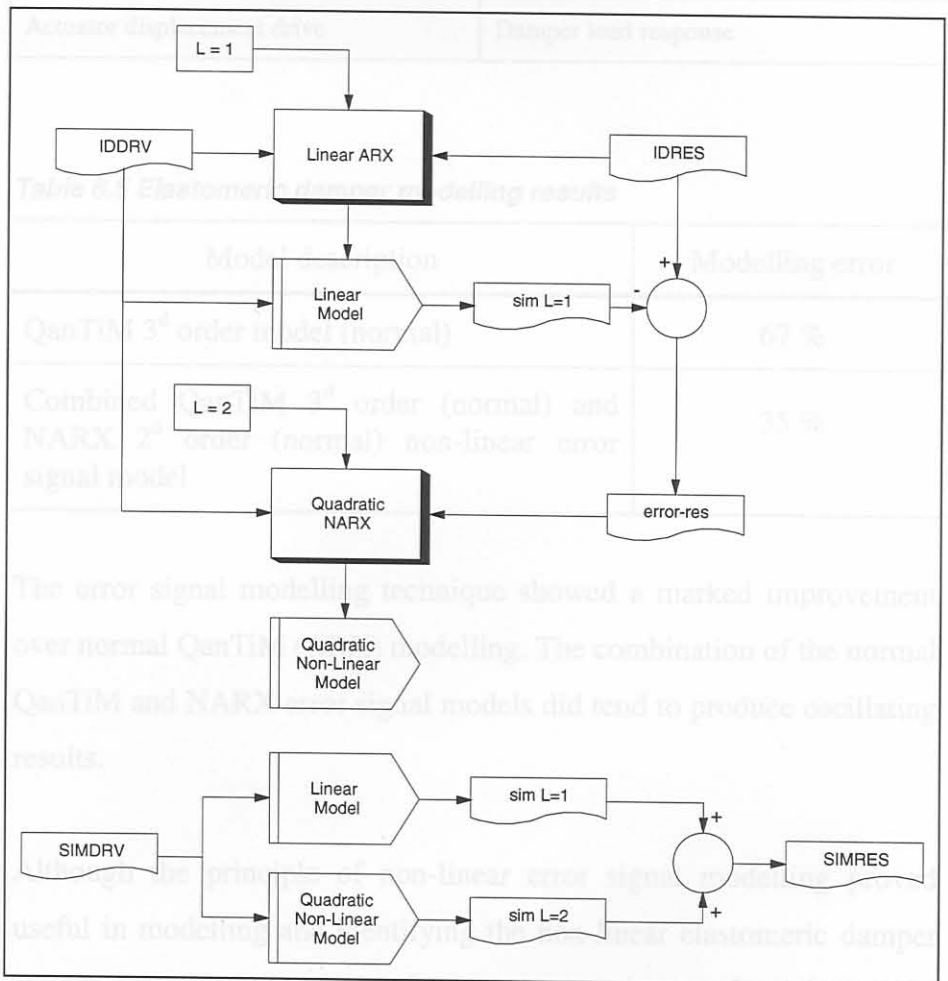


Figure 6.3 Quadratic non-linear error signal modelling

A 3<sup>d</sup> order linear normal QanTiM model was used to characterise the damper unit's linear response. A 2<sup>d</sup> order quadratic model was then used to model the error signal. No cubic model was used. The non-linear error signal modelling process is shown in Figure 6.3. The modelling results are shown in Figure 6.4.

**Table 6.4 Elastomeric damper modelling – System summary**

Test description:	Identification and modelling of elastomeric damper load response	
Model bandwidth:	0 Hz to 25 Hz	
	System Inputs	System Outputs
	Actuator displacement drive	Damper load response

**Table 6.5 Elastomeric damper modelling results**

Model description	Modelling error
QanTiM 3 <sup>d</sup> order model (normal)	67 %
Combined QanTiM 3 <sup>d</sup> order (normal) and NARX 2 <sup>d</sup> order (normal) non-linear error signal model	35 %

The error signal modelling technique showed a marked improvement over normal QanTiM (ARX) modelling. The combination of the normal QanTiM and NARX error signal models did tend to produce oscillating results.

Although the principle of non-linear error signal modelling proved useful in modelling and identifying the non-linear elastomeric damper system, the added complexity does not warrant its use above that of the condensed NARX formulation.

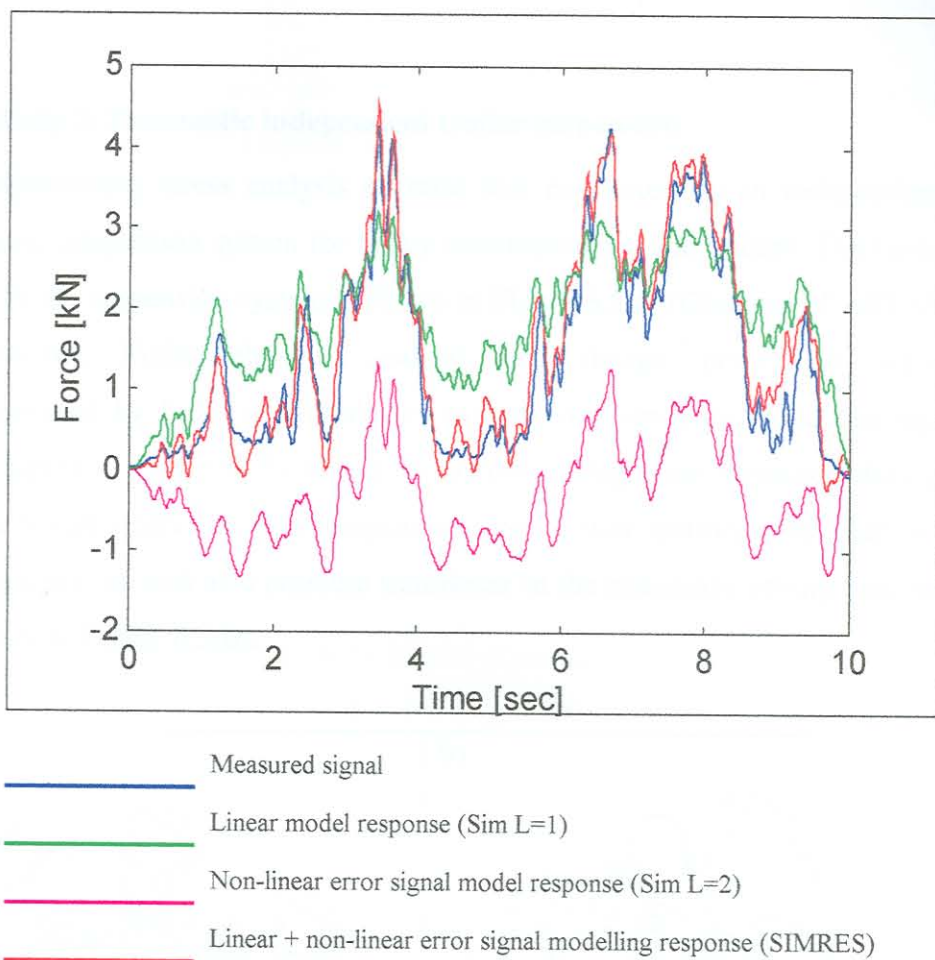


**Figure 6.4 Non-linear error signal modelling response for an elastomeric damper**



## 6.2. Case study 2: Pneumatic independent trailer suspension

A comprehensive stress analysis exercise was conducted on an independent pneumatic suspension system for heavy commercial vehicle trailers. The basic layout of the suspension system is shown in Figure 6.5(a) (Courtesy of ASTAS Automotive). Finite element analysis and design procedures were complimented by full-scale simulation testing on a servo-hydraulic test rig. Strain inputs to both the FEA and simulation testing were measured during normal trailer operation. The suspension system was instrumented with 10 strain gauges, as well as a pressure transducer in the pneumatic spring unit, as indicated in Figure 6.5(b).

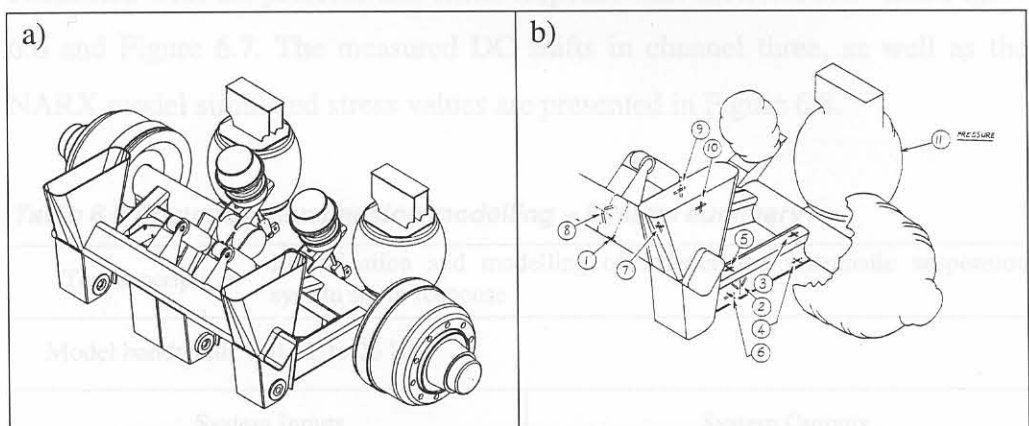


**Figure 6.5 Independent pneumatic suspension: layout and instrumentation**

The most critical stress area was found to be on the top flange of the suspension swing arm, in the region of strain channel three. While driving with an over-laden trailer on rough road conditions, a substantial DC shift was recorded for channel three (see Figure 6.8 – measured data). Such a large DC shift could typically indicate plastic deformation of the component. Alternatively, instrumentation errors, or so-called welding shakedown could cause the DC shift. Due to the critical location of channel three, it was of paramount importance to determine whether plastic deformation did indeed occur in the suspension swing arm.

Part of the investigation into the possible plastic deformation involved modelling strain (or approximate stress) responses with NARX techniques. A dynamic model was identified between the pressure response in the pneumatic spring unit, and the strain response at channel three. The dynamic model was identified and validated on Sections of true data, and subsequently used to predict the suspect strain response at channel three as a function of the pressure in the pneumatic spring.

Linear normal QanTiM models failed to model strain response as a function of pneumatic spring pressure, whereas NARX models provided accurate results (see Table 6.6 through Table 6.7). Model identification and validation were conducted with the pressure and strain response time histories shown in Figure 6.6 and Figure 6.7. The measured DC shifts in channel three, as well as the NARX model simulated stress values are presented in Figure 6.8.

**Table 6.6 Pneumatic suspension modelling – System summary**

Test description:	Identification and modelling of independent pneumatic suspension system strain response	
Model bandwidth:	0 Hz to 25 Hz	
	System Inputs	System Outputs
	Pneumatic spring unit pressure response	Channel three strain response

**Table 6.7 Pneumatic suspension modelling results**

Model description	Modelling error
QanTiM 5 <sup>th</sup> order model (normal)	95 %
NARX 3 <sup>d</sup> order quadratic model (normal)	34 %



Figure 6.8 Measured vs. simulated channel three stress response

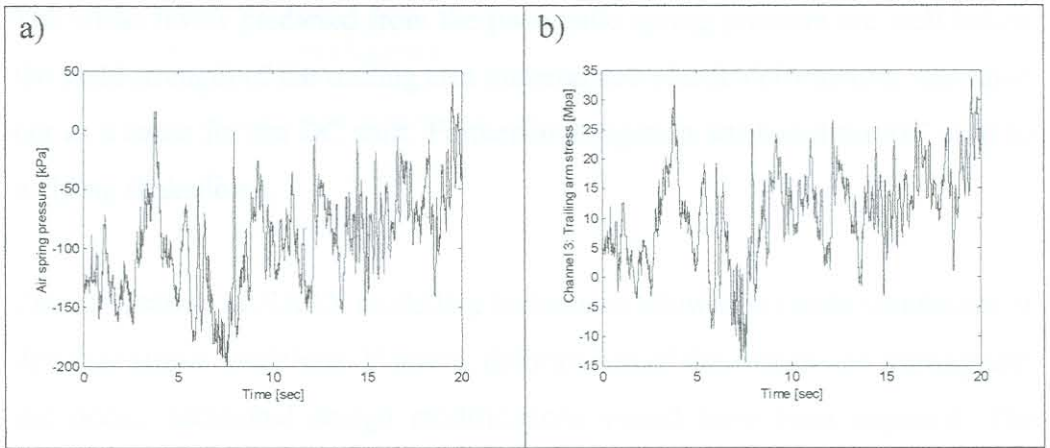


Figure 6.6 Modelling and validation response time histories for the independent suspension system

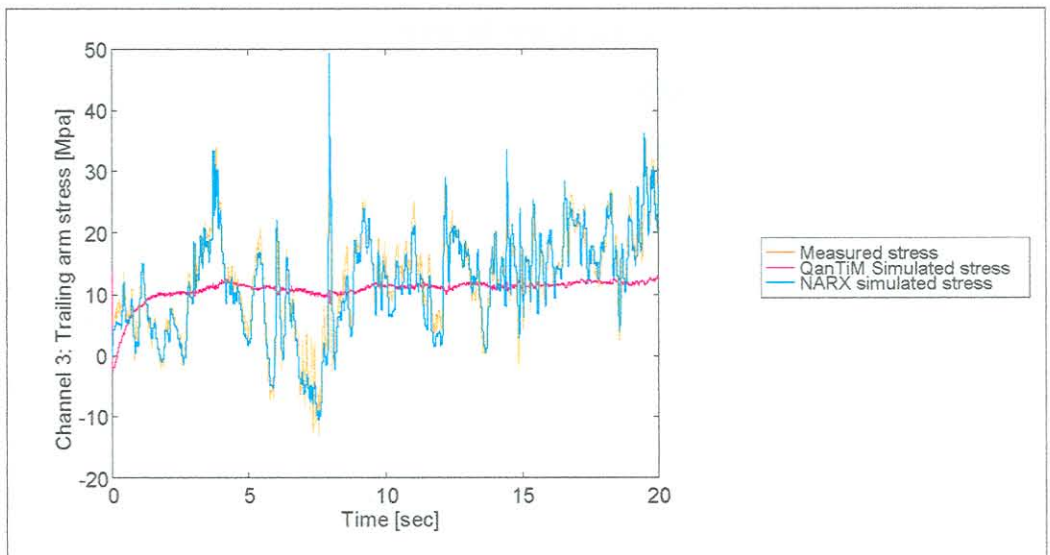


Figure 6.7 Linear vs. non-linear modelling results for the independent suspension system

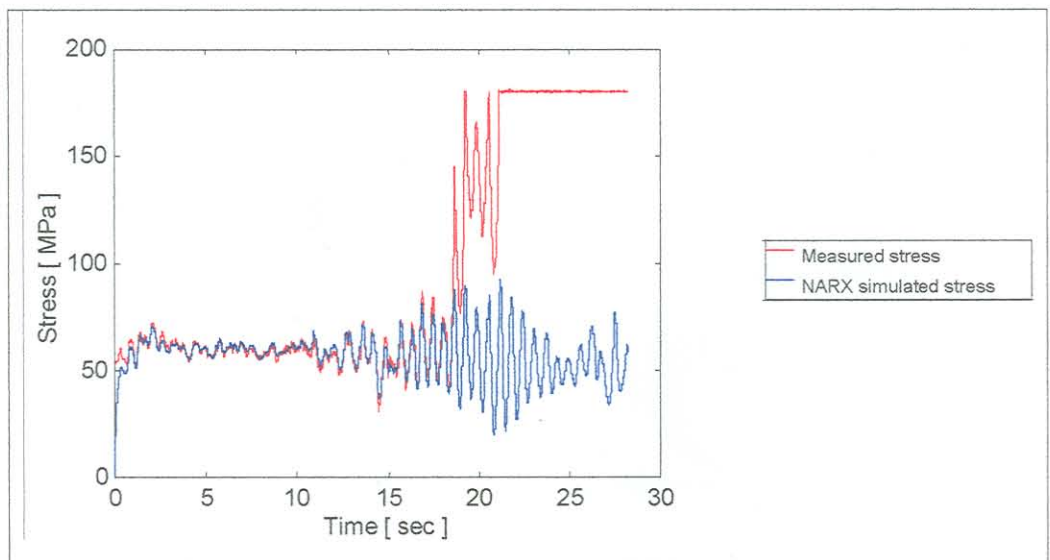


Figure 6.8 Measured vs. simulated channel three stress response

The stress levels predicted from the pneumatic spring pressure are well below the yield strength of the trailing arm material and plastic deformation was ruled out as a cause for the DC shift. Further investigation attributed the DC shift to welding shakedown.

The application of NARX modelling techniques allowed accurate simulation of dynamic stress conditions. If plastic deformation of the suspension trailing arm did occur, additional design modifications would have been required. The simulated stress results obtained with the NARX model averted any such modifications.

The front suspension of the truck was extensively instrumented with strain gauges. The wheels were instrumented to measure input loads to the suspension system. The first example models the longitudinal force in the upper suspension ball joint as a function of the wheel input loads. The second example models forces in, and displacements of the upper and lower suspension control arms as a function of the wheel input loads. A schematic representation of the suspension system is shown in Figure 6.9.



Figure 6.9 Light truck front suspension system



### 6.3. Case study 3: Light truck front suspension

Two examples are presented where split spectra linear-non-linear modelling techniques were used to describe the dynamic behaviour of systems too complex for linear normal QanTiM modelling. The two applications further show the capability of the condensed NARX model formulation to describe non-square systems (number of inputs  $\neq$  number of outputs). Both application examples are concerned with modelling, and subsequently simulating, suspension system stresses as a function of wheel loads for the front suspension of a light truck [ 16 ] (courtesy of GM corporation, Pontiac, Michigan). The front suspension of the truck was extensively instrumented with strain gauges. The wheels were instrumented to measure input loads to the suspension system. The first example models the longitudinal force in the upper suspension ball joint as a function of the wheel input loads. The second example models forces in, and displacements of the upper and lower suspension control arms as a function of the wheel input loads. A schematic representation of the suspension system is shown in Figure 6.9.

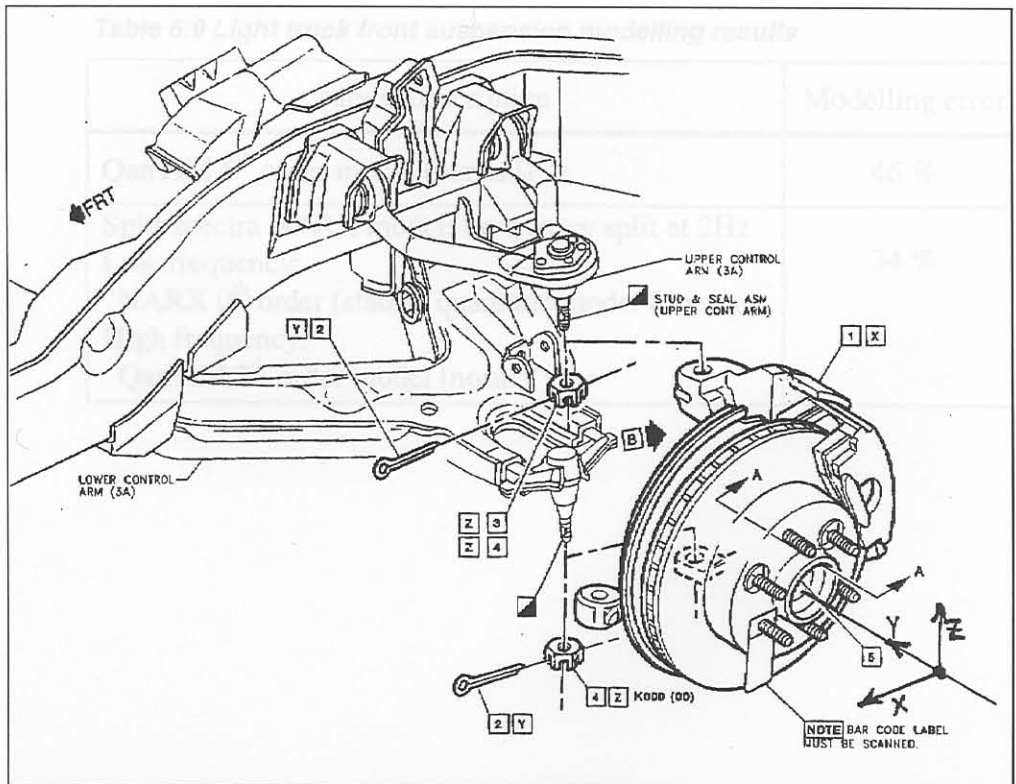


Figure 6.9 Light truck front suspension system

### 6.3.1. Light truck suspension: Wheel $\Rightarrow$ upper ball joint forces

The upper ball joint longitudinal reactions are modelled to wheel input loads. This MISO system illustrates the effect of the non-linear terms, and its improved accuracy achieved over linear modelling.

**Table 6.8 Light truck front suspension modelling – System summary**

Test description:	Identification and modelling of light truck front suspension system strain response	
Model bandwidth:	0 Hz to 25 Hz	
	System Inputs	System Outputs
	<ul style="list-style-type: none"> <li>• Spindle longitudinal force X</li> <li>• Spindle lateral force Y</li> <li>• Spindle vertical force Z</li> <li>• Moment about X axis</li> <li>• Moment about Y axis</li> <li>• Moment about Z axis</li> </ul>	<ul style="list-style-type: none"> <li>• Longitudinal forces at the upper suspension ball joint</li> </ul>

**Table 6.9 Light truck front suspension modelling results**

Model description	Modelling error
QanTiM 5 <sup>th</sup> order model (normal)	46 %
Split spectra NARX model: Frequency split at 2Hz Low frequency: NARX 0 <sup>th</sup> order (static), quadratic model (normal) High frequency: QanTiM 2 <sup>d</sup> order model (normal)	34 %

*Figure 6.10 Split spectra model response*

Both drive and response data are split using a 4<sup>th</sup> order digital filter. A static quadratic model is used to describe the low frequency part, whereas a second order linear model is used for the high frequency part. The two frequency ranges are modelled and simulated independently, the responses are summed to obtain simulation over the whole spectrum.

The measured and simulated response signals for both the low and high frequency ranges are shown in Figure 6.10. Note that the low frequency model produced a near perfect fit (in the graph below, the two lines are plotted on one another), but the high frequency model is less accurate.

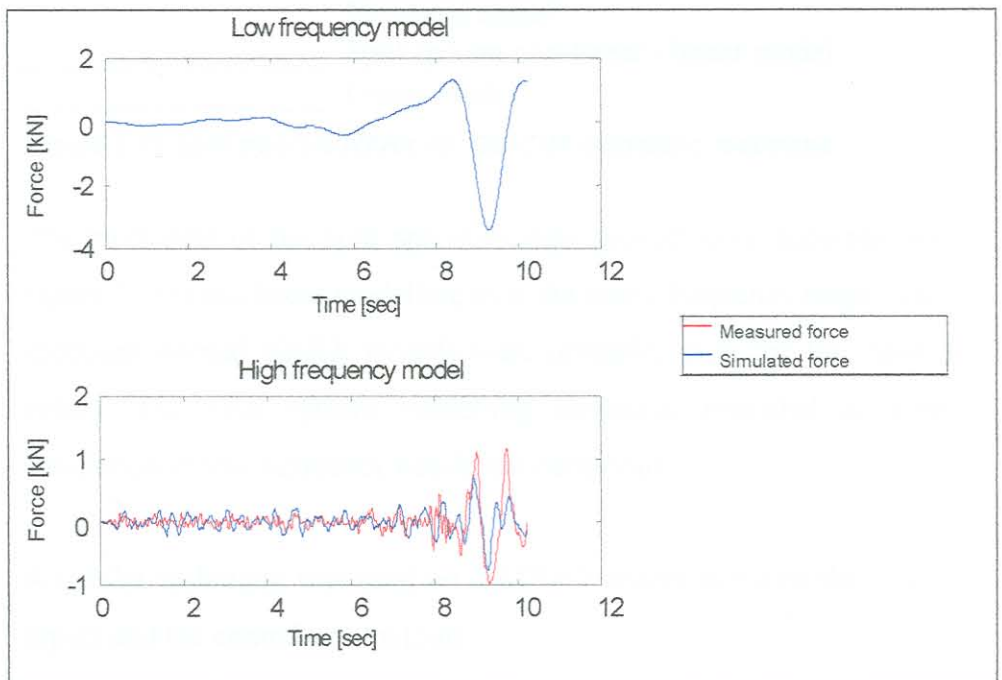


**Figure 6.10 Split spectra model response**

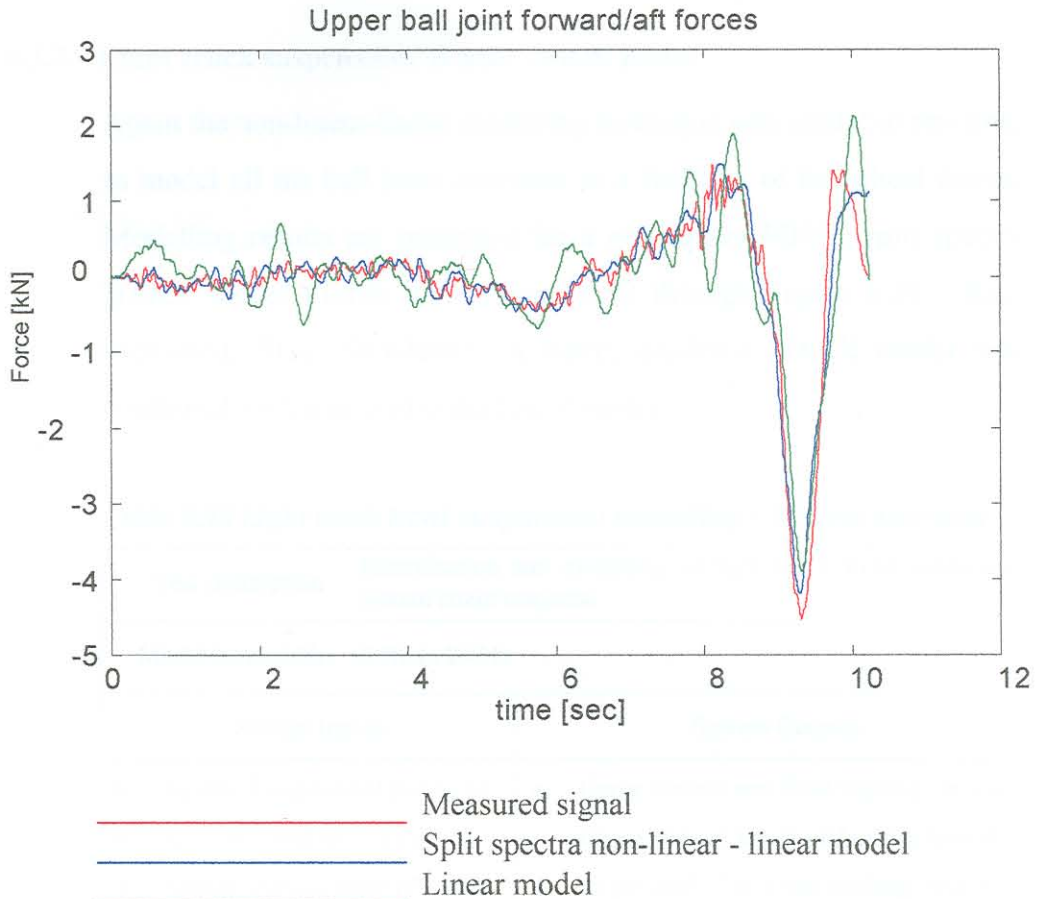


**Figure 6.11 Split spectra NARX vs. QanTiM modelling response**

The modelling of the split spectrum data proved more accurate (see Figure 6.11) than linear modelling over the entire frequency range. Full spectrum normal NARX models were unstable, even for low model orders. The split spectra modelling technique provided accurate simulation of low frequency non-linear behaviour

A similar technique was used on a MIMO system between the wheel inputs and the control arm outputs.



### 6.3.2. Light truck suspension: Wheel $\Rightarrow$ ball joints

Again the non-linear-linear modelling technique was used, but this time to model all the ball joint reactions as a function of the wheel forces. Modelling results are presented for a non-square MIMO split spectra NARX model (Table 6.10, Figure 6.12 through Figure 6.20 - Red: Measured, Blue: Simulated). A static, quadratic NARX model was combined with a second order linear model.

**Table 6.10 Light truck front suspension modelling – System summary**

Test description:	Identification and modelling of light truck front suspension system strain response	
Model bandwidth:	0 Hz to 25 Hz	
	System Inputs	System Outputs
	<ul style="list-style-type: none"> <li>• Spindle Longitudinal force (X)</li> <li>• Spindle lateral force (Y)</li> <li>• Spindle vertical force (Z)</li> <li>• Moment about X axis</li> <li>• Moment about Y axis</li> <li>• Moment about Z axis</li> </ul>	<ul style="list-style-type: none"> <li>• Upper control arm front bushing vertical</li> <li>• Upper control arm front bushing lateral</li> <li>• Upper control arm rear bushing vertical</li> <li>• Upper control arm rear bushing lateral</li> <li>• Lower control arm front bushing vertical</li> <li>• Lower control arm front bushing lateral</li> <li>• Lower control arm rear bushing vertical</li> <li>• Lower control arm rear bushing lateral</li> <li>• Lower control arm angular displacement</li> </ul>

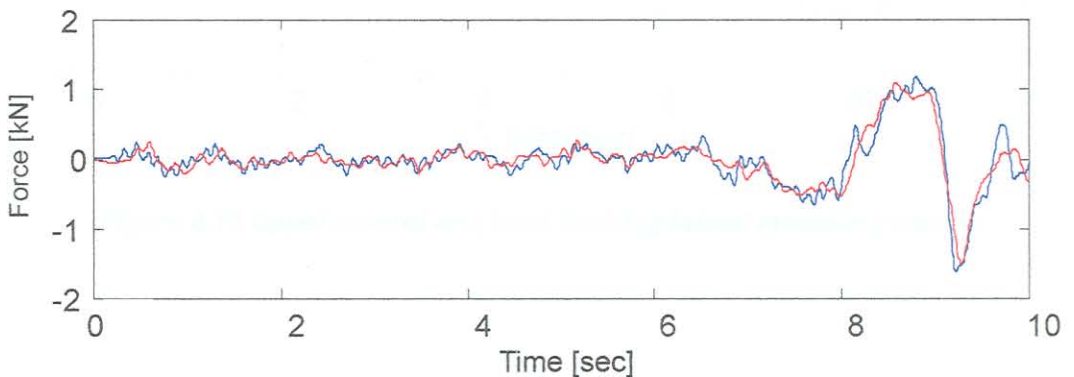


**Figure 6.12 Upper control arm front bushing vertical modelling results**

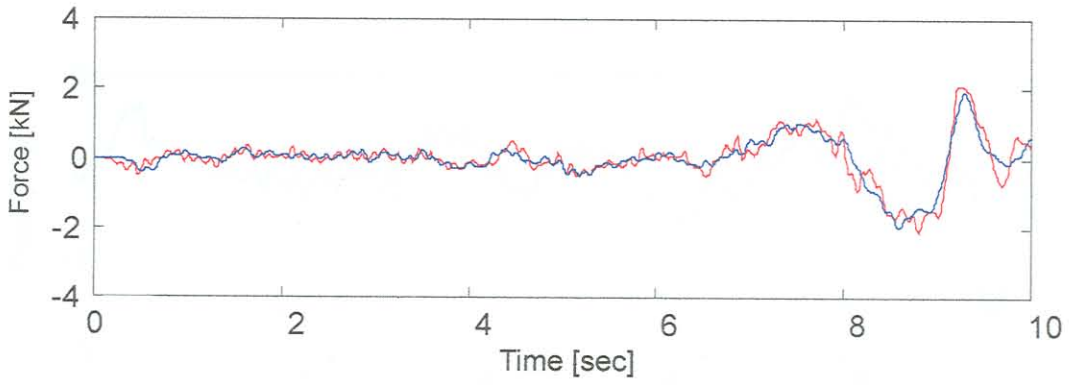


*Figure 6.13 Upper control arm front bushing lateral modelling results*

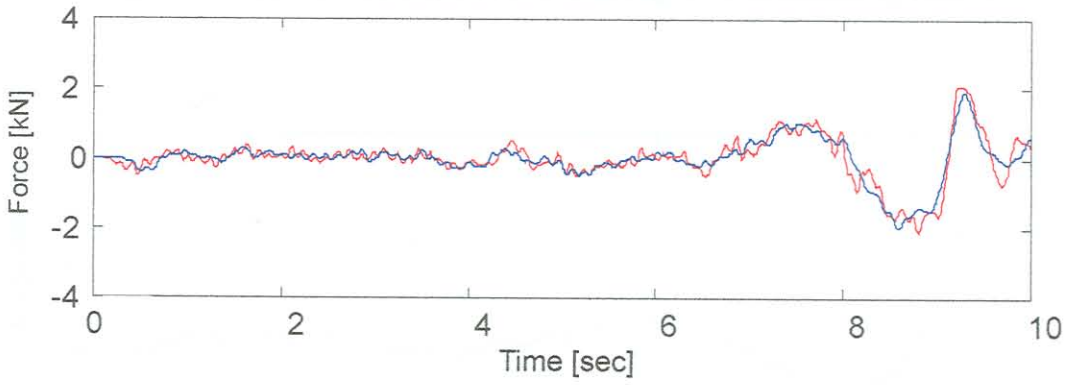


*Figure 6.14 Upper control arm rear bushing vertical modelling results*

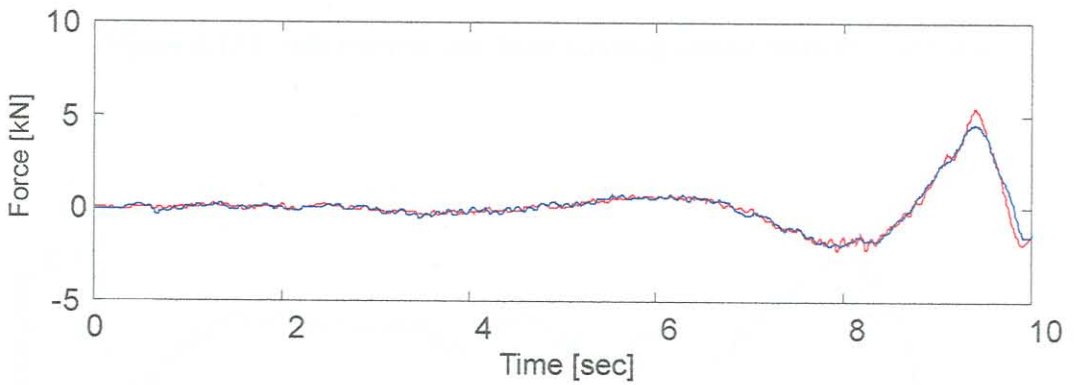


*Figure 6.15 Upper control arm front bushing lateral modelling results*

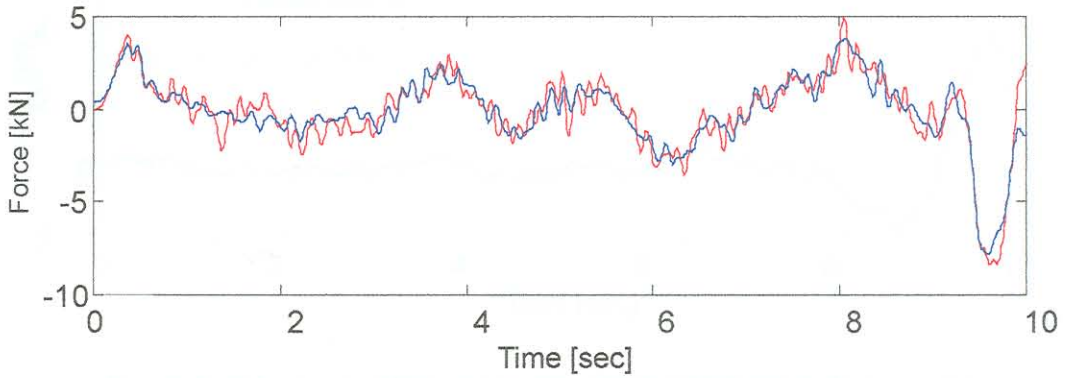


**Figure 6.16 Lower control arm front bushing vertical modelling results**

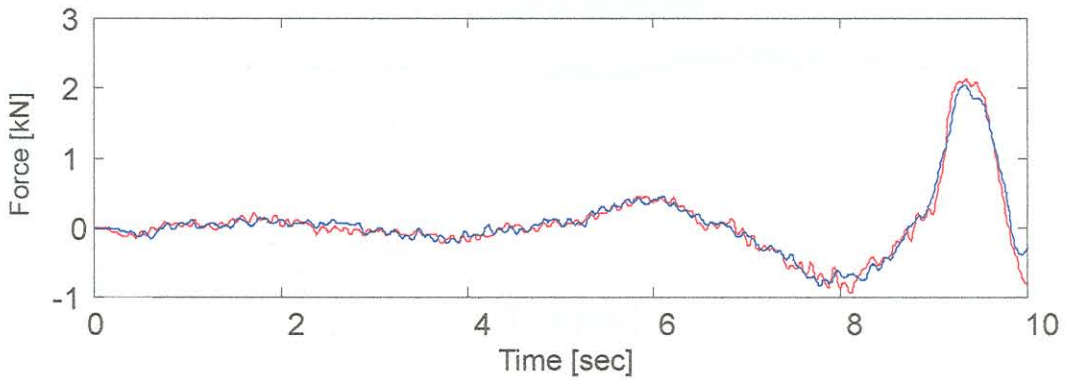


**Figure 6.17 Lower control arm front bushing lateral modelling results**

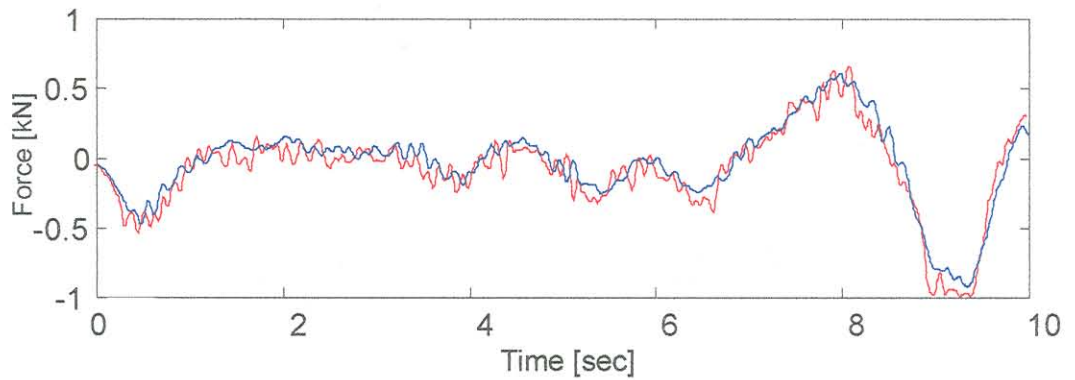


**Figure 6.18 Lower control arm rear bushing vertical modelling results**

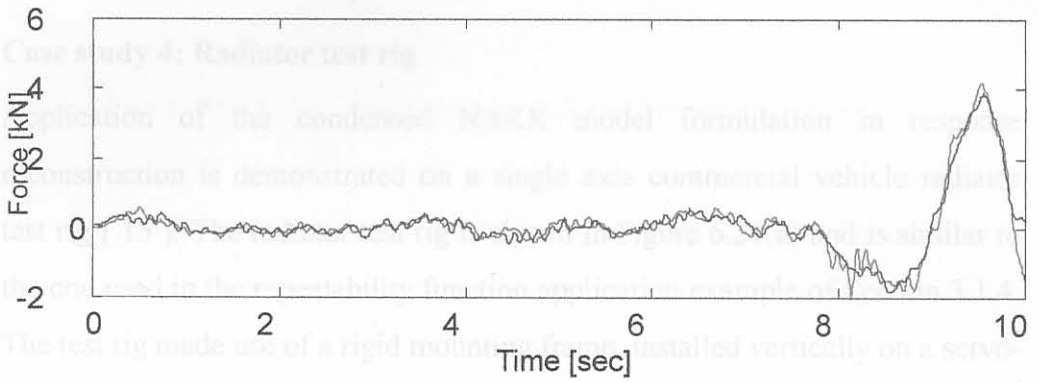


**Figure 6.19 Lower control arm rear bushing lateral modelling results**

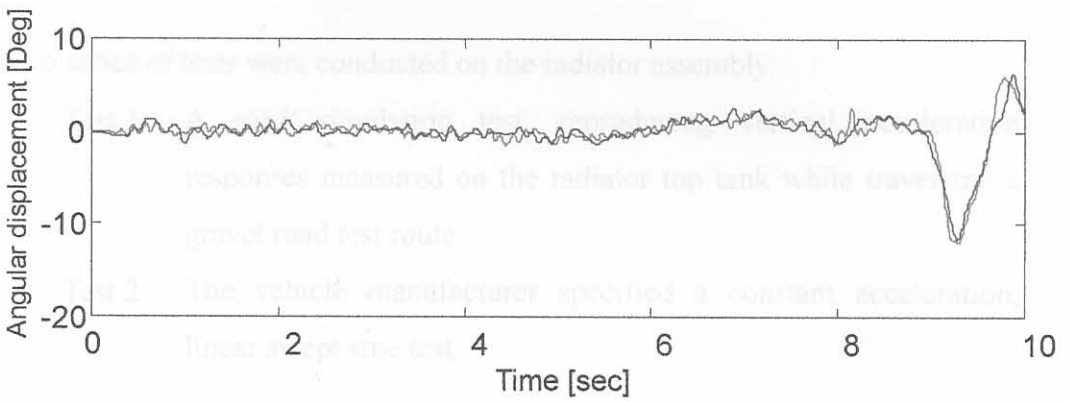


**Figure 6.20 Lower control arm angular displacement modelling results**



**Figure 6.21 Radiator test rig**



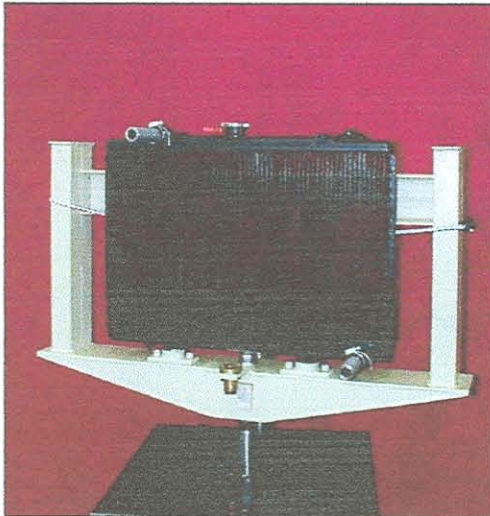
#### 6.4. Case study 4: Radiator test rig

Application of the condensed NARX model formulation in response reconstruction is demonstrated on a single axis commercial vehicle radiator test rig [ 15 ]. The radiator test rig is shown in Figure 6.21(a) and is similar to the one used in the repeatability function application example of Section 3.1.4. The test rig made use of a rigid mounting frame, installed vertically on a servo-hydraulic actuator. Mounting pins on the top and bottom radiator tanks fitted into doughnut shaped rubber mounts. These rubber mounts were fitted to the rigid mounting frame as per normal vehicle installation.

Two series of tests were conducted on the radiator assembly:

- Test 1: A road simulation test, reproducing vertical acceleration responses measured on the radiator top tank while traversing a gravel road test route.
- Test 2: The vehicle manufacturer specified a constant acceleration, linear swept sine test.

a)



b)

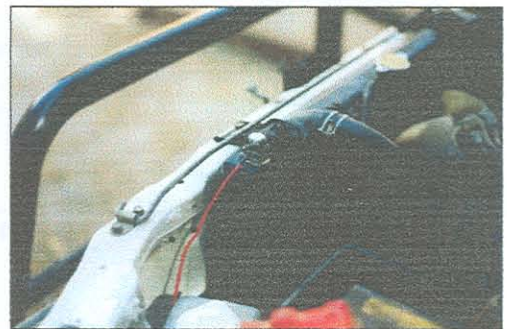


**Figure 6.21 Radiator test rig**

#### 6.4.1. Reconstruction of radiator top tank field acceleration response

Structural durability tests required the field acceleration response, recorded on the radiator top tank, to be reproduced in the laboratory. Figure 6.21 (b) shows an accelerometer applied to the top tank of the test vehicle's radiator for field measurements. An additional accelerometer was applied to the vehicle chassis, centred below the radiator. Field responses were recorded while travelling on a gravel road test route.

*Table 6.12 Radiator simulation results*

Results are presented for three simulation exercises, namely a linear QanTiM simulation, a NARX simulation and a non-square NARX simulation. The non-square simulation utilises both the acceleration response channels to predict the actuator drive signals. The non-square dynamic system is shown schematically in Figure 6.22. The use of a second response transducer serves as an aid to improve top tank acceleration simulation.

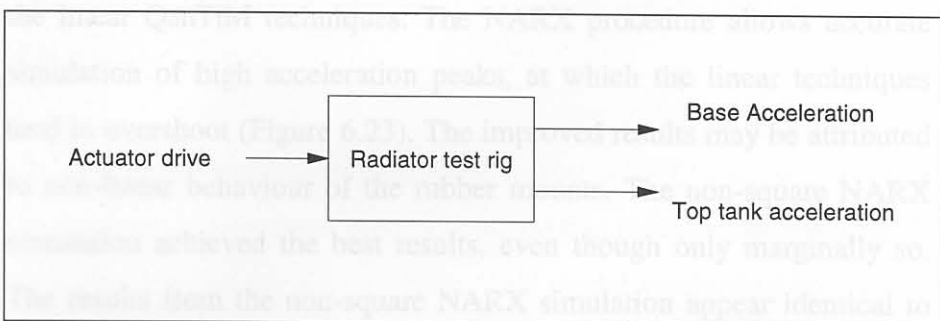


**Figure 6.22 Non-square dynamic system**

The accuracy of simulation is determined by the accuracy with which the top tank acceleration is reproduced. The simulation results are presented in Table 6.12. The simulation error values (see Section 5.7) are calculated for simulation results prior to any iteration, i.e. a comparison of DESRES with IT00RES.

**Table 6.11 Radiator road simulation test - System summary**

Test description: Simulation of radiator acceleration response	
Model bandwidth: 2 Hz to 30 Hz	
System Inputs	System Outputs
<ul style="list-style-type: none"> <li>Actuator displacement drive</li> </ul>	<ul style="list-style-type: none"> <li>Radiator top tank acceleration</li> <li>Radiator base acceleration (only for non-square simulation)</li> </ul>

**Table 6.12 Radiator simulation results**

Simulation procedure	Simulation error
QanTiM 6 <sup>th</sup> order model (inverse)	35 %
NARX 6 <sup>th</sup> order quadratic model (inverse)	16 %
Non-square NARX 6 <sup>th</sup> order quadratic model (inverse)	14 % (base acceleration: 12 %)

The NARX simulation procedure produced results superior to that of the linear QanTiM techniques. The NARX procedure allows accurate simulation of high acceleration peaks, at which the linear techniques tend to overshoot (Figure 6.23). The improved results may be attributed to non-linear behaviour of the rubber mounts. The non-square NARX simulation achieved the best results, even though only marginally so. The results from the non-square NARX simulation appear identical to that of the SISO NARX and are not shown.



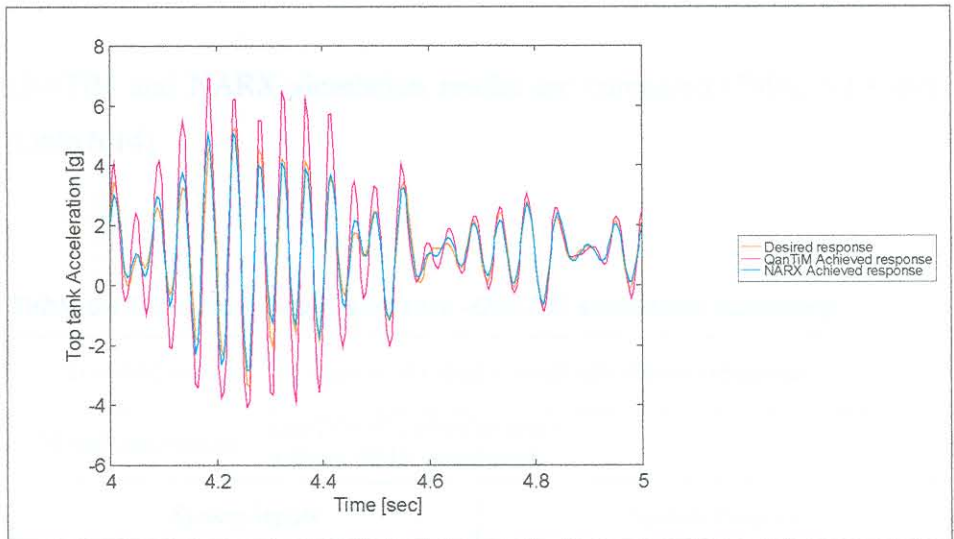


**Figure 6.23 Radiator simulation test, QanTiM vs. NARX results**

#### 6.4.2. Radiator sine sweep tests

The second phase of the radiator test series consisted of a constant acceleration swept sine test. The test prescribed a 10 Hz to 50 Hz swept sine response at a constant acceleration amplitude of 1.5 g, measured at the base of the mounting frame. Due to inherent system resonance, the prescribed test response fell beyond the capabilities of the actuator's servo control system. A response reconstruction technique was subsequently employed, with the 1.5 g swept sine as desired response (DESRES).

The aim of the simulation procedure was to identify a model between the actuator displacement drive signal and the acceleration response on the radiator mounting frame's base. This model would then be used to calculate actuator drive signals, which compensate for the system resonance, resulting in the desired test response. It is known that QanTiM has difficulty simulating over areas of resonance [ 45 ][ 50 ]. This application will indicate whether the NARX techniques improve simulation results over areas of resonance.



QanTiM and NARX simulation results are compared (Table 6.13 and Table 6.14)

**Table 6.13 Radiator swept sine test –QanTiM simulation summary**

Test description: Simulation of radiator swept sine desired response	
Model description: QanTiM 9 <sup>th</sup> order (inverse) 8 Hz to 60 Hz Bandwidth	
System Inputs	System Outputs
Actuator displacement drive	Radiator base acceleration

**Table 6.14 Radiator swept sine test - NARX simulation summary**

Test description: Simulation of radiator swept sine desired response	
Model description: NARX 6 <sup>th</sup> order quadratic (inverse) 8 Hz to 60 Hz Bandwidth	
System Inputs	System Outputs
Actuator displacement drive	Radiator base acceleration

The PSD graphs of QanTiM and NARX simulation results (IT00RES) are presented in Figure 6.24. The graphs show the constant PSD amplitude of the desired response, and the achieved resonant for both QanTiM and NARX responses. It is important to note that the effects of resonance appear worsened in the NARX simulation. The best results were achieved with extensive iteration of QanTiM simulation results, as shown in Figure 6.25. Small iteration gain factors were used throughout the iteration process, but even this approach did not relieve the resonance problems.

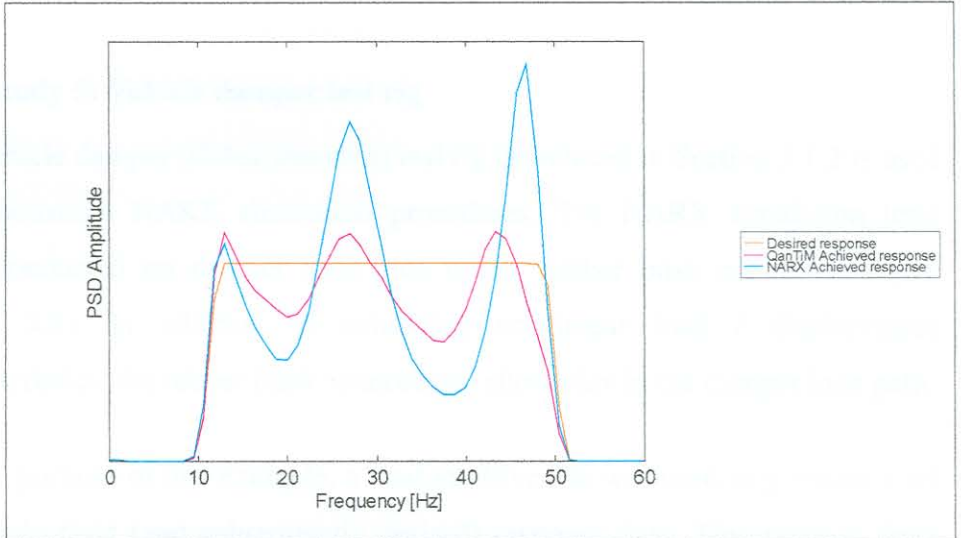


Figure 6.24 Radiator swept sine test simulation results (IT00RES)

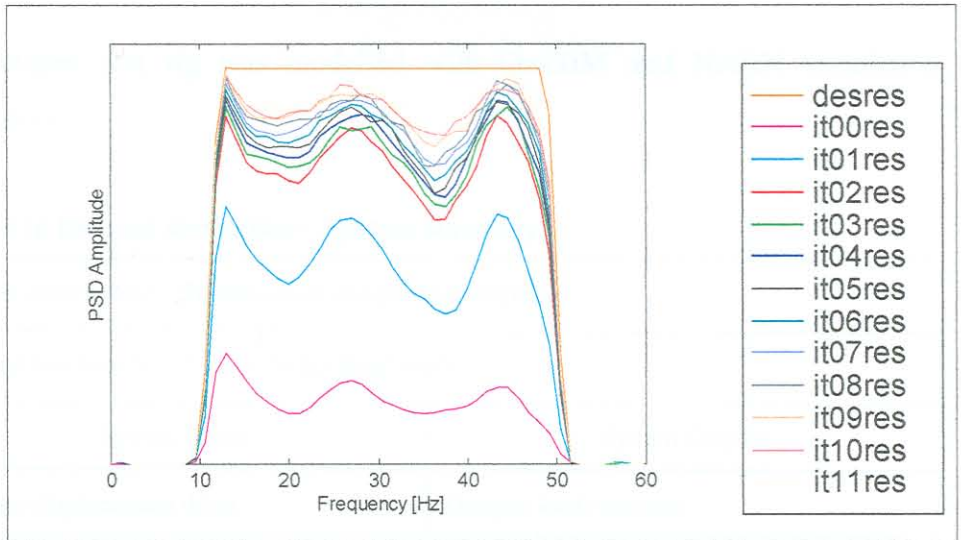


Figure 6.25 Radiator swept sine test simulation and iteration results

## 6.5. Case study 5: Vehicle damper test rig

The vehicle damper (shock absorber) test rig introduced in Section 3.1.2 is used to demonstrate NARX simulation procedures. The NARX simulation tests were conducted on damper units that utilise rubber bush connections (see Figure 3.3). In addition to exhibiting non-linear load / displacement characteristics, the rubber bush connections allow play in the damper load path.

For the purpose of this example, a random drive file was used to generate a set of pseudo field (and subsequently desired) response data. This random drive file will be referred to as DESDRV, and the subsequent response as DESRES.

The damper test rig was modelled with QanTiM and NARX simulation procedures.

**Table 6.15 Damper simulation - System summary**

Test description: Simulation of damper load response	
Model bandwidth: 0 Hz to 10 Hz Bandwidth	
System Inputs	System Outputs
Actuator displacement drive	Damper load response

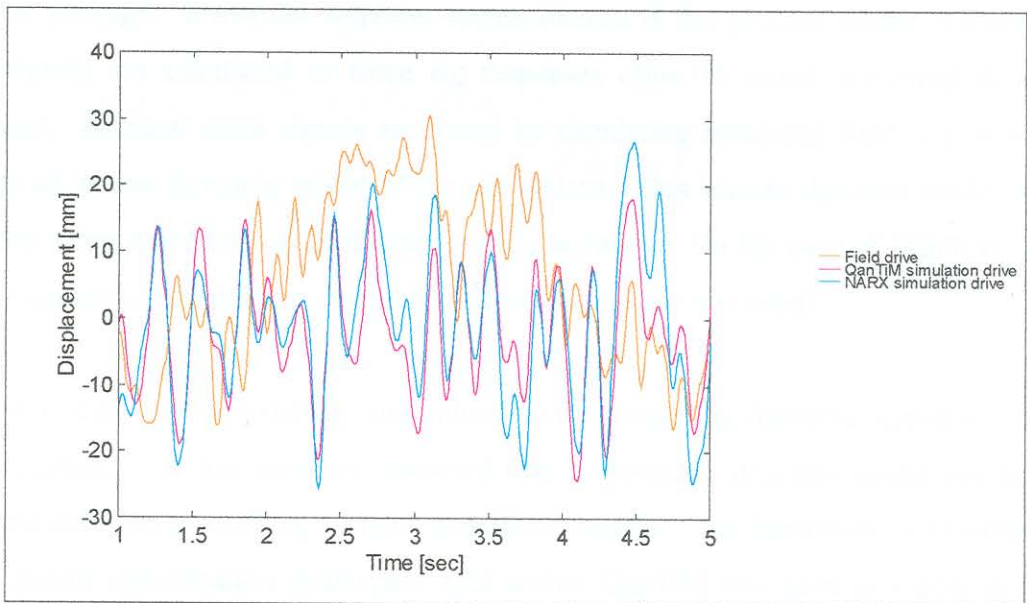
**Table 6.16 Damper simulation results**

Simulation procedure	Simulation error
QanTiM 4 <sup>th</sup> order model (inverse) IT00RES	27 %
QanTiM 4 <sup>th</sup> order model (inverse) IT05RES	17 %
NARX 4 <sup>th</sup> order cubic model (inverse) IT00RES	18 %

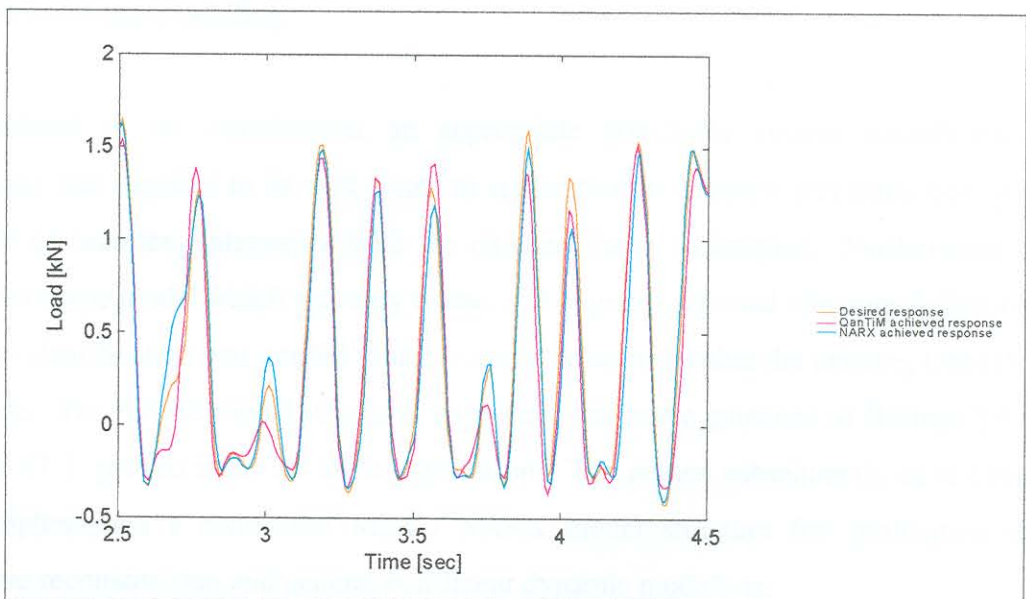
NARX simulation results surpassed linear results achieved with QanTiM. Iteration of the QanTiM results improved on the NARX achievement and produced the best simulation.

Figure 6.37 Damper test rig response reconstruction

Both the QanTiM and NARX techniques rendered good simulation results, i.e. good response reconstruction. Good response reconstruction intuitively implies good reconstruction of system inputs. Thus if FINRES is equal to DESRES, then FINDRV should intuitively be equal to DESDRV. For the damper test rig however, the final drive displays no similarity to the drive used to create the desired response, i.e. FINDRV is not equal to DESDRV. Figure 6.26 compares DESDRV with the NARX (IT00DRV) and QanTiM (IT05DRV) simulation drive files. The corresponding response files are compared in Figure 6.27



**Figure 6.26 Damper test rig drive reconstruction**



**Figure 6.27 Damper test rig response reconstruction**



## Chapter 7

### Conclusions and recommendations for further research - Part II

Research into the application of non-linear time domain system identification techniques in general modelling and simulation of dynamic systems, and more specifically implementation into structural response reconstruction, was prompted by a large scale research program surrounding the time domain based QanTiM simulation software package. Structural response reconstruction is the process where actuator drive signals are calculated to force rig responses close to actual measured field responses. Actuator drive signals are found by simulating measured field responses through an inverse dynamic model of the test system. This inverse dynamic model is found by using a dynamic system identification technique. In the case of QanTiM, a linear parametric time domain system identification technique is used.

QanTiM is capable of modelling and subsequently simulating dynamic responses in most structures. It has however occurred that a dynamic structure could not be modelled accurately, resulting in poor simulation results. The limitation of existing linear system identification techniques used within QanTiM was seen as a potential cause of such modelling difficulty, hence this study into non-linear system identification and modelling

As outlined in the introduction, an appropriate non-linear system identification technique was required to be well suited to application in response reconstruction, yet capable of seamless integration with the existing linear techniques. Furthermore a black-box type model which was easy to use, and required minimal structure definition prior to identification was needed to allow implementation within the existing QanTiM software. The NARX model structure, introduced under the guidance of Billings [ 5 ] [ 46 ] [ 47 ] proved ideal for these applications. The author subsequently developed and implemented a condensed MIMO NARX model structure for application in response reconstruction and general non-linear dynamic modelling.

### 7.1. Non-linear system identification: The condensed NARX model formulation

Non-linear system identification is relatively new, and limited practical case study research contributions were available on the subject. Valuable research contributions were made under the guidance of Billings, who presented the NARX model formulation (See references [ 4 ] through [ 8 ] [ 46 ] & [ 47 ]). The NARX model formulation proved to be well suited to application within time domain system identification and response reconstruction [ 54 ]. The author subsequently combined the NARX formulation with the so called 'full order approach' (suggested by Raath [ 53 ]). These techniques were adapted and refined, resulting in a condensed NARX model structure, which evolved into a time domain based non-linear system identification 'toolbox' of Matlab functions. The condensed NARX model structure is capable of identifying, modelling and simulating systems with polynomial non-linear behaviour. The condensed NARX functions require minimal structure definition prior to identification. Two parameters need to be specified for each response channel, namely the model order and degree of non-linearity.

### 7.2. NARX as a general non-linear modelling tool

The NARX model formulation showed notable potential as a general non-linear system identification and modelling tool, capable of accurately and efficiently modelling MISO and MIMO non-linear dynamic systems. Chapter 6 presented four case studies in which the condensed NARX model structure outperformed normal QanTiM modelling techniques. The NARX based techniques proved valuable in modelling the dynamic behaviour of rubber and elastomeric components. Section 6.2 implemented NARX techniques to model stress levels as a function of pneumatic spring pressure in a trailer suspension system. In Section 6.3, the condensed NARX model description was used to identify a model between wheel inputs and ball joint loads for a vehicle front suspension system. This application showed the condensed NARX model structure's ability to model both indeterminate and redundant non-square



systems. The NARX techniques were further extended to make use of a split-spectra modelling approach.

Application of the condensed NARX model structure in normal system identification and modelling is summarised below:

- Accurate, and relatively easy, modelling of MISO and MIMO systems with severe polynomial non-linearity.
- Well suited to modelling non-square systems, typically modelling more than one output channels from a single input.
- Potential application would typically be modelling between critical points on a complex dynamically loaded, non-linear structure.
- The NARX formulation excelled if used in a split-spectra modelling technique to accommodate low frequency, high displacement non-linear system behaviour.

### 7.3. NARX structural response reconstruction

In general, the NARX formulation did not allow successful simulation of systems that could not be simulated using the linear QanTiM software. More important, most test structures encountered did not show enough non-linearity to warrant the extra computational effort required by the NARX technique. Only in a few test systems did the NARX technique render improved simulation results. Examples of successful non-linear response reconstruction using the condensed NARX model structure were presented in Chapter 6. The newly developed NARX techniques allowed accurate simulation of load responses within an elastomeric damper unit. Similarly, NARX accurately simulated required load responses within a vehicle suspension damper. However, after four iterations the results achieved with QanTiM surpassed the non-linear results. NARX outperformed QanTiM in the simulation of operational acceleration responses of a vehicle radiator. The non-linear techniques did however not improve on QanTiM in simulating responses in areas of system resonance.

### 7.4.3. Modified NARX model structures

## 7.4. Recommendations for further research

NARX system identification techniques were implemented and subsequently applied in structural mechanics. The newly developed, condensed NARX model formulation showed potential as a general, non-linear normal modelling tool with limited potential in dynamic response reconstruction. The case studies presented in Chapter 6 showed the potential of NARX techniques, and prompted recommendations for feature research.

### 7.4.1. Alternative non-linear modelling capabilities

Test systems for which NARX modelling capabilities did not improve on poor QanTiM simulation results were presented in Table 6.1. These test systems were generally concerned with simulating operational acceleration response. Furthermore, these test systems made use of fixtures that allowed some backlash in the load path. The sensitivity of accelerometer response to system backlash may be the cause of the poor simulations. The NARX technique's polynomial structure is not ideally suited to model backlash response. Dead-band, non-linear system identification and modelling techniques may resolve backlash related problems, and improve simulation results.

### 7.4.2. Non-square modelling and simulation

The application examples showed potential in modelling and simulation of non-square systems. Section 6.4.1 showed improved simulation results when two remote response transducers were used to calculate the actuator drive signals. Non-square modelling capabilities are not restricted to the condensed NARX model structure. QanTiM techniques can be modified to accommodate non-square systems. Non-square simulation may prove valuable to calculate road simulator drive signals, utilising two remote transducers for each drive channel.



### 7.4.3. Modified NARX model structures

Split spectra techniques proved valuable to recreate high frequency linear dynamics, together with low frequency non-linear behaviour. The split spectra procedures are however computationally taxing. An alternative approach to split spectra modelling may be the application of the quasi-static modified NARX model formulation presented in Section 5.5.2.

- [ 1 ] Astrom, K.J. "Identification of systems with non-linearities", *Automatica*, Vol. 16, Pergamon Press, 1980.
- [ 2 ] Bernard, T.M. "Identification of systems with non-linearities", *Mechanical and Aeronautical Engineering, University of Pretoria*, 1993.
- [ 3 ] Barrowclif, B.K., Eblert, R.E., "Full scale road simulated endurance test", Paper 680148 presented at SAE Automotive Engineering Congress, Detroit, 1968.
- [ 4 ] Billings S.A., Fakhouri S.Y., "Identification of Systems Containing Linear Dynamic and Static Non-linear Elements", *Automatica*, Vol. 18 No. 1, pp 15-26, Pergamon Press, 1982.
- [ 5 ] Billings, S.A., "Identification of non-linear systems-a survey", *IEEE Proceedings* vol. 128, November, 1980.
- [ 6 ] Billings, S.A., Fadzil, M.B., "The practical identification of Systems with Nonlinearities", *IFAC proceedings* no. 7, 1985, York, pp 155-160.
- [ 7 ] Billings, S.A., Voon, W.S.F., "A prediction-error and stepwise-regression estimation algorithm for non-linear systems", *Int. J. Control*, Vol. 48, No. 3, 1986, pp 803-822.
- [ 8 ] Billings, S.A., Voon, W.S.F., "Least squares parameter algorithms for non-linear systems", *Int. J. Control*, Vol. 15, No. 6, 1984, pp 601-615.
- [ 9 ] Billings, S.A., Chen, S., Korenberg, M.J., "Identification of MIMO non-linear systems using a forward-regression orthogonal estimator", *International Journal of Control*, Vol. 49, No. 6, 1989, pp 2157-2189.
- [ 10 ] Björck, A., Plemmons, R.J., Schneider, H., "Large scale matrix problems", Elsevier North Holland, New York, 1981.
- [ 11 ] Burden, R.L., Faires, J.D., "Numerical analysis", 5th ed, PWS-Kent, Boston, 1993.
- [ 12 ] Cater, C.R., "Dakota engine cradle fatigue testing", Report no LGE 98-005, Structural Mechanics & Dynamics, Laboratory for Advanced Engineering, Pretoria, 1998.

## References

- [ 1 ] Aström, K.J., "Maximum likelihood and prediction error methods", Automatica, Vol.16, Pergamon Press, Oxford, 1981.
- [ 2 ] Barnard, T.M., "Refined excitation techniques", Master's thesis, Department of Mechanical and Aeronautical Engineering, University of Pretoria, 1990.
- [ 3 ] Barrowclif, B.K., Ehlert, R.E., "Full scale road simulated endurance test", Paper 680148 presented at SAE Automotive Engineering Congress, Detroit, 1968.
- [ 4 ] Billings S.A. Fakhouri S.Y., "Identification of Systems Containing Linear Dynamic and Static Non-linear Elements", Automatica, Vol. 18 No. 1, pp 15-26, Pergamon Press, 1982.
- [ 5 ] Billings, S.A., "Identification of non-linear systems-a survey", IEEE Proceedings no6, November, 1980.
- [ 6 ] Billings, S.A., Fadzil, M.B., "The practical Identification of Systems with Nonlinearities", IFAC proceedings no. 7, 1985, York, pp 155-160.
- [ 7 ] Billings, S.A., Voon, W.S.F., "A prediction-error and stepwise-regression estimation algorithm for non-linear systems", Int. J. Control, Vol. 48, No. 3, 1986, pp 803-822.
- [ 8 ] Billings, S.A., Voon, W.S.F., "Least squares parameter algorithms for non-linear systems", Int. J. Control, Vol. 15, No. 6, 1984, pp 601-615
- [ 9 ] Billings, S.A., Chen, S., Kroenberg, M.J., "Identification of MIMO non-linear systems using a forward-regression orthogonal estimator", International Journal of Control, Vol. 49, No. 6, 1989, pp 2157-2189.
- [ 10 ] Björck, A., Plemmons, R.J., Schneider, H., "Large scale matrix problems", Elsevier North Holland, New York, 1981
- [ 11 ] Burden, R.L., Faires, J.D., "Numerical analysis", 5th-ed, PWS-Kent, Boston, 1993
- [ 12 ] Cater, C.R., "Dakota engine cradle fatigue testing", Report no LGI 98-005, Structural Mechanics & Dynamics, Laboratory for Advanced Engineering, Pretoria, 1998.

- [ 13 ] Cater, C.R., "Durability rig testing of Isuzu load boxes", Report no LGI 97-054, Structural Mechanics & Dynamics, Laboratory for Advanced Engineering, Pretoria, 1997.
- [ 14 ] Cater, C.R., "General non-linear system identification for MIMO systems", Report no VLG 94- 020, Centre for Structural Mechanics, Laboratory for Advanced Engineering, Pretoria, 1994
- [ 15 ] Cater, C.R., "Mitsubishi P-Car radiator tests", Report no LGI 98-018, Structural Mechanics & Dynamics, Laboratory for Advanced Engineering, Pretoria, 1998.
- [ 16 ] Cater, C.R., "Modelling results: GM-Truck Data", Report no LGI 97-069, Structural Mechanics & Dynamics, Laboratory for Advanced Engineering, Pretoria, March 1996.
- [ 17 ] Cater, C.R., "Summary of Tests Conducted at Ford Building 4, Dearborn USA", Report no LGI 97-070, Structural Mechanics & Dynamics, Laboratory for Advanced Engineering, Pretoria, April 1996.
- [ 18 ] Chen, S., Billings, S.A., Luo, W., "Orthogonal least squares methods and their application to non-linear system identification", *Int. J. Control*, Vol. 50, No. 5, 1989, pp 1873-1890
- [ 19 ] Craig, J., "The laboratory simulation of vehicle response to road profile excitation", Paper presented at the Symposium on Dynamic Analysis of Structures, Glasgow, 1975.
- [ 20 ] Creyer B.W., Nawrocki P.E., Lund R.A., "A Road Simulation System for Heavy Duty Vehicles", Paper 760361 presented at SAE Automotive Engineering Congress and Exposition, Detroit, February 1976.
- [ 21 ] Dodds, C.J., "The laboratory simulation of vehicle service stress", *Journal of Engineering for Industry*, May, 1974, pp 391-398.
- [ 22 ] Dodds, C.J., "Simulation of Random Environments for Structural Dynamics Testing", *Experimental Mechanics*, November 1976, pp 416-424.
- [ 23 ] Dodds, C.J., Robson, J.D., "Simulated Road Testing", *Journal of Automotive Engineering*, April 1972, pp 17-19.



- [ 24 ] Eksteen, J.J.A., Raath, A.D., Cater, C.R., "Road simulator durability test of the 2020 imported light weight pick-up vehicle", Report no LGI 96-031, Structural Mechanics & Dynamics, Laboratory for Advanced Engineering, Pretoria, 1996.
- [ 25 ] Engels, F., "Vibrations in vehicles and methods of investigating them", Proceedings of the Institution of Mechanical Engineers, Vol. 182, 1967, pp 140-151.
- [ 26 ] Fasol, K.H., Jörgl, H.P., "Principles of model building and identification", Automatica, Vol.16, Pergamon Press, Oxford, 1981.
- [ 27 ] Foster, S.A., "Electrodynamic multi-shaker test systems", Environmental Engineering, September 1989, pp 16-19.
- [ 28 ] Galyardt, D., Quantz, C., "Comparative results for time domain and frequency domain modal parameter estimation algorithms:", Proceedings of the 3rd IMAC, Vol. 1, London, 1987, pp 115-121.
- [ 29 ] Golub G.H., van Loan C.F., "Matrix computations", The John Hopkins University Press, Baltimore, 1983.
- [ 30 ] Harral, B.B., "The application of a statistical fatigue life prediction method to agricultural equipment", International Journal of Fatigue, Vol. 9, 1987, pp 115-118
- [ 31 ] Hodkin, R.K., "Hydraulic vibrators in automobile testing with special reference to the Roots suspension parameter rig", Proceedings of the Institution of Mechanical Engineers, Vol. 182, 1967, pp 54-62.
- [ 32 ] Householder, A.S., "The theory of matrices in numerical analysis", Dover publications inc, New York, 1964.
- [ 33 ] Kana, D.D., Chu, W., "Electromechanical Simulation of Helicopter Blade Responses to Random Excitation During Forward Flight", Journal of Engineering for Industry, May 1974, pp 405-410
- [ 34 ] Kelsey Instruments, "Ki Catalogue", Kelsey Instruments Group, Coventry, 1996
- [ 35 ] Kelsey Instruments, "QanTiM version 3.1 Operational manual", Kelsey Instruments Limited, Coventry, England, 1995.



- [ 36 ] Korenberg, M., Billings, S.A., Liu, Y.P., McIlroy, P.J., "Orthogonal Parameter Estimation Algorithm for non-linear stochastic systems", Int. J. Control, Vol. 48, No. 1, 1988, pp 193-210.
- [ 37 ] Kraus, A.D., "Matrices for engineers", Hemisphere publishing co., Washington, 1976
- [ 38 ] Leontaritis, I.J., Billings, S.A., "Input-Output Parametric Models for Non-linear Systems", Int.J. Control, Vol. 41, No.2, pp 303-344
- [ 39 ] Leontaritis, I.J., Billings, S.A., "Model selection and validation methods for non-linear systems", International Journal of Control, Vol. 45, No. 1, 1987, pp 311-341.
- [ 40 ] Ljung, L. "System Identification theory for the user", Prentice Hall, Englewood Cliffs, New Jersey., 1987.
- [ 41 ] Ljung, L., "System Identification Toolbox User's Guide", The Math Works Inc., Natick, Massachusetts, 1991.
- [ 42 ] Lund, R.A., Donaldson, K.H., "Approaches to vehicle dynamics and durability testing", SAE Transactions, Vol. 91, 1983, pp 289-298.
- [ 43 ] Marcus, M., "Matrices and Matlab - a tutorial", Prentice Hall, New Jersey, 1993.
- [ 44 ] Mathews J.H., "Numerical Methods for computer science, engineering and mathematics", Prentice-Hall, London, 1987.
- [ 45 ] Niemand L.J., Cater C.R., "Bell equipment B25B ADT engine/cooler assembly qualification test", Centre for Structural Mechanics, Laboratory for Advanced Engineering, Pretoria, 1995.
- [ 46 ] Peyton Jones, J.C., Billings, S.A., "Recursive algorithm for computing the frequency response of a class of non-linear difference models", International Journal of Control, Vol. 50, No. 5, 1989, pp 1925-1040.
- [ 47 ] Peyton Jones, J.C., Billings, S.A., "Interpretation of non-linear frequency response functions", International Journal of Control, Vol. 52, No. 2, 1990, pp 319-346.

- [ 48 ] Phillips C.L., Nagle H.T., "Digital control system analysis and design", Prentice-Hall, Englewood Cliffs, N.J. 1984
- [ 49 ] Pierce P.R., "Using Simulated Road Surface Inputs for Dynamic Analysis of Heavy Truck Combination Vehicles", Paper 820096 presented at SAE International Congress & Exposition, Detroit, February 1982.
- [ 50 ] Raath A.D., Cater C.R., "Simulation testing of Isuzu fuel tank assemblies", Report no LGI 95-021, Centre for Structural Mechanics, Laboratory for Advanced Engineering, Pretoria, 1995
- [ 51 ] Raath, A.D., "Dynamic system identification for general multivariable black-box state space formulations", Report no LGI 90- 079, Centre for Structural Mechanics, Laboratory for Advanced Engineering, Pretoria, 1990
- [ 52 ] Raath, A.D., "Dynamic System Identification", Report no VLG/90/050 Centre for Structural Mechanics, Laboratory for Advanced Engineering, Pretoria, 1990.
- [ 53 ] Raath, A.D., "Structural Dynamic Response Reconstruction in the Time Domain", PHD Thesis, Department of Mechanical and Aeronautical Engineering, University of Pretoria, 1992.
- [ 54 ] Raath, A.D., Verwey, W.H., Non-linear Extension of time domain based structural testing techniques - Literature Survey-", Report no LGI 93-042, Centre for Structural Mechanics, Laboratory for Advanced Engineering, Pretoria, 1993.
- [ 55 ] Sales, K.R., Billings, S.A., "Self-tuning of non-linear ARMAX models", International Journal of Control, Vol. 51, No. 4, 1990, pp 753-769.
- [ 56 ] Schutte, R., "Implementation of the NARX model for structural dynamic response reconstruction", Undergraduate thesis, Department of Mechanical and Aeronautical Engineering, University of Pretoria, 1993.
- [ 57 ] Scott, D., "Test rig simulates actual motoring", Automotive Industries, February 15, 1967, pp 88 - 89

- [ 58 ] Strejc, V., "Least squares parameter estimation", Automatica, Vol.16, Pergamon Press, Oxford, 1981.
- [ 59 ] Van der Bijl, S.H., Cater, C.R., "Durability rig testing of Mitsubishi load boxes", Report no LGI 98-008, Structural Mechanics & Dynamics, Laboratory for Advanced Engineering, Pretoria, 1998.
- [ 60 ] Van der Westhuizen, S.F., "Multi-excitation techniques", Master's thesis, Department of Mechanical and Aeronautical Engineering, University of Pretoria, 1990.
- [ 61 ] Van Waveren C.C, Cater C.R., "Fatigue tests on aircraft wing components", Centre for Structural Mechanics, Laboratory for Advanced Engineering, Pretoria, 1996
- [ 62 ] Whittemore, A.P., "A technique for measuring 'effective' road profiles", Paper 720094 presented at SAE automotive engineering congress, Detroit, 1972.
- [ 63 ] Zomotor, A., Schwarz, K., Weiler, W., "Simulation Methods for Evaluating Passenger Car Ride Comfort and the Fatigue Strength of Vehicle Components", Paper 820095 presented at SAE International Congress & Exposition, Detroit, 1982.

$$y(t) = \sum_{n=0}^{\infty} \int \dots \int h_n(\tau_1, \tau_2, \dots, \tau_n) \prod_{i=1}^n u(t-\tau_i) d\tau_i$$

$$= \sum_{n=0}^{\infty} w_n(t) \dots \dots \dots \quad (A-1)$$

The functions  $h_n(\tau_1, \tau_2, \dots, \tau_n)$  are known as the Volterra kernels that form the basis of the identification of non-linear systems represented by functional series.



## Appendix A

### Survey of non-linear system identification models

Linear system identification boasts with a host of widely applicable, well tried techniques, however the identification of non-linear systems has not received such attention or exposure. This can of course be attributed to the inherent complexity of non-linear systems, and the difficulty of deriving identification algorithms that can be applied to a reasonably large class on non-linear systems. This survey presents non-linear model formulations, extracted from published literature, for possible application in response reconstruction. The available models are presented in three groups, functional series methods, block-orientated methods and finally input-output model descriptions.

#### A.1. Functional series methods

In a survey of non-linear system identification techniques, Billings [ 5 ] indicated that functional series all stem from the analytic functionals introduced by Volterra in 1887. Among these methods are the two formulations postulated by Weiner and the Volterra-series methods. Volterra's functional series can be represented as:

$$\begin{aligned}
 y(t) &= \sum_{n=1}^{\infty} \int \dots \int h_n(\tau_1, \tau_2, \dots, \tau_n) \prod_{i=1}^n u(t - \tau_i) d\tau_i \\
 &= \sum_{n=1}^{\infty} w_n(t)
 \end{aligned}
 \tag{ A-1 }$$

The functions  $h_n(\tau_1, \tau_2, \dots, \tau_n)$  are known as the Volterra kernels that form the basis of the identification of non-linear systems represented by functional series.



## A.2. Block-orientated systems

### A.1.1. Wiener methods

One of the first authors to consider non-linear system identification was Wiener who devised two distinct approaches using functional series methods. In theory, these methods are functionally elegant, but Billings [ 5 ] indicated Wiener methods to be impractical due to the excessive number of coefficients required. Further discussions on the Wiener methods are not included in this study, as it holds no practical use in any applications.

### A.1.2. Volterra-series methods

Consider a system that can be described by just the first two Volterra kernels [ 5 ][ 6 ]:

$$y(t) = \int_0^{\infty} h_1(\tau_1)u(t - \tau_1)d\tau_1 + \iint_0^{\infty} h_2(\tau_1, \tau_2)u(t - \tau_1)u(t - \tau_2)d\tau_1 d\tau_2 \quad (\text{A-2})$$

Many methods of identifying the kernels can be found [ 5 ][ 8 ][ 9 ]. These methods however require extensive data and great computational effort. Due to the complexity of the models, the first two kernels as shown above represent the largest practical model of this type. To specify the first two Volterra kernels for a simple quadratic non-linearity in cascade with a first order linear system Billings and Voon [ 8 ] predict 400-500 coefficients would be needed. Again the model would prove to be impractical in actual system identification techniques.

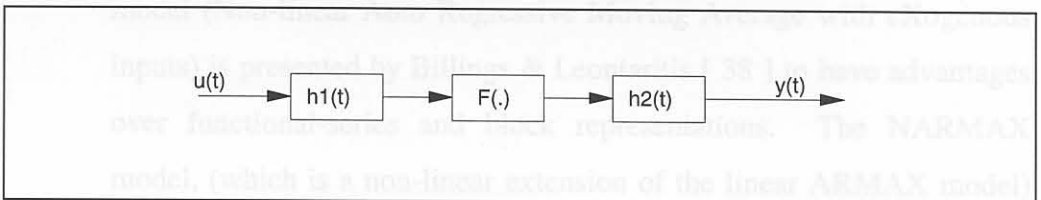


Figure A.2 Schematic representation of Uryson's model

### A.3. Input - output model descriptions

#### A.2. Block-orientated systems

A number of systems consisting of interconnections of linear dynamic systems and non-linear static elements have been formulated to reduce the complexity and computational effort involved with the functional-series methods. One of the most studied models, known as the General model, consists of a linear system followed by a non-linear element in cascade (Figure. A.1 ). Examples of such models are the Hammerstein model and the Uryson's model, shown in Figure A.2 (See Billings [ 5 ]). For the block oriented models,  $h(t)$  represents the dynamic linear part, while  $H(\bullet)$  or  $F(\bullet)$  represents the non-linear part. Schematically such models may be represented as [ 55 ]:



**Figure. A.1** The General Model

Billings [ 5 ] indicated that the Hammerstein model is found by omitting  $h1(t)$  from the general model. It then represents a realisation of the Hammerstein operator, and Uryson's model consists of several Hammerstein models in parallel.

$$H_h [u(t)] = \int h(t, \tau) F[\tau, u(\tau)] d\tau \quad (\text{A-3})$$

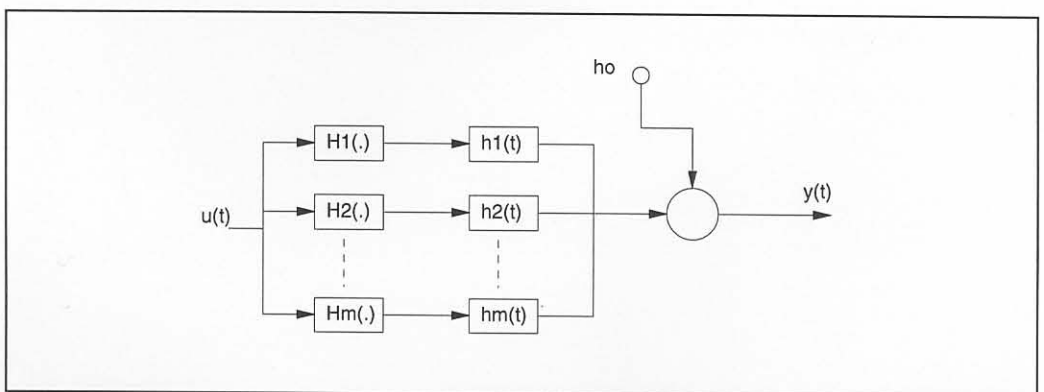


**Figure A.2** Schematic representation of Uryson's model

### A.3. Input - output model descriptions

Billings [ 5 ] and Sales [ 55 ] indicated that input-output model descriptions are generally applicable to systems of which little or no *a priori* information is available. Furthermore, these systems can be represented by extensions of linear models and thus form linear-in-the-parameters models. Systems of this kind form the focus of this study, to enable a general non-linear system identification technique for multiple-input, multiple-output (MIMO) systems. A special case of the input/output model description is the so-called NARMAX model.

#### A.3.1. The NARMAX model

The non-linear difference equation model known as the NARMAX model (Non-linear Auto Regressive Moving Average with eXogenous inputs) is presented by Billings & Leontaritis [ 38 ] to have advantages over functional-series and block representations. The NARMAX model, (which is a non-linear extension of the linear ARMAX model) may be represented as:

$$y(t) = F^L[y(k-1), \dots, y(k-na), u(t), \dots, u(t-nb), e(t-1), \dots, e(t-nc)] + e(t)$$

According to Chen & Billings [ 18 ] it is however impos (A-4)

With  $F^L[\bullet]$  some non-linear polynomial function, normally the degree of the polynomial,  $L=1,2,3$ . Various special cases of the NARMAX model have been identified, some of which are presented in the next Sections.

### A.3.2. Bilinear model

The bilinear input-output model takes the following form [ 18 ]:

$$y(t) = a_0 + \sum_{i=1}^{ny} a_i \cdot y(t-i) + \sum_{i=1}^{nu} b_i \cdot u(t-i) + \sum_{i=1}^{ny} \sum_{j=1}^{nu} c_{ij} \cdot y(t-i) \cdot u(t-j) \quad (\text{A-5})$$

In state space formulation the model representation is:

$$\begin{aligned} x(t+1) &= A \cdot x(t) + B \cdot u(t) + u(t) \cdot C \cdot x(t) \\ y(t) &= D \cdot x(t) \end{aligned} \quad (\text{A-6})$$

where:  $x(t)$  = state vector

$A$  = state matrix

$B$  = input matrix

$C$  = output matrix

$D$  = direct transmission matrix

According to Chen & Billings [ 18 ] it is however impossible to approximate all discrete-time systems within the class of discrete-time bilinear systems.

These two models are initially valid, however, the response function is restricted to polynomial response.

According to Chen & Billings [ 18 ] it is however impossible to approximate all discrete-time systems within the class of discrete-time bilinear systems.

Exogenous input) by removal of the noise model and moving average terms (See Billings [ 5 ] and Peyton Jones [ 46][ 47 ]).

NARX is a parametric difference equation that forms a convenient linear-in-the-parameters equation capable of describing systems with severe non-linearity. The NARX model description was selected to investigate the application of non-linear system identification in dynamic response reconstruction. The NARX model is discussed in detail in Chapter 5.

$$y(t) = F^L [ y(t-1), \dots, y(t-na), u(t), \dots, u(t-nb) ] \quad (\text{A-9})$$

With  $F^L(\cdot)$  again some non-linear polynomial function



## Appendix B

A.3.3. *Output-Affine and rational models*

Chen *et al.* [ 18 ] presented rational and subsequently output-affine models for identification of non-linear dynamic systems. The rational model with polynomial order  $r$  and finite polynomials  $a(\bullet)$  and  $b(\bullet)$  may be written as:

$$y(t) = \frac{b \cdot (y(t-1), \dots, y(t-r), u(t-1), \dots, u(t-r))}{a \cdot (y(t-1), \dots, y(t-r), u(t-1), \dots, u(t-r))} \quad (\text{A-7})$$

The output affine model is a logical expansion of the rational model:

$$y(t) = \sum_{i=1}^r \frac{a_i \cdot (u(t-1), \dots, u(t-r))}{a_0 \cdot (u(t-1), \dots, u(t-r))} \cdot y(t-i) + \frac{a_{r+1} \cdot (u(t-1), \dots, u(t-r))}{a_0 \cdot (u(t-1), \dots, u(t-r))} \quad (\text{A-8})$$

These two models are globally valid, however, the response function is restricted to polynomial response.

A.3.4. *The NARX-model*

The NARMAX model may be reduced to NARX (Non-linear Auto Regressive with eXogenous input) by removal of the noise model and moving average terms (See Billings [ 5 ] and Peyton Jones [ 46][ 47 ]). NARX is a parametric difference equation that forms a convenient linear-in-the-parameters equation capable of describing systems with severe non-linearity. The NARX model description was selected to investigate the application of non-linear system identification in dynamic response reconstruction. The NARX model is discussed in detail in Chapter 5.

$$y(t) = F^L[y(k-1), \dots, y(k-na), u(t), \dots, u(t-nb)] \quad (\text{A-9})$$

With  $F^L[\bullet]$  again some non-linear polynomial function

## Appendix B

### NARX Regression techniques

Various methods were developed to rewrite the NARX difference equation of ( 5-8 ) into a matrix notation for implementation within Matlab. The first and most logical method was to directly implement the difference equation in a sample point loop algorithm. This however proved extremely slow, especially for MIMO systems with large numbers of inputs and outputs. The advantages of Matlab were slightly shadowed by the inherent difficulty to execute loop structures efficiently. On the other hand lateral use of Matlab's matrix manipulation capabilities did, in a way, compensate for the lacking loop performance.

#### B.1. General sample point loop approach

Direct implementation of the NARX difference equation [ 44 ] resulted in an extremely slow method. The algorithm made use of a sample point loop, as well as loop functions to calculate the non-linear terms. It clearly illustrates the NARX construction and served as a solid foundation on which improved algorithms were built.

### Algorithm B.1: Sample point loop regression of the NARX difference equation

INPUT:	Dynamic system input/output data:	$u_1(t), u_2(t) \dots, u_{nu}(t)$ $y_1(t), y_2(t) \dots, y_{ny}(t)$
	Dynamic model order for each o/p channel:	$n_k$
	Degree of non-linearity for each o/p channel:	$L_k$
	Number of sample points to use in regression	$N$
	Number of input and output channels	$nu, ny$
OUTPUT:	Regression matrix for each o/p channel	$\mathbf{X}_1, \mathbf{X}_2, \dots, \mathbf{X}_{ny}$

```

FOR k = 1,2,...,ny      Main loop: output channels
  FOR t = 1,2,...,N    Sample point loop

    Linear regression
    FOR a = 1,2,..., ny Output channel loop
      FOR i = 1,2,.. n_k Output delay loop
         $X_k(t,i) = y_a(t-i)$  Include response data
      FOR b = 1,2,...,nu Input channel loop
        FOR j = 0,2,.. n_k Input delay loop
           $X_k(t,n_k+1+j) = u_b(t-i)$  Include drive data

        IF  $L_k \geq 2$  Quadratic manipulation
          c = 1 Counter
           $M_{L1} = 2n_k + 1$  Number of linear terms
          FOR p = 1,2,...,  $M_{L1}$ 
            FOR q = p+1, p+2,...,  $M_{L1}$ 
              c = c+1 Increment counter
               $X_k(t, M_{L1} + c) = X_k(t,p) \cdot X_k(t,q)$  Calculate quadratic terms

            IF  $L_k \geq 3$  Cubic manipulation
               $M_{L2} = 2n_k + 1 + c$  Number of quadratic terms
              c = 1 Reset counter
              FOR p = 1,2,...,  $M_{L1}$ 
                FOR q = p+1, p+2,...,  $M_{L1}$ 
                  FOR r = q+1, q+2,...,  $M_{L1}$ 
                    c = c+1 Increment counter
                     $X_k(t, M_{L2} + c) = X_k(t,p) \cdot X_k(t,q) \cdot X_k(t,r)$  Calculate cubic terms

```

## B.2. Column-wise Linear regression of the NARX difference equation

An improved method was devised to compute the linear part of the regression matrix without executing the sample point loop. The algorithm made use of Matlab's matrix manipulation capabilities. In each step an entire column is appended to the regression matrix by selecting the correct indices within the input-output data. This reduced calculation times from hours, to seconds. Various methods to further remove the channel and delay order loops were also developed, but proved too cumbersome to warrant practical implementation.

### Algorithm B.2: Linear regression without sample point loop

<i>FOR</i> $k = 1, 2, \dots, n_y$	<i>FOR</i> $a = 1, 2, \dots, n_y$	<i>FOR</i> $i = 1, 2, \dots, n_k$	$X_k = [ X_k \ y_a(n_k + 1 - i : N - 1) ]$	<i>FOR</i> $b = 1, 2, \dots, n_u$	<i>FOR</i> $j = 0, 2, \dots, n_k$	$X_k = [ X_k \ u_b(n_k + 1 - j : N - 1) ]$

*Main loop: output channels*

*Linear regression*

*Output channel loop*

*Output delay loop*

*Include response data*

*Input channel loop*

*Input delay loop*

*Include drive data*

## B.3. Non-linear regression

Construction of the non-linear part of the regression matrix proved difficult to implement generally for all degrees of non-linearity, hence the cubic modelling limitation. Calculating the non-linear terms as described in Algorithm B.1 proved computationally expensive, prompting the development of more elegant methods.



### B.3.1. Loop methods:

As described in Algorithm B.1 a combination of  $L$  nested loops construct the correct indices of the linear regression matrix to be multiplied for each non-linear term. This method proved extremely slow, especially if combined with a sample point loop as shown in Algorithm B.3.

### Algorithm B.3: Loop method for calculation of non-linear terms

```

IF  $L_k \geq 3$ 
   $M_{L2} = 2n_k + 1 + c$ 
   $c = 1$ 
  FOR  $p = 1, 2, \dots, M_{L1}$ 
    FOR  $q = p+1, p+2, \dots, M_{L1}$ 
      FOR  $r = q+1, q+2, \dots, M_{L1}$ 
         $c = c+1$ 
         $X_k(t, M_{L2} + c) = X_k(t, p) \cdot X_k(t, q) \cdot X_k(t, r)$ 

```

### B.3.2. Matrix manipulation methods

Matlab's matrix manipulation capabilities were used in a method for finding the non-linear parts of the regression matrix and proved the forerunner of more advanced methods. This method presented a substantial improvement over the loop method of Algorithm B.3, but was still restricted by a sample point outer loop.

### Algorithm B.4: Matrix manipulation of non-linear terms

```

FOR  $k = 1, 2, \dots, n_y$ 
  FOR  $t = 1, 2, \dots, N$ 
    Find  $X_{L1_k}(t)$  the linear part of the regression matrix  $X_k(t)$  as in Algorithm B.1
     $X_{L1_k}(t) = [y_1(t-1) \ \dots \ y_{n_y}(t-na) \ \dots \ u_1(t) \ u_1(t-1) \ \dots \ u_{n_u}(t-nb)]$ 
Step 1:
           $= [X_{k_1}(t) \ X_{k_2}(t) \ \dots \ \dots \ \dots \ X_{k_{m_1}}(t)]$ 

```

### B.3.3. Indexed matrix manipulation methods

Step 2: Create the first term matrix. A square matrix called  $\mathbf{P}_1(t)$  is created by multiplying a  $(M1 \times 1)$  unity column matrix with  $\mathbf{XLI}_k(t)$ .

$$\mathbf{P}_1(t) = \begin{bmatrix} 1 \\ 1 \\ \vdots \\ \vdots \\ 1 \end{bmatrix} \cdot \begin{bmatrix} X_{k_1}(t) & X_{k_2}(t) & \cdots & \cdots & X_{k_{M1}}(t) \\ X_{k_1}(t) & X_{k_2}(t) & \cdots & \cdots & X_{k_{M1}}(t) \\ \vdots & \vdots & \ddots & \ddots & \vdots \\ \vdots & \vdots & & \ddots & \vdots \\ X_{k_1}(t) & X_{k_2}(t) & \cdots & \cdots & X_{k_{M1}}(t) \end{bmatrix} =$$

Step 3: Create the second term matrix,  $\mathbf{P}_2(t)$  by simply transposing  $\mathbf{P}_1(t)$ :

$$\mathbf{P}_2(t) = \mathbf{P}_1(t)^T$$

Step 4: The matrices  $\mathbf{P}_1(t)$  and  $\mathbf{P}_2(t)$  are then reduced by discarding their upper triangular parts. Taking the elements in a column-wise fashion matrix  $\mathbf{P}_1(t)$  and  $\mathbf{P}_2(t)$  are reshaped into vectors.

$$\mathbf{P}_1(t) = \begin{bmatrix} X_{k_1}(t) \\ X_{k_1}(t) & X_{k_2}(t) \\ \vdots & \ddots & \ddots \\ \vdots & & \ddots & \ddots \\ X_{k_1}(t) & X_{k_2}(t) & \cdots & \cdots & X_{k_{M1}}(t) \end{bmatrix} \Rightarrow$$

$$\mathbf{P}_1(t) = [X_{k_1}(t) \quad X_{k_1}(t) \quad \cdots \quad X_{k_1}(t) \quad X_{k_2}(t) \quad \cdots \quad X_{k_2}(t) \quad \cdots \quad \cdots \quad X_{k_{M1}}(t)] \quad (B-1)$$

Similarly

$$\mathbf{P}_2(t) = \begin{bmatrix} X_{k_1}(t) \\ X_{k_2}(t) & X_{k_2}(t) \\ \vdots & \ddots & \ddots \\ \vdots & & \ddots & \ddots \\ X_{k_{M1}}(t) & X_{k_{M1}}(t) & \cdots & \cdots & X_{k_{M1}}(t) \end{bmatrix} \Rightarrow$$

$$\mathbf{P}_2(t) = [X_{k_1}(t) \quad X_{k_2}(t) \quad \cdots \quad X_{k_{M1}}(t) \quad X_{k_2}(t) \quad \cdots \quad X_{k_{M1}}(t) \quad \cdots \quad \cdots \quad X_{k_{M1}}(t)]$$

Step 5: The non-linear part of  $\mathbf{X}_k(t)$  is found by multiplying vectors  $\mathbf{P}_1(t)$  and  $\mathbf{P}_2(t)$  in an element-by-element fashion. The regression matrix  $\mathbf{X}_k(t)$  is formed by appending  $\mathbf{XLI}_k(t)$  and  $\mathbf{XL2}_k(t)$  (\* implies element-by-element multiplication.)

$$\mathbf{XL2}_k(t) = \mathbf{P}_1(t) \cdot \mathbf{P}_2(t) =$$

$$[X_{k_1}(t) \cdot X_{k_1}(t) \quad X_{k_1}(t) \cdot X_{k_2}(t) \quad \cdots \quad X_{k_2}(t) \cdot X_{k_2}(t) \quad X_{k_2}(t) \cdot X_{k_3}(t) \quad \cdots \quad \cdots \quad X_{k_{M1}}(t) \cdot X_{k_{M1}}(t)]$$

$$\mathbf{X}_k(t) = [\mathbf{XLI}_k(t) \quad \mathbf{XL2}_k(t)]$$

### B.3.3. Indexed matrix manipulation methods

The limiting factor in the matrix manipulation technique of Algorithm B.4 remained the sample point loop (the number of samples,  $N$ , is typically in the order of  $10^4$ ). A more general method in which the non-linear calculations need not be done for each sample was devised. This indexed matrix manipulation method creates a set of matrices containing the indices for non-linear combinations of the linear terms. The procedure is similar to that of Algorithm B.4, but does not manipulate the actual ARX-terms, only the indices thereof. The indexed matrix manipulation method presented in Algorithm B.5 may be used with techniques that implement sample point loops (Algorithm B.1) as well as those that do not (Algorithm B.2). If used in conjunction with a sample point loop algorithm, the index vectors  $P_1$  and  $P_2$  must be calculated prior to initiating the loop. The non-linear terms,  $XL2_k(t)$ , are then calculated for each sample by evaluating:

$$\begin{aligned} XL2_k(t) &= X_{L1_k}(t, P_1) \cdot X_{L1_k}(t, P_2) \\ &= X_{L1_k}(t, [1,1,1, \dots, 2,2, \dots, M_{L1}]) \cdot X_{L1_k}(t, [1,2,3, \dots, 2,3, \dots, M_{L1}]) \end{aligned} \quad (\text{B-1})$$

The indexed matrix manipulation method is best suited for use with column-wise linear regression (Algorithm B.2). The linear regression is completed for each channel  $k$  prior to finding the non-linear combinations. Combining Algorithm B.2 and Algorithm B.5 provides a system capable of easily calculating the NARX regression matrix, with minimal use of loop structures.

## Appendix C

**Algorithm B.5: Indexed matrix manipulation of non-linear terms**

FOR  $k = 1, 2, \dots, ny$

Step 1: Create the first term matrix. A square matrix called  $\mathbf{P}_1$  is created by multiplying a  $(M_{L1} \times 1)$  unity column matrix with the vector  $[1, 2, 3, \dots, M_{L1}]$ .

$$\mathbf{P}_1 = \begin{bmatrix} 1 \\ 1 \\ \vdots \\ \vdots \\ 1 \end{bmatrix} \cdot [1 \ 2 \ 3 \ \dots \ M_{L1}] = \begin{bmatrix} 1 & 2 & 3 & \dots & M_{L1} \\ 1 & 2 & 3 & \dots & M_{L1} \\ 1 & 2 & 3 & \dots & M_{L1} \\ \vdots & \vdots & \vdots & \ddots & \vdots \\ 1 & 2 & \dots & \dots & M_{L1} \end{bmatrix}$$

Step 2: Create the second term matrix,  $\mathbf{P}_2$  by simply transposing  $\mathbf{P}_1$

$$\mathbf{P}_2 = \mathbf{P}_1^T = \begin{bmatrix} 1 & 1 & 1 & \dots & 1 \\ 2 & 2 & 2 & \dots & 2 \\ 3 & 3 & 3 & \dots & 3 \\ \vdots & \vdots & \vdots & \ddots & \vdots \\ M_{L1} & M_{L1} & M_{L1} & \dots & M_{L1} \end{bmatrix} \quad (C-1)$$

Step 3: The matrices  $\mathbf{P}_1$  and  $\mathbf{P}_2$  are again reduced by discarding their upper triangular parts. Taking the elements in a column-wise fashion matrix  $\mathbf{P}_1$  and  $\mathbf{P}_2$  are reshaped into vectors.

$$\mathbf{P}_1 = \begin{bmatrix} 1 \\ 1 \ 2 \\ 1 \ 2 \ 3 \\ \vdots \\ 1 \ 2 \ 3 \ \dots \ M_{L1} \end{bmatrix} \Rightarrow \mathbf{P}_2 = \begin{bmatrix} 1 \\ 2 \ 2 \\ 3 \ 3 \ 3 \\ \vdots \\ M_{L1} \ M_{L1} \ \dots \ M_{L1} \end{bmatrix} \Rightarrow$$

$$\mathbf{P}_1 = [1 \ 1 \ \dots \ 2 \ 2 \ \dots \ 3 \ 3 \ \dots \ M_{L1}] \quad \mathbf{P}_2 = [1 \ 2 \ 3 \ \dots \ 2 \ 3 \ \dots \ 3 \ \dots \ M_{L1}]$$

Step 4: The vectors  $\mathbf{P}_1$  and  $\mathbf{P}_2$  are the indices of the linear regression matrix  $\mathbf{X}_{L1_k}$  to be multiplied to form the non-linear  $\mathbf{X}_{L2_k}$  so that

$$\mathbf{X}_{L2_k} = \mathbf{X}_{L1_k}(:, \mathbf{P}_1) .* \mathbf{X}_{L1_k}(:, \mathbf{P}_2)$$

Step 5: Lastly the matrices  $\mathbf{X}_{L1_k}$  and  $\mathbf{X}_{L2_k}$  are appended to form the complete regression matrix:

$$\mathbf{X}_k = [\mathbf{X}_{L1_k} \ \mathbf{X}_{L2_k}]$$



## Appendix C

### NARX Parameter estimation: full parameter set solutions

Parameter estimation for NARX models was presented in Section 5.3, defining the concept of orthogonal decomposition to solve the Least Squares equation. Consider again the Least Squares Equation ( 5-17 ) for finding the NARX coefficient vector  $\Theta_k$ .

$$\mathbf{X}^T \cdot \mathbf{X} \cdot \Theta - \mathbf{X}^T \cdot \mathbf{Y} = 0$$

$$\Downarrow$$

$$\Theta = [\mathbf{X}^T \cdot \mathbf{X}]^{-1} \cdot \mathbf{X}^T \cdot \mathbf{Y} \quad (\text{C-1})$$

The simplest method would be to implement Matlab functions to directly solve the inverse  $[\mathbf{X}^T \cdot \mathbf{X}]^{-1}$  and then find the  $\Theta_k$  according to ( C-1 ).

#### C.1. Solving the normal Least Squares equation

Implementation within Matlab gives access to a multitude of numerical functions and toolboxes which are easily and generally applied to most engineering problems. It was thus a logical first choice to make use of Matlab's matrix *INVERSE* function to find a solution to the Least Squares equation. The algorithm for finding the NARX parameter vector for channel  $k$ ,  $\Theta_k$  can thus be written as shown in Algorithm C.1

#### Algorithm C.1: Solving the Least Squares equation using Matlab

INPUT:	Dynamic system output data:	$y_1(t), y_2(t) \dots, y_{ny}(t)$
	Regression matrix for each channel	$X_k$
	Number of output channels	$ny$
OUTPUT:	NARX coefficient vector for each o/p channel	$\Theta_1, \Theta_2, \dots, \Theta_{ny}$

for $k = 1, 2, \dots, ny$	<i>Loop channel numbers</i>
$\Theta_k = INV(X_k^T * X_k) * X_k^T * y_k$	<i>Calculate NARX coefficient vector using INVERSE and matrix manipulation functions</i>

This simple and effective solution is unfortunately not ideally suited for application in large NARX systems. It has major limitations concerning the size of the system and ill-conditioning of matrices. It is not uncommon for the NARX matrix  $[\mathbf{X}^T \cdot \mathbf{X}]^{-1}$  to consist of more than  $10^3$  elements, which poses a problem for conventional matrix inversion techniques.

Alternatively the Least Squares equation may be considered as a set of linear equations and solved by a Gaussian elimination scheme. Rewrite Equation (C-1) into the familiar  $\mathbf{A}x = b$  format for systems of linear equations:

$$\begin{aligned} \mathbf{X}^T \cdot \mathbf{X} \cdot \Theta - \mathbf{X}^T \cdot \mathbf{Y} &= 0 \\ \Downarrow \\ [\mathbf{X}^T \cdot \mathbf{X}] \cdot \Theta &= \mathbf{X}^T \cdot \mathbf{Y} \\ \Downarrow \\ \mathbf{A} \cdot x = b &\quad \begin{cases} \mathbf{A} = [\mathbf{X}^T \cdot \mathbf{X}] \\ x = \Theta \\ b = \mathbf{X}^T \cdot \mathbf{Y} \end{cases} \end{aligned} \quad (\text{C-2})$$

An elegant and effective method for solving Equation (C-2) is by Crout factorisation of Algorithm C.2, as presented by Burden and Faires [ 11 ].

The matrix  $\mathbf{X}^T \cdot \mathbf{X}$  may further tend to be ill-conditioned, which makes inversion by conventional techniques impossible. If inversion of an ill conditioned  $\mathbf{X}^T \cdot \mathbf{X}$  matrix is possible the NARX coefficient vector  $\Theta$  may be inaccurate due to an accumulation of round off errors within the inversion process. The ill conditioning of a matrix  $\mathbf{X}$  can be quantified by its rank  $K[\mathbf{X}]$ , the ratio of the largest to the smallest non-zero singular value of  $\mathbf{X}$  [ 37 ]. According to Chen [ 18 ], a normal equation for solving the Least Squares problem can not be used unless  $K[\mathbf{X}] \leq 2^{M/2}$ , with M the number of NARX coefficients within  $\Theta$ . This creates the demand for more general solution methods.

**Algorithm C.2: Crout factorisation**

INPUT:	Dynamic system output data:	$y_1(t), y_2(t) \dots, y_{ny}(t)$
	Regression matrix for each channel	$X_k$
	Number of output channels	$ny$
OUTPUT:	NARX coefficient vector for each o/p channel	$\Theta_1, \Theta_2, \dots, \Theta_{ny}$

<pre> for k = 1, 2, ..., ny   A = X_k^T * X_k   b = X_k^T * y_k   n = max(size(A));   A = [A b];   l(1,1) = A(1,1);   u(1,2) = A(1,2)/l(1,1);   for i = 2:n-1     l(i,i-1) = A(i,i-1);     l(i,i) = A(i,i)-l(i,i-1)*u(i-1,i);     u(i,i+1) = a(i,i+1)/l(i,i);   l(n,n-1) = A(n,n-1);   l(n,n) = A(n,n)-l(n,n-1)*u(n-1,n);   z(1) = a(1,n+1)/l(1,1);   for i = 2:n     z(i) = (a(i,n+1)-l(i,i-1)*z(i-1))/l(i,i);   x(n) = z(n);   for i = n-1:-1:1     x(i) = z(i) - u(i,i+1)*x(i+1);   Theta_k = x^T; </pre>	<p><i>Loop channel numbers</i> (C-3)</p> <p><i>Create A matrix</i></p> <p><i>Create b vector</i></p> <p><i>Calculate number of columns in A</i></p> <p><i>Create augmented matrix</i></p> <p><i>Initialise lower triangular matrix L</i></p> <p><i>Initialise upper triangular matrix U</i></p> <p><i>Backward substitution</i></p>
--	---

Thus the solution to the Least Squares problem is:

$$\Theta = Y \cdot Y \quad (C-7)$$

Finding the NARX parameters using the singular value decomposition scheme proved accurate, but time consuming due to the complexity of finding the singular values of a large matrix (C-3).

## C.2. Singular value decomposition

The solution to the Least Squares problem is no longer unique if the rank of  $\mathbf{X}$  is less than  $2^{M/2}$ . The singular value decomposition offers a general solution to the Least Squares problem. The procedure starts with the singular value decomposition theorem as presented by Marcus [ 43 ]:

$$\mathbf{X}=\mathbf{U}\cdot\mathbf{S}\cdot\mathbf{V}^T \quad (\text{C-3})$$

The matrix can be the product of a diagonal matrix,  $\mathbf{S}$ , of the same dimension as  $\mathbf{X}$  and with nonnegative diagonal elements in decreasing order, and unitary matrices  $\mathbf{U}$  and  $\mathbf{V}$ .

$$\mathbf{S}=\text{diag}[s_1,s_2,\dots,s_M] \quad (\text{C-4})$$

The pseudo-inverse of  $\mathbf{S}$  is defined as:

$$\mathbf{S}^+=\text{diag}[s_1^+,s_2^+,\dots,s_M^+] \quad (\text{C-5})$$

$$s_i^+ = \begin{cases} \frac{1}{s_i}, & \text{for } s_i > 0 \\ 0, & \text{for } s_i = 0 \end{cases}$$

So that:

$$\mathbf{X}^+=\mathbf{V}\cdot\mathbf{S}^+\cdot\mathbf{U}^T \quad (\text{C-6})$$

Thus the solution to the Least Squares problem is:

$$\Theta=\mathbf{X}^+\cdot\mathbf{Y} \quad (\text{C-7})$$

Finding the NARX parameters using the singular value decomposition scheme proved accurate, but time consuming due to the complexity of finding the singular values of a large matrix (C-3 ).



### C.3. Orthogonal decomposition

Matrix inversion methods based on orthogonalization of the matrix  $\mathbf{X}^T \cdot \mathbf{X}$  proved the most convenient for parameter estimation applications of large NARX systems [ 18 ][ 36 ]. These methods are generally fast and can be implemented to be insensitive to low matrix ranks and thus produce accurate results for most systems.

Recall that a matrix  $\mathbf{X}$  can be transformed into an orthogonal matrix  $\mathbf{Q}$  and an upper triangular matrix  $\mathbf{R}$  so that [ 32 ].

$$\mathbf{X} = \mathbf{Q} \cdot \mathbf{R} \quad (\text{C-8})$$

Transform the Least Squares equation, in order to find the parameter vector  $\Theta$ .

$$\begin{aligned} \Theta &= [\mathbf{X}^T \cdot \mathbf{X}]^{-1} \cdot \mathbf{X}^T \cdot \mathbf{Y} \\ \mathbf{X}^T \cdot \mathbf{X} \cdot \Theta &= \mathbf{X}^T \cdot \mathbf{Y} \end{aligned} \quad (\text{C-9})$$

Substitute  $\mathbf{X} = \mathbf{Q} \cdot \mathbf{R}$

$$\begin{aligned} [\mathbf{Q} \cdot \mathbf{R}]^T \cdot \mathbf{Q} \cdot \mathbf{R} \cdot \Theta &= [\mathbf{Q} \cdot \mathbf{R}]^T \cdot \mathbf{Y} \\ \mathbf{Q}^T \cdot \mathbf{R}^T \cdot \mathbf{Q} \cdot \mathbf{R} \cdot \Theta &= \mathbf{Q}^T \cdot \mathbf{R}^T \cdot \mathbf{Y} \end{aligned} \quad (\text{C-10})$$

but  $\mathbf{Q}^T \cdot \mathbf{Q} = \mathbf{I}$

$$\begin{aligned} \mathbf{R}^T \cdot \mathbf{R} \cdot \Theta &= \mathbf{Q}^T \cdot \mathbf{R}^T \cdot \mathbf{Y} \\ \mathbf{R} \cdot \Theta &= [\mathbf{R}^T]^{-1} \cdot \mathbf{Q}^T \cdot \mathbf{R}^T \cdot \mathbf{Y} \end{aligned} \quad (\text{C-11})$$

thus (C-12)

$$\Theta = [\mathbf{R}^T]^{-1} \cdot \mathbf{Q}^T \cdot \mathbf{Y}$$

Again direct implementation of built in Matlab functions provided a simple and convenient first approach to finding the NARX parameter vector  $\Theta_k$ .

**Algorithm C.3** shows the use of Matlab's *QR* orthogonalization function.

**Algorithm C.3: Parameter estimation using Matlab orthogonal decomposition**

INPUT:	Dynamic system output data:	$y_1(t), y_2(t) \dots, y_{ny}(t)$
	Regression matrix for each channel	$X_k$
	Number of output channels	$ny$
OUTPUT:	NARX coefficient vector for each o/p channel	$\Theta_1, \Theta_2, \dots, \Theta_{ny}$

<i>for</i> $k = 1, 2, \dots, ny$	<i>Loop channel numbers</i>
$[Q, R] = QR(X_k)$	<i>Orthogonal decomposition of regression vector <math>X</math>, using Matlab's <i>QR</i> function</i>
$\Theta_k = INV(R^T) * Q^T * y_k$	<i>Calculate NARX coefficient vector using <i>INVERSE</i> and matrix manipulation functions</i>

The parameter estimation technique presented in Algorithm C.3 proved accurate and extremely convenient, but is unfortunately slow for large non-linear systems. A faster, more elegant approach to orthogonal decomposition was needed. Various methods are discussed: Golub [ 29 ] reviews methods applicable to matrix orthogonalization, Chen *et all.* [ 18 ] present a classical and modified Gram Schmidt process specifically for application in parameter estimation. A Gram Schmidt process as presented by Burden and Faires [ 11 ] as well as a method proposed by Householder [ 32 ] was modified by the author for application in NARX parameter estimation.

$$W^T W = D \quad (C-15)$$

With  $D$  a positive diagonal matrix such that:

$$X^T X = A^T D A \quad (C-16)$$

### C.3.1. Gram Schmidt

The Gram Schmidt process is commonly used in numerical analysis for applications ranging from finding eigen values, solving sets of numerical equations, finding matrix inverses and more specifically orthogonalization of matrices. A typical example is that presented by Burden and Faires [ 11 ]. A more formal Gram Schmidt approach, specifically adapted for parameter estimation, is presented by Chen *et all* [ 18 ]. This procedure is an adaptation of the method presented by Golub [ 29 ] and makes use of an auxiliary model:

$$\mathbf{Y} = \mathbf{W} \cdot \mathbf{g} \quad (\text{C-13})$$

With  $\mathbf{W}$  an orthogonal regression matrix and  $\mathbf{g}$  an auxiliary parameter vector. Consider the factorisation of the regression matrix  $\mathbf{X}$  into an upper triangular matrix  $\mathbf{A}$  and an orthogonal matrix  $\mathbf{W}$ . The matrices  $\mathbf{W}$  and  $\mathbf{A}$  are calculated according to Algorithm C.4

$$\mathbf{X} = \mathbf{W} \cdot \mathbf{A}$$

$$\mathbf{A} = \begin{bmatrix} 1 & \alpha_{12} & \alpha_{13} & \cdots & \alpha_{1M} \\ & 1 & \alpha_{23} & \cdots & \alpha_{2M} \\ & & \ddots & \ddots & \vdots \\ & & & 1 & \alpha_{M-1M} \\ & & & & 1 \end{bmatrix} \quad (\text{C-14})$$

$$\mathbf{W} = [\mathbf{w}_1 \quad \cdots \quad \mathbf{w}_M]$$

The  $N$  by  $M$  matrix  $\mathbf{W}$  has orthogonal columns that satisfy:

$$\mathbf{W}^T \cdot \mathbf{W} = \mathbf{D} \quad (\text{C-15})$$

With  $\mathbf{D}$  a positive diagonal matrix such that:

$$\mathbf{X}^T \cdot \mathbf{X} = \mathbf{A}^T \mathbf{D} \mathbf{A} \quad (\text{C-16})$$

**Algorithm C.4: Calculation of W and A for Gram Schmidt process**

INPUT:	Regression matrix for each channel	$X_k$
	Number of NARX parameters	$M$
OUTPUT:	Orthogonal regression matrix	$W$
	upper triangular matrix	$A$

$W_1 = X_1$       *Initiate process by setting column 1 of W equal to column 1 of X*

for  $k = 2, 3, \dots, M$

    for  $i = 1, 2, \dots, k-1$

$$\alpha_{ik} = \frac{W_i \cdot X_k}{W_i \cdot W_i}$$

*Calculate the  $k^{\text{th}}$  column of W and  $k^{\text{th}}$  row of A*

*(for W and X the subscript indicates the column number)*

$$W_k = X_k - \sum_{i=1}^{k-1} \alpha_{ik} W_i$$

The auxiliary parameter vector  $\mathbf{g}$  is defined so that:

$$\mathbf{g} = \mathbf{D}^{-1} \cdot \mathbf{W}^T \cdot \mathbf{Y} \quad (\text{C-17})$$

Using back substitution, the parameter vector  $\Theta$  can now readily be calculated from:

$$\mathbf{A} \cdot \Theta = \mathbf{g} \quad (\text{C-18})$$

This classical Gram Schmidt process proved fast, but is very sensitive to round-off errors [ 18 ].

The elements of the auxiliary parameter vector  $\mathbf{g}$  are calculated according to Algorithm C.6.



### C.3.2. Modified Gram Schmidt

Due to the inherent inaccuracies associated with the classical Gram Schmidt process, Chen *et al* [ 18 ] further presented a modified Gram Schmidt procedure for finding the NARX coefficients. The orthogonalization process for the modified Gram Schmidt method is presented in Algorithm C.5

#### Algorithm C.5: Calculation of W and A for modified Gram Schmidt process

INPUT:	Regression matrix for each channel	$X_k$
	Number of NARX parameters	$M$
OUTPUT:	Orthogonal regression matrix	$W$
	upper triangular matrix	$A$

$X^{(0)} = X$	Initiate process by setting the matrix $X^{(0)}$ equal to $X$
for $k=1, 2, 3, \dots, M-1$	
$W_k^{(0)} = X_k^{(k-1)}$	Calculate the $k^{\text{th}}$ column of $W$ and $k^{\text{th}}$ row of $A$
for $i=1, 2, \dots, k-1$	(for $W$ and $X$ the subscript indicates the column number)
$w_k = x_k^{(k-1)}$	
$\alpha_{ki} = \frac{w_k^T \cdot x_i^{(k-1)}}{w_k^T \cdot w_k}$	
$x_i^{(k)} = x_i^{(k-1)} - \alpha_{ki} w_k$	
$W_M = X_M^{(M-1)}$	

The elements of the auxiliary parameter vector  $g$  are calculated according to Algorithm C.6.

**Algorithm C.6: Calculation of auxiliary parameter vector  $\mathbf{g}$  for the modified Gram Schmidt process**

INPUT:	Orthogonal regression matrix	$W$
	Number of NARX parameters	$M$
OUTPUT:	Auxiliary parameter vector	$\mathbf{g}$

$Y^{(0)} = Y$	<i>Initiate process by setting <math>Y^{(0)}</math> equal to <math>X</math></i>
for $k=1, 2, 3, \dots, M-1$	<i>Loop channel numbers</i>
$\mathbf{g}_k = \frac{\mathbf{w}_k^T \cdot \mathbf{Y}^{(k-1)}}{\mathbf{w}_k^T \cdot \mathbf{w}_k}$	<i>Calculate the <math>k^{\text{th}}</math> element of <math>\mathbf{g}</math> and rewrite <math>Y^k</math></i>
$\mathbf{Y}^{(k)} = \mathbf{Y}^{(k-1)} - \mathbf{g}_k \mathbf{w}_k$	<i>(for <math>W</math> the subscript indicates the column number)</i>

This modified Gram Schmidt procedure is not as fast as the classical method, but proved numerically superior and very accurate since round off errors are not accumulated. The modified Gram Schmidt procedure is slow due to the complex loop structures required during the orthogonalization process. An adapted version of this modified Gram Schmidt algorithm proved to be the most effective method for NARX parameter estimation. This method combined the classical Gram Schmidt technique with Matlab's  $QR$  function as shown in Algorithm C.7.

### Algorithm C.7: Combined Matlab Gram Schmidt parameter estimation

INPUT:	Dynamic system output data:	$y_1(t), y_2(t) \dots, y_{ny}(t)$
	Regression matrix for each channel	$X_k$
	Number of output channels	$ny$
OUTPUT:	NARX coefficient vector for each channel	$\Theta_1, \Theta_2, \dots, \Theta_{ny}$

for  $k = 1, 2, \dots, ny$

$[Q, R] = QR(X_k)$

$[dum, M] = size(X_k);$

$g = Q^* * y;$

$\Theta_k(M) = g(M)/R(M, M);$

for  $j = M-1:-1:1$

$\Theta_k(j) =$

$(g(j) - (R(j, j+1:M) * \Theta_k(j+1:M, 1))) / R(j, j)$

*Loop channel numbers*

*Orthogonal decomposition of regression vector  $X$ , using Matlab's  $QR$  function*

*Calculate number of columns in regression matrix  $X$*

*Calculate NARX coefficient vector*

### C.3.3. Householder

A parameter estimation technique based on the orthogonalization proposed by Householder [ 32 ] and again presented by Golub [ 29 ] and Chen [ 18 ] for application in parameter estimation, is given in Algorithm C.8. Augment the matrix  $\mathbf{Q}$  with a further  $N-M$  orthonormal columns to make up a full set of  $N$  orthonormal vectors for an  $N$ -dimensional Euclidean space:

$$\tilde{\mathbf{Q}} = [\mathbf{Q} \quad \tilde{\mathbf{q}}_{M+1} \quad \cdots \quad \tilde{\mathbf{q}}_N] = [\mathbf{Q}_M \quad \tilde{\mathbf{Q}}_{N-M}] \quad (\text{C-19})$$

Then

$$\mathbf{X} = \tilde{\mathbf{Q}}\tilde{\mathbf{R}} = \mathbf{Q} \begin{bmatrix} \mathbf{R} \\ \mathbf{0} \end{bmatrix} \quad (\text{C-20})$$

Where  $\mathbf{R}$  is a  $M \times M$  upper triangular matrix and  $\tilde{\mathbf{Q}}^T$  can be used to triangularize  $\mathbf{X}$ .

If  $\tilde{\mathbf{Q}}^T \mathbf{y}$  is partitioned into:

$$\tilde{\mathbf{Q}}^T \mathbf{y} = \mathbf{Q} \begin{bmatrix} \mathbf{y}_1 \\ \mathbf{y}_2 \end{bmatrix} \begin{matrix} \} M \\ \} N - M \end{matrix} \quad (\text{C-21})$$

We have:

$$\|\mathbf{y} - \mathbf{X} \cdot \Theta\| = \|\tilde{\mathbf{Q}}^T (\mathbf{y} - \mathbf{X} \cdot \Theta)\| = \|\mathbf{y}_1 - \mathbf{R} \cdot \Theta\| + \|\mathbf{y}_2\| \quad (\text{C-22})$$

The Least Squares estimates can therefore be obtained by solving the triangular system:

$$\mathbf{R} \cdot \Theta = \mathbf{y}_1 \quad (\text{C-23})$$



## Appendix D

**Algorithm C.8: Householder parameter estimation**

INPUT:	Dynamic system output data:	$y_1(t), y_2(t) \dots, y_{ny}(t)$
	Regression matrix for each channel	$X_k$
	Number of output channels	$ny$
OUTPUT:	NARX coefficient vector for each channel	$\Theta_1, \Theta_2, \dots, \Theta_{ny}$

```

[N,M]=size(x);
x = [x y];
for j = 1:M;
    sj = norm(x(j:N,j));
    bj = 1/(sj*(sj+abs(x(j,j))));
    vj = zeros(N,1);
    vj(j,1) = x(j,j)+sign(x(j,j))*sj;
    vj(j+1:N,1) = x(j+1:N,j);
    x = x - vj*bj*vj'*x;
z1 = x(1:M,M+1);
z2 = x(M+1:N,M+1);
x = x(1:M,1:M);
th = inv(x)*z1;

```

## Appendix D

### NARX Parameter estimation: Reduced parameter set solutions

Because the number of possible NARX candidate terms can easily run into several thousands even for ‘moderately’ non-linear MIMO systems optimal multiple selection methods could reduce the computational effort involved in the system identification process. Unfortunately the model structure of real systems is rarely known *a priori* and methods of model structure determination must therefore be developed and included as a vital part of the identification procedure. Korenberg [ 36 ] indicates that “provided the significant terms in the model can be detected, models with fewer than ten terms are usually sufficient to capture the dynamics of highly non-linear processes.” Various studies [ 38 ][ 36 ][ 6 ], have been undertaken into structure detection for non-linear parametric models. More specifically Chen [ 18 ] surveyed methods for finding a reduced NARX equation i.e. discarding terms in the NARX equation which do not contribute to the dynamic behaviour of the system. These structure reduction schemes are presented for the parameter estimation techniques of Appendix C. These methods all require the full set of NARX coefficients to be available for evaluation, thus an initial full set regression and parameter estimation is required prior to structure detection. Research into finding the significant terms within the NARX model prior to parameter estimation proved fruitless. The basic structure detection scheme is presented in Figure D.1.

1	Least squares regression
2	Singular value decomposition
3	Orthogonal decomposition
	Gram Schmidt
	Modified Gram Schmidt
	Householder
4	Diverse methods
5	Eigen value methods

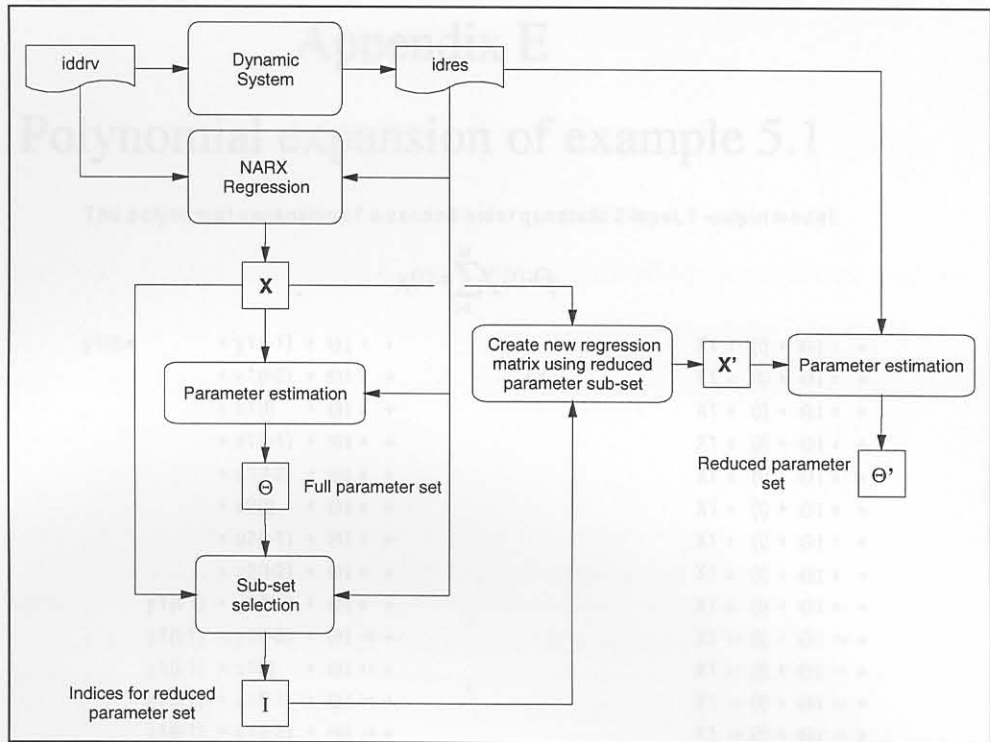


**Figure D.1: Reduced sub-set selection**

The structure detection processes proved computationally cumbersome. More importantly simulation of the NARX models proved insensitive to the number of terms involved. The general conclusion is that the amount of effort concerned with model reduction does not warrant the implementation thereof. Full parameter set modelling proved more practical. Some of the reduction techniques investigated are listed in Table D.1.

**Table D.1 Parameter reduction methods**

1	Stepwise regression
2	Singular value decomposition
3	Orthogonal decomposition
	Gram Schmidt
	Modified Gram Schmidt
	Householder
4	Diverse methods
5	Eigen value methods

# Appendix E

## Polynomial expansion of example 5.1

The polynomial expansion of a second order quadratic 2-input, 1-output model.

$$y_1(t) = \sum_{i=1}^M X_i(t) \cdot \Theta_i$$

$y_1(t) =$	$+ y_1(t-1) + \Theta_{11} +$ $+ y_1(t-2) + \Theta_{12} +$ $+ u_1(t) + \Theta_{13} +$ $+ u_1(t-1) + \Theta_{14} +$ $+ u_1(t-2) + \Theta_{15} +$ $+ u_2(t) + \Theta_{16} +$ $+ u_2(t-1) + \Theta_{17} +$ $+ u_2(t-2) + \Theta_{18} +$ $y_1(t-1) + y_1(t-1) + \Theta_{19} +$ $y_1(t-1) + y_1(t-2) + \Theta_{110} +$ $y_1(t-1) + u_1(t) + \Theta_{111} +$ $y_1(t-1) + u_1(t-1) + \Theta_{112} +$ $y_1(t-1) + u_1(t-2) + \Theta_{113} +$ $y_1(t-1) + u_2(t) + \Theta_{114} +$ $y_1(t-1) + u_2(t-1) + \Theta_{115} +$ $y_1(t-1) + u_2(t-2) + \Theta_{116} +$ $y_1(t-2) + y_1(t-2) + \Theta_{117} +$ $y_1(t-2) + u_1(t) + \Theta_{118} +$ $y_1(t-2) + u_1(t-1) + \Theta_{119} +$ $y_1(t-2) + u_1(t-2) + \Theta_{120} +$ $y_1(t-2) + u_2(t) + \Theta_{121} +$ $y_1(t-2) + u_2(t-1) + \Theta_{122} +$ $y_1(t-2) + u_2(t-2) + \Theta_{123} +$ $u_1(t) + u_1(t) + \Theta_{124} +$ $u_1(t) + u_1(t-1) + \Theta_{125} +$ $u_1(t) + u_1(t-2) + \Theta_{126} +$ $u_1(t) + u_2(t) + \Theta_{127} +$ $u_1(t) + u_2(t-1) + \Theta_{128} +$ $u_1(t) + u_2(t-2) + \Theta_{129} +$ $u_1(t-1) + u_1(t-1) + \Theta_{130} +$ $u_1(t-1) + u_1(t-2) + \Theta_{131} +$ $u_1(t-1) + u_2(t) + \Theta_{132} +$ $u_1(t-1) + u_2(t-1) + \Theta_{133} +$ $u_1(t-1) + u_2(t-2) + \Theta_{134} +$ $u_1(t-2) + u_1(t-2) + \Theta_{135} +$ $u_1(t-2) + u_2(t) + \Theta_{136} +$ $u_1(t-2) + u_2(t-1) + \Theta_{137} +$ $u_1(t-2) + u_2(t-2) + \Theta_{138} +$ $u_2(t) + u_2(t) + \Theta_{139} +$ $u_2(t) + u_2(t-1) + \Theta_{140} +$ $u_2(t) + u_2(t-2) + \Theta_{141} +$ $u_2(t-1) + u_2(t-1) + \Theta_{142} +$ $u_2(t-1) + u_2(t-2) + \Theta_{143} +$ $u_2(t-2) + u_2(t-2) + \Theta_{144}$	or	$X_{11}(t) + \Theta_{11} +$ $X_{12}(t) + \Theta_{12} +$ $X_{13}(t) + \Theta_{13} +$ $X_{14}(t) + \Theta_{14} +$ $X_{15}(t) + \Theta_{15} +$ $X_{16}(t) + \Theta_{16} +$ $X_{17}(t) + \Theta_{17} +$ $X_{18}(t) + \Theta_{18} +$ $X_{19}(t) + \Theta_{19} +$ $X_{110}(t) + \Theta_{110} +$ $X_{111}(t) + \Theta_{111} +$ $X_{112}(t) + \Theta_{112} +$ $X_{113}(t) + \Theta_{113} +$ $X_{114}(t) + \Theta_{114} +$ $X_{115}(t) + \Theta_{115} +$ $X_{116}(t) + \Theta_{116} +$ $X_{117}(t) + \Theta_{117} +$ $X_{118}(t) + \Theta_{118} +$ $X_{119}(t) + \Theta_{119} +$ $X_{120}(t) + \Theta_{120} +$ $X_{121}(t) + \Theta_{121} +$ $X_{122}(t) + \Theta_{122} +$ $X_{123}(t) + \Theta_{123} +$ $X_{124}(t) + \Theta_{124} +$ $X_{125}(t) + \Theta_{125} +$ $X_{126}(t) + \Theta_{126} +$ $X_{127}(t) + \Theta_{127} +$ $X_{128}(t) + \Theta_{128} +$ $X_{129}(t) + \Theta_{129} +$ $X_{130}(t) + \Theta_{130} +$ $X_{131}(t) + \Theta_{131} +$ $X_{132}(t) + \Theta_{132} +$ $X_{133}(t) + \Theta_{133} +$ $X_{134}(t) + \Theta_{134} +$ $X_{135}(t) + \Theta_{135} +$ $X_{136}(t) + \Theta_{136} +$ $X_{137}(t) + \Theta_{137} +$ $X_{138}(t) + \Theta_{138} +$ $X_{139}(t) + \Theta_{139} +$ $X_{140}(t) + \Theta_{140} +$ $X_{141}(t) + \Theta_{141} +$ $X_{142}(t) + \Theta_{142} +$ $X_{143}(t) + \Theta_{143} +$ $X_{144}(t) + \Theta_{144}$
------------	---	----	--



## Appendix F

### Summary of functions

The research into application of NARX system identification procedures led to the development of a toolbox of Matlab M-functions for non-linear system identification, and response reconstruction. Some of the M-functions, together with a short description, are listed below:

NLID.M	Non-linear system identification to condensed NARX formulation
NLSIM.M	Simulation of SISO condensed NARX models
NLMIMO.M	Simulation of MIMO condensed NARX models
NLINVID.M	Inverse Non-linear system identification to condensed NARX formulation for use in response reconstruction
NLINVSIM.M	Inverse simulation of MIMO condensed NARX models for use in response reconstruction
IDARX.M	Linear ARX system identification. User friendly implementation of Matlab's ARX function
SIMARX.M	Linear simulation of ARX models. User friendly implementation of Matlab's IDSIM function
THQR.M	NARX parameter estimation using Orthogonal decomposition
REGRES.M	Regression of time history data sets for use with NLID.M and NLINVID.M

REPEAT.M	Repeatability function
MAKEMOD.M	Random non-linear model generator
NEWPSD.M	Rig specific identification PSD generator
QFIT.M	Modified QanTiM error function

## Appendix G

### QanTiM: a practical solution to response reconstruction

Figure G.1 is a simplified schematic representation of the QanTiM simulation process (See [ 34 ] & [ 35 ]). The flow diagram shows relevant file names, and their locations within the process. The general response processing icon represents possible high-pass and low-pass filtering, as well as DC-offset removal as applied to all response data. The IDDRV processing icon represents filtering operations to identification drive data. Both these processing functions make use of parameters set up in the data processing window and are implemented into QanTiM as a direct result of the empirical research presented in Chapter 3.

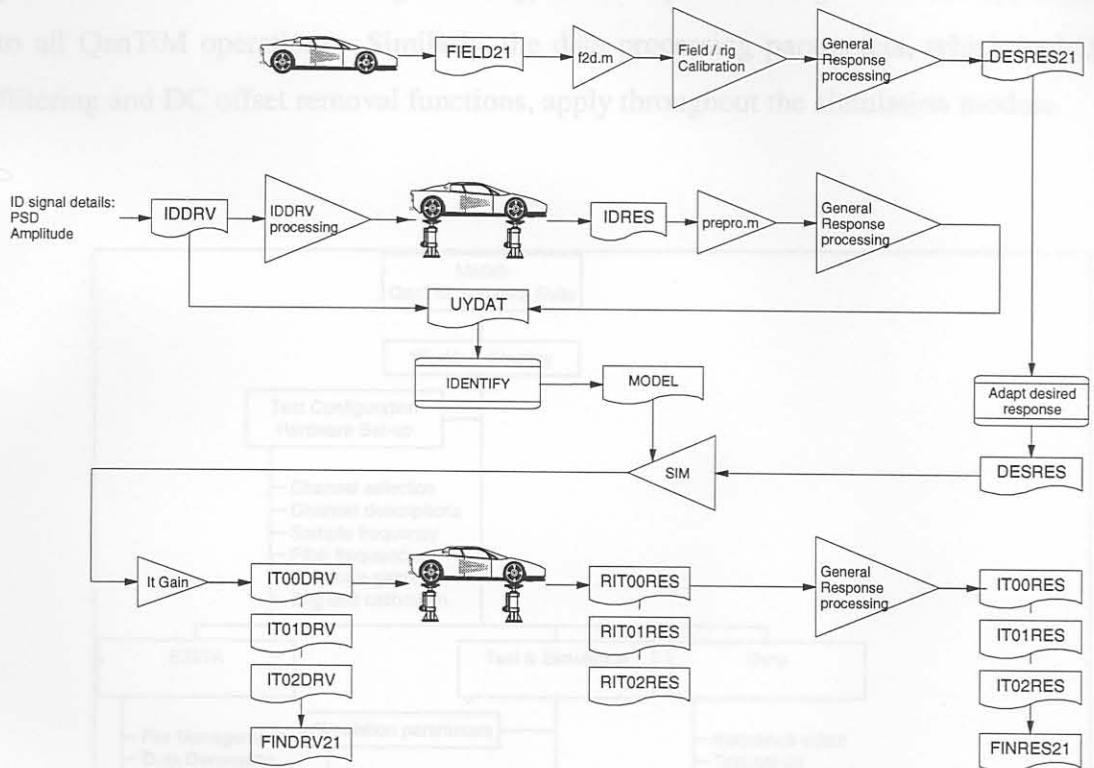
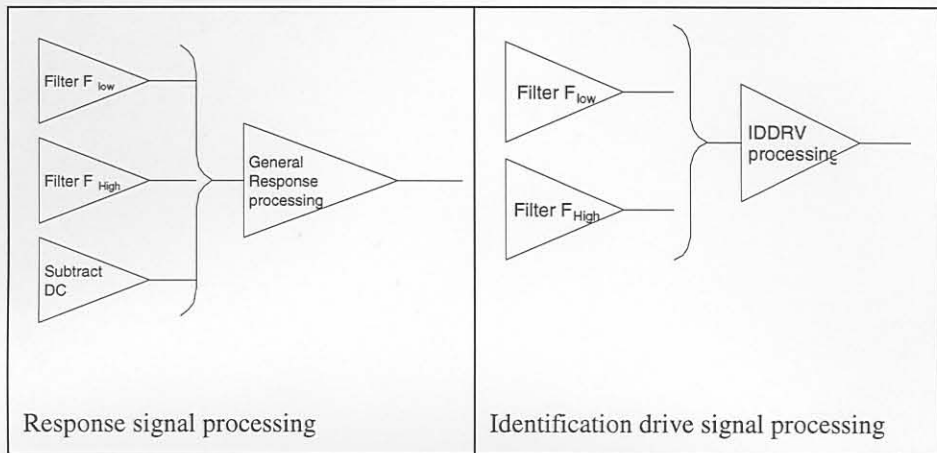


Figure G.1 QanTiM process

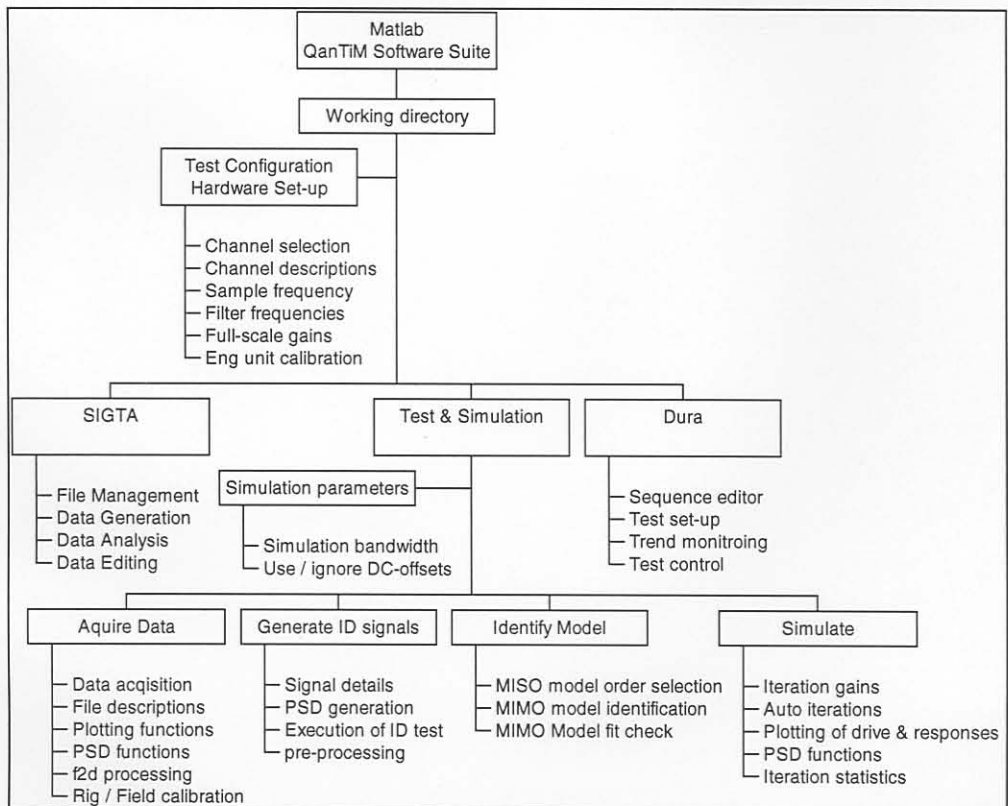


Figure G.3 QanTiM software map



**Figure G.2 General processing functions**

Figure G.3 shows a map of QanTiM windows and relevant operations. Initial test parameters such as the working directory, and the system configuration are applicable to all QanTiM operations. Similarly, the data processing parameters, which include filtering and DC offset removal functions, apply throughout the simulation module.



**Figure G.3 QanTiM software map**